Influence of Saharan dust on phytoplankton in the Eastern equatorial Atlantic

J.A. van Hateren

14-01-2016

Supervisors: Jan-Berend Stuut (NIOZ)

Gert-Jan Reichart (NIOZ & University of Utrecht)

NIOZ Royal Netherlands Institute for Sea Research

Universiteit Utrecht

Acknowledgements

First and foremost, I want to thank Jan-Berend Stuut for this opportunity, the daily supervision and help with every section of the research. Furthermore, I want to thank Gert-Jan Reichart for his supervision and for bringing me to the NIOZ. I want to thank Michelle van der Does for help with grain-size analysis and other questions, Laura Korte for help with C/N analysis and other questions, Rick Hennekam and Rineke Giles for all the time they spent helping me with XRF measurements, Wim Boer for aiding me with the scanning electron microscope, Sharyn Ossebaar for help with C/N analysis, Morton Iversen for help with gel-trap photography and Karine Deboudt for advice on analysis of minerals using the scanning electron microscope. Furthermore, I want to thank the captain, crew and scientific party aboard cruise 64PE395 of the RV Pelagia for making the drifting trap deployments possible and for the nice time on-board. Last, I want to thank Thomas Oudman for recovering the Mauritanian dust samples and Sidi and Camara from parc national du banc D'arguin in Mauritania without whom sampling dust year-round would be impossible.

Index

1. Introduction

Mineral dust has major impacts on the planet and human life. For instance, mineral dust causes asthma in the Caribbean (Gyan et al., 2005), fertilises the Amazon rainforest (Yu et al., 2015) and impacts climate through its effects on albedo (Slingo et al., 2006) and marine phytoplankton (Martin, 1990). In the mid 80's, John Martin hypothesized that mineral dust may have been one of the major drivers of past atmospheric CO_2 fluctuations in glacial-interglacial cycles by supplying iron to oceanic regions low in iron and high in nutrients (High Nitrate Low Chlorophyll regions (HNLC)). Iron fertilisation has been most thoroughly studied in the strongly iron-limited southern ocean (e.g. Blain et al., 2007), but may also play a significant role in oceanic regions where iron is not the proximal limiting nutrient. Such indirect iron limitation was proposed for the oligotrophic eastern equatorial Atlantic by Mills et al (2004). In contrast to the southern ocean, nitrogen is the proximal limiting nutrient for the phytoplankton community in the oligotrophic eastern equatorial Atlantic (Moore et al, 2008). The deficiency in nitrogen accentuates the importance of nitrogen fixation in this area. As the tropical Atlantic receives a high input of mineral dust from the Sahara, iron limitation is least likely to develop in these regions. Nevertheless, Mills et al (2004) performed bioassays and fertilisation experiments in which they found nitrogen fixation to be co-limited by iron and phosphorus, thus indicating the possibility of indirect iron limitation even in waters receiving a relatively high flux of iron. Such iron limitation was also shown to occur in the northeast Atlantic, where dissolved iron is also relatively abundant (Blain et al., 2004).

The current study describes samples collected on a transect within the oligotrophic Northern Equatorial Atlantic (NEA). Due to low ambient nutrient concentrations in this region, nutrients supplied by Saharan dust may play a significant role. Saharan dust has been shown to supply the major nutrients nitrogen, phosphorus and silicate as well as important trace metals that function as essential cofactors in metalloenzymes, including iron, manganese, zinc, copper, cobalt and nickel (Formenti et al., 2003; Sunda, 2013). Earlier dust fertilisation studies in the NEA performed bioassays or fertilisation experiments (e.g. Mills et al., 2004). In doing so, they effectively identified limiting nutrients and the fertilising potential of dust, but their experiments lacked the many complexities associated with natural dust seedings. An exception is the biannual study of Neuer et al. (2004) near the Canary Islands, in which no correlation was found between aerosol concentration and primary nor export production. However, they made use of moored sediment traps at relatively large depths (330-640m), which may have led to dispersion of the signal. Together with the collection intervals of 9.5-19 days, these data had sufficient temporal resolution to show seasonal or sub-seasonal trends, but may not have had sufficient resolution to identify biological responses to individual dust events, which last only a few days to a week at a surface sampling station (Prospero et al., 1987).

Like other dense materials, such as diatom frustules or coccolithophorids, dust may form aggregates with- or adhere to organic matter. As such, it may act as an anchor for organic matter, increasing its settling velocity and thereby decreasing residence time in the water column during which the organic matter could be respired. This process, which effectively transfers CO_2 to the deeper ocean, has been termed the ballasting hypothesis (Bressac et al., 2013). Their study found evidence for ballasting in the Mediterranean Sea through artificial dust seedings. A time lag of 2-3 days was observed between the seeding and the biological response (the fertilising effect), whereas POC export immediately increased due to the ballasting effect. Ballasting by Saharan dust in the NEA has been studied before. By analysing marine snow and measuring its sinking velocity, direct evidence was found of Saharan dust ballasting phytoplankton (Ploug et al., 2008). However, the interaction between the dust events and ballasting remained unclear.

Hypothetically, ballasting by Saharan dust depends on grain size and its fertilisation potential depends on the chemical composition and grain size. In general, clays are the main source of bioavailable iron because they show high iron solubility and are abundant in Saharan dust (Journet et al., 2008). Ideal grain size for ballasting has not been reported. From a conceptual perspective, particles should have enough surplus density to act as an effective anchor. However, very dense particles may not allow sufficient time in the upper water column to form aggregates with- or adhere to OM. In general, Saharan dust is a mixture consisting mainly of quartz and clay particles. Due to preferential deposition of quartz grains, relative amounts of quartz decrease from ~20 to ~14 percent during transport across the Atlantic (Glaccum and Prospero, 1980). Grain size depends on lateral and vertical transport distance from the source (Torres-Padrón et al., 2002) and also shows seasonal fluctuations, with lower grain size in winter than in summer (Neuer et al., 1997; Skonieczny et al., 2013). Over the Atlantic, the zone of maximum dust transport shows a seasonal shift from ~5^{o} N in winter to ~20^{o} N during summer, associated with the latitudinal shift of the inter-tropical convergence zone (ITCZ) from the summer to winter monsoon season (Moulin et al., 1997). Three wind systems dominate dust lofting and transport in northwest Africa and transport dust from separate source areas. In winter, northern coastal trades and (north)eastern Harmattan trades dominate dust transport (Stuut et al., 2005). In summer, Harmattan trades weaken and coastal trades and westward transport in the Saharan air layer dominate dust transport (Stuut et al., 2005). The Saharan air layer overlies the trade winds layer causing an altitude shift of maximum dust transport from 1-2 km in winter to 2-3 km in summer (Liu et al., 2008).

The current study aimed to improve knowledge on fertilisation and ballasting by Saharan dust. The research consisted of two main sections. First, it focussed on ballasting and fertilisation by a dust event. Two questions were central to this work: Does a dust event lead to increased production of organic matter? Can we prove or disprove the ballasting hypothesis under natural dust seeding? In the second section, Mauritanian dust was studied to investigate variability in dust flux and characteristics that may influence its fertilisation and ballasting potential. Three questions were central to this work: What are the seasonal trends in flux, chemical and physical characteristics of low-level transported Saharan dust? What may be the influence of these shifts in dust transport and characteristics on phytoplankton production and ballasting? Can we define possible source areas of the dust samples?

The first part of this research made use of six drifting traps with traps at 100, 200 and 400 m depth, deployed on an east to west transect across the northern equatorial Atlantic. These traps gathered settling organic matter with accompanying dust during and after a major dust event which lasted from the 11th to the 15th of January. Carbon and nitrogen were measured as an indication of OM content in the water column. To examine ballasting, three complementary indicators were used: vertical trends in POC and PON flux, C/N ratio (Müller, 1977) and intact marine snow from gel traps (McDonnell and Buesseler, 2010). The latter enabled us to study the extent of aggregation of the organic matter. The biological response was compared to the timing and quantity of dust supplied during the dust event, as sampled by two dust samplers on board research vessel (RV) the Pelagia (bachelor project Katarina Wetterauer, 2015). In the second part, characteristics of low-level transported Saharan dust were studied in monthly samples from two dust sampling masts in Iwik, Mauritania (19º 53’ 05’’ N, 16º 17’ 04’’ W). The samples were examined for flux, grain size and chemistry and provide the first in-situ data of low-level dust properties and flux.

2. Material and Methods

2.1 Material

2.1a. Drifting traps samples

Sampling fresh marine snow using drifting traps

During cruise 64PE395 of the Royal Dutch Institute for Sea Reseach (NIOZ), drifting traps were deployed for ± 24 hours at station M1, M2, M4a , M4b, M5 and for 44 hours at station M3 (appendix 1, fig. 1). The main goal was to sample fresh marine snow. In a strike of luck, a dust storm passed during deployment of M1 and to a lesser extent M2.

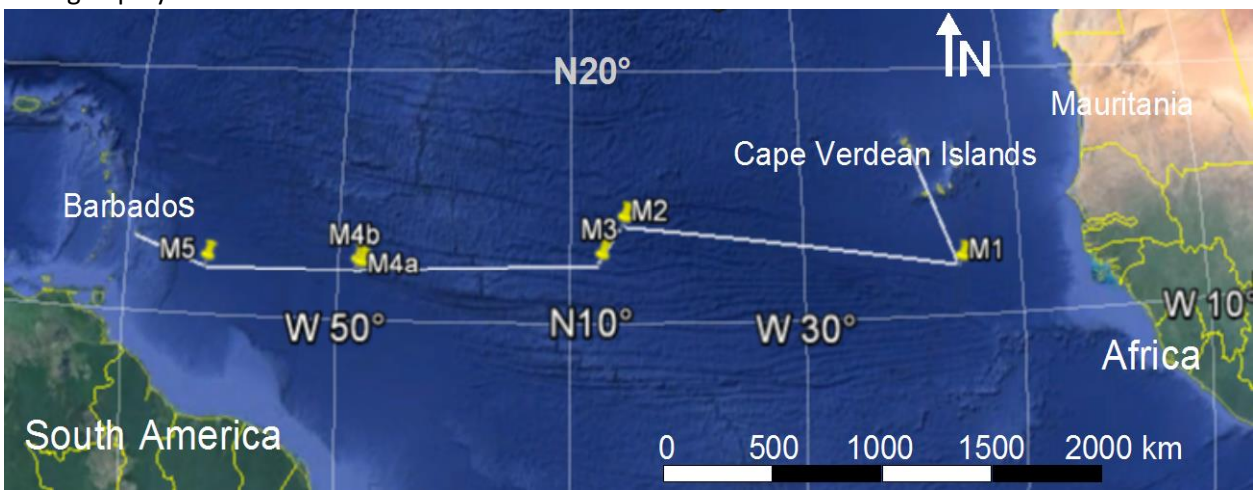

Figure 1. Cruise track and drifting trap deployments of cruise 64PE395. Adapted from: google earth (2015), imagery: SIO, NOAA, U.S. navy, NGA, GEBCO image landsat.

The drifting traps sampled at three depths: 100, 200 and 400 m (fig. 3). Hereafter, the respective traps will be referred to as “M1 100” etcetera. Each level consisted of four Perspex tubes attached to a metal frame, numbered 1 to 4. The traps were 1 m long with an inner diameter of 10.5 cm. Each level contained three regular traps and one gel trap. This trap held a shorter Perspex tube, 5 cm deep and with 9 cm inner diameter, which was filled with medical tissue gel (water, polyvinyl alcohol and carbowax) (McDonnell and Buesseler, 2010) (fig. 2). At station M3 and M4B no gel trap was deployed. The tubes held 8 L and were kept upright by a ballast weight in the bottom of the tube. Before deployment, the traps were filled with filtered seawater. Seawater from appropriate depths was taken from CTD deployments, directly filtered through a 0.20µ folded cellulose-acetate filter and densified using 1.225 g/L Borax. After station M3, Borax was replaced by sodium chloride. Originally, the gel traps were also densified using Borax. Because the first gel had developed a white impenetrable top layer during deployment, it was decided to replace borax by sodium chloride, which greatly improved the performance of the gel.

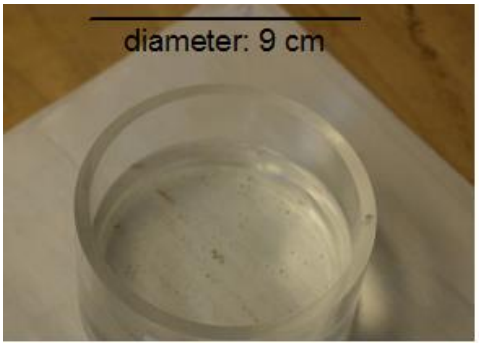

Figure 2. Clear gel trap.

Once on deck, the tubes were left to settle for approximately 5 hours. Since we were only interested in the settling fraction and not the stationary fraction, tubes 2-4 of each depth were emptied to approximately 2 l after settling. Subsequently, they were filtered using a vacuum pump.
Material of tube 2 was used in the current study. This tube was filtered over a Whatman 47 mm Ø glass-fibre filter with approximately 0.4 µm mesh size. These filters had been baked at 400 degrees beforehand to remove organics. After filtering, they were re-wrapped in tin-foil and frozen at -80 degrees to be analysed for C/N ratio and pigments back at NIOZ. The gel traps (tube 1) were emptied to approximately 3L. Subsequently, the short Perspex tubes containing the gels with trapped marine snow were removed from the tube. The gels were stored at -20 °C.

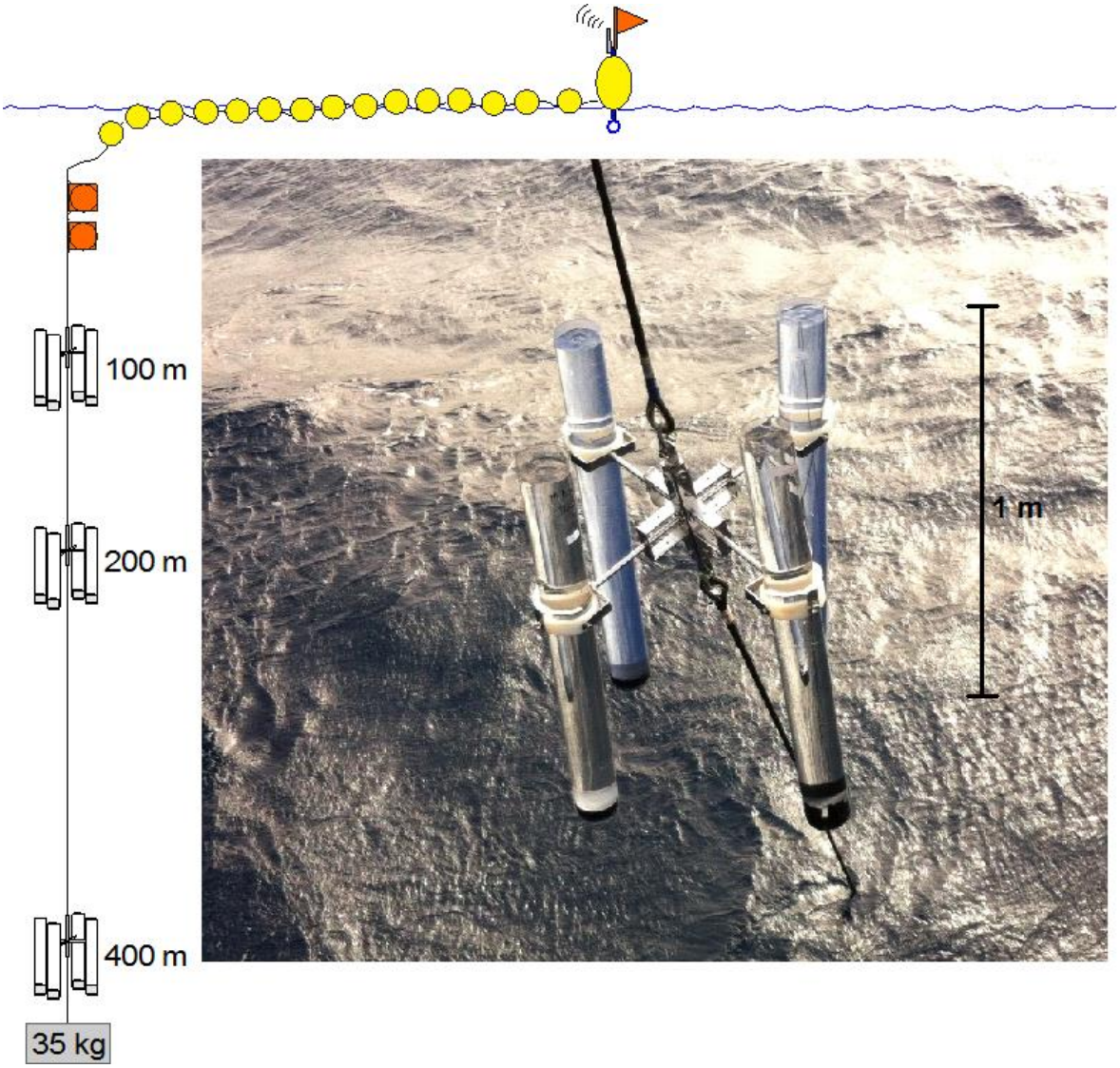

Figure 3. Setup of the drifting traps with floats and a radio- and iridium beacon to aid retrieval. The picture shows one of the drifting trap deployments during cruise 64PE395.

Sampling dust at high temporal resolution using ship-based dust samplers
Dust flux data used in the current study were produced in an unpublished bachelor research project of Katarina Wetterauer (2015) titled "Mineral-dust Samples of the RV Pelagia Cruise 64PE395". Two SIERRA type Anderson high volume active dust samplers were employed on-board the ship (fig. 4). One was equipped with a 20.3 x 25.4 cm glass fibre filter (GFF, +- 0.7 µ) and the other with a 20.3 x 25.4 cm, 0.4µ cellulose filter. A wind vane stopped the sampling procedure if the wind came from the aft of the ship to prevent pollution with soot from the exhaust stacks. During the dust event that lasted from the 11th to the 15th of January, the filters were swapped approximately every 5 hours

during daytime and left overnight. After the dust event, sampling intensity decreased to approximately daily.

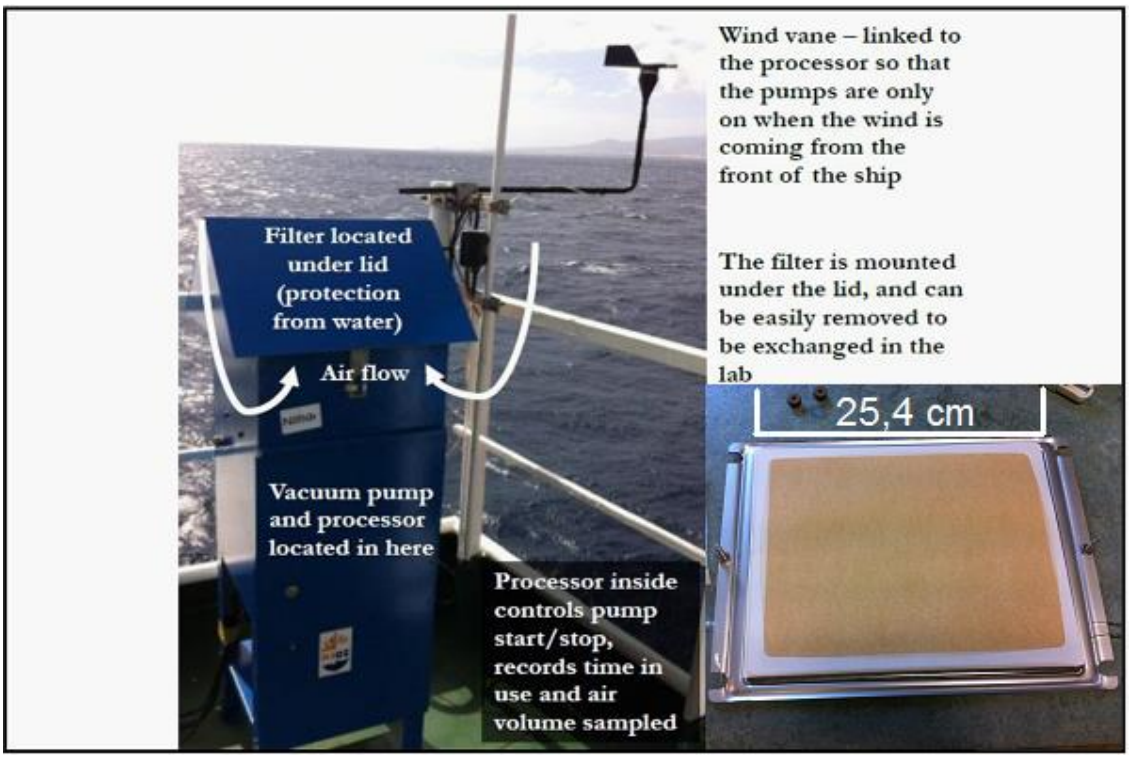

Figure 4. High-volume Anderson dust collector on top of the bridge of Pelagia and a dusty filter of the current cruise (adapted from Stuut et al., 2015).

2.1b. Mauritanian dust samples

The NIOZ dust sampling station in Iwik, Mauritania, is located at the tip of a spit in national park Banc D'Arguin. Mast 1 is located at 19°53.116'N 016°17.639'W and mast 2 at 19°53.121'N 016°17.634'W. Each mast samples at 5 heights: 90, 140, 190, 240 and 290 cm. At each level, two Modified Wilson And Cooke (MWAC) samplers are clamped into sockets (fig. 5). The MWAC sampling bottles are 9.5 cm long with a diameter of 4.5 cm. Two glass tubes, 7.5 mm in diameter, lead air through the cap into the bottle and then out again. The large volume of the bottle relative to the inlet diameter causes dust to settle in the bottle. A wind vane is used to align the mast with the current wind direction. The record has monthly resolution and contains four duplicate samples per height. Samples used in the current study range from the 27th of January, 2013 to the 31st of December, 2014. Samples were switched around the 15th each month (appendix 2). In September 2013 the bottles were not switched, hence these bottles contained dust from the 15th of August to the 15th of October.

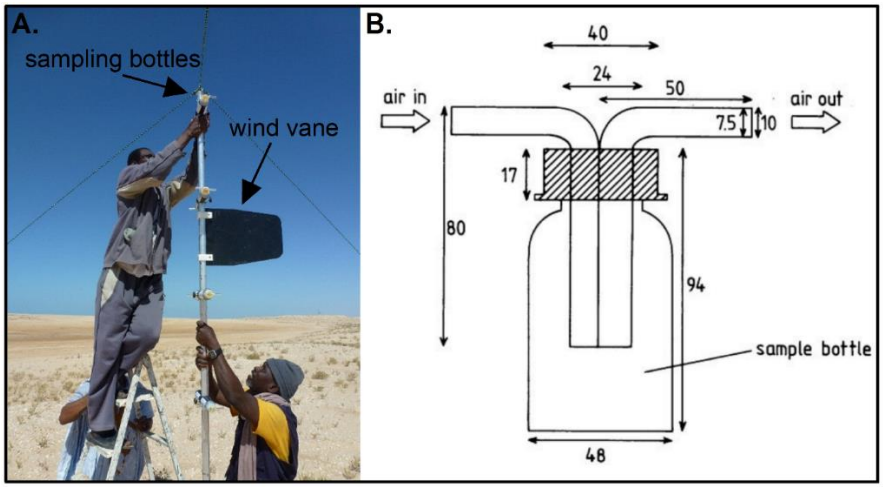

Figure 5. A. Bottles are being replaced at one of the sampling masts. B. Drawing of the MWAC sampling bottle with sizes in mm (Goossens and Offer, 2000).

2.2 Methods

2.2.1 Drifting trap samples

POC, PON and C/N ratio from drifting traps

One quarter of each GF/F filter was cut off using a cutting tool (fig. 6) and refrozen in a glass tube at -20 degrees Celsius. The lid of the glass tube was replaced by a Kimtech precision wipe before freeze-drying. Samples were freeze-dried for at least 6 hours. They were treated with HCL to remove carbon in the form of calcium carbonate. First, freeze-dried filters were transferred to glass petri-dishes and fumed with HCL overnight in a desiccator. Subsequently, they were packed in silver foil cups which were left open at the top. To each silver cup 70 µl of HCL was added. They were dried at 60 degrees Celsius for approximately one hour before the procedure was repeated. After four iterations they were dried overnight and measured. Filter blanks were derived from quarters of a baked filter. They were treated similar to the samples except for the freeze-drying, which was skipped. The cups were closed, compressed to a ball-shape and analysed for carbon and nitrogen using a Thermo-Interscience Flash EA112 Series NC Analyser with a detection limit of 100 ppm and a precision of 0.3%. The analysis was based on the original flash combustion method of Verardo et al. (1990). C and N were measured separately by a thermal conductivity sensor. The area under the peaks was converted to mass of C and N present in the sample using known acetanilide standards (Thermoquest). Fluxes of C and N into the drifting trap were calculated as:

$$F = \frac{M}{A * t} * 4$$

Where F is the flux (mmol/m2/day) of N or C, M is the amount of N or C on a quarter filter in mmol, A is the cross-sectional area of the tube (m_2) and t is the duration of deployment (days). The flux was corrected for the fact that a quarter filter was used in the analysis.


Figure 6. 1/8 cutting tool and Stanley knife used to split filter samples.

Gel trap photography

A camera mounted on a tripod was used to take pictures of the gel traps. The gels were placed on a luminous plate and approximately 13 overlapping pictures were shot. The camera was first focused on the bottom of the gel, where the largest and densest particles were found. Gels that showed high particle density at mid-depth were also photographed with focus at mid-depth. The photos were stitched using the panorama stitching programme Hugin.

2.2.2 Mauritanian dust samples

Meteorological data for comparison to the Mauritanian dust samples

At the sampling location in Iwik, Mauritania, meteorological variables were measured using a Davis Corporation Vantage Vue weather station. Precipitation measurements were deemed unreliable since only two precipitation events were recorded in the course of the 2 year sampling period. Instead, rainfall was estimated using the dataset TRMM_3B42_daily v7 in Giovanni 4 (Giovanni [online], 2015). An area averaged time series was obtained for a 1x1 degree bounding box around Iwik: 16.8° W to 15.8° W, 19.415° N to 20.415° N. Daily precipitation was averaged per sampling month for convenient comparison to dust samples. Daily air parcel back trajectories ending at noon were obtained from the National Oceanic and Atmospheric Administration HYSPLIT model, using the reanalysis (1948-present) dataset (air resources laboratory [online], 2015). As a quality check of the meteorological station at the sampling location and the backward trajectories, data were obtained from the international airports of Nouakchott and Nouadhibou. Nouakchott is located 200 km south of Iwik and Nouadhibou 140 km north-northwest of Iwik. Unfortunately, the airport data lacked precipitation measurements. In order to analyse the relationship between dust characteristics and wind direction, wind direction was averaged per sampling month. This was achieved by vector addition of wind direction and wind speed. In vector addition, strong wind influences the average direction more than weak wind, which correctly represents that strong winds transport more dust on average than do weak winds.

Dust flux

The dust samples were weighed on a Mettler-Toledo AT261 Delta Range balance with a readability of 0.01 mg and a specified reproducibility of 0.015 mg. Each sampling bottle was percussed by hand in order to loosen dust from its sides. The sample was transferred to a measuring cup and weighed. Subsequently, it was stored for further analysis. Mean dust loading per sampling month was estimated as:

$$DL = \frac{MAR}{v * A} * \frac{1}{\eta} * 10^{-6}$$

Where DL is the mean dust loading (µg/m^3), MAR is the mass accumulation rate (g/s), v is the mean wind speed per sampling month (m/s), A is the cross-sectional area of the inlet tube of the MWAC sampler (m^2) and η is the estimated sampling efficiency of MWAC bottles. The diameter of the MWAC inlet was 7.5 mm. An efficiency of 90% was used for the MWAC sampler in accordance to a study by Goossens and Offer (2000).

Grain-size analysis

A Beckmann Coulter laser particle sizer LS 13 320 was used to analyse grain-size distributions. From four duplicate samples (two samples per height, two masts) the sample with highest mass was selected because it was presumed that this sample had been collected with highest efficiency (see:

discussion). Before each run the measuring cell was filled with degassed water to measure background obscuration during 60 s. Scoops of dust were added to a 20 ml beaker until optimum obscuration was reached (defined here as 8-12% with a maximum of 20%). To reach optimum obscuration small samples had to be used entirely. In these cases, duplicate samples were used for subsequent chemical analysis. Approximately 15 ml of degassed water and 3 drops of sodium pyrophosphate were added. The contents of the beaker were stirred for 10 s. Part of the mixture was added to the cell until it was filled completely. The cell was immediately placed in the particle sizer. A stirring magnet in the cell was set at an optimum pace at which particles remained in suspension but no air bubbles were created. The runtime was 90 seconds and offset and alignment were corrected every 60 min. At least three runs were performed. More runs were performed if a significant change in grain-size distribution was observed between run two and three. The first run was selected (if of good quality) to include dust aggregates.

ED-XRF

Chemistry was determined qualitatively by energy dispersive X-ray fluorescence (ED-XRF) using an AVAATECH XRF core scanner. Special measuring cups had to be developed to deal with the small samples. After testing different plastics we settled for clean, paint-free poly-ethylene cups with a circular recess of 6 mm diameter and 1 mm or 2.5 mm depth. A thin plastic film for XRF (thickness 4µ, SPEX SamplePrep) was placed over the cylinder using a plastic ring. Samples were placed at 5 cm intervals in a sample-cup holder (fig. 8). A short test was performed to obtain a current at which acceptable dead times were reached (between approximately 15 and 30%). Different live times were tested for 10, 30 and 50 Kv. It was found that respectively 20, 40 and 80 s live time produced sufficient counts at acceptable measurement durations. The slit size was set at 4x4 mm. The settings used in the measurements are shown in table 1.

Table 1. Final XRF settings.

Voltage	**10 Kv**	**30 Kv**	**50 Kv**
Live time	20 s	40 s	80 s
Current	1500 µA	1300 µA	800 µA
Dead time	18 %	27 %	26 %
Filter	-	Palladium - thin	Cu
Y-axis alignment	+2 mm	+2 mm	+2 mm
Slit size	4x4 mm	4x4 mm	4x4 mm

The cups were tested against regular tablet standards SARM 4 (NIM-N Norite, Mintek), MESS 3 (Beaufort Sea. Produced by the national research council of Canada) and PACS 2 (harbour of Esquimalt, Canada); (fig. 7). Produced by the national research council of Canada). The 1 mm cups showed slightly more deviation from the tablet standards compared to 2.5 mm cups. However, the deviation is negligible compared to the differences between standards. It was decided to use the 1 mm cups because they provide the opportunity to measure small samples and hence months with low dust flux. Due to shallowness of the recess, measurements of heavy elements at 50 Kv may have penetrated through the sample into the measuring cylinder. This was not problematic since the paint-free poly-ethylene did not contain measurable amounts of the elements we were interested in.

However, it may have lowered the counts of the heavy elements somewhat relative to counts of lighter elements.

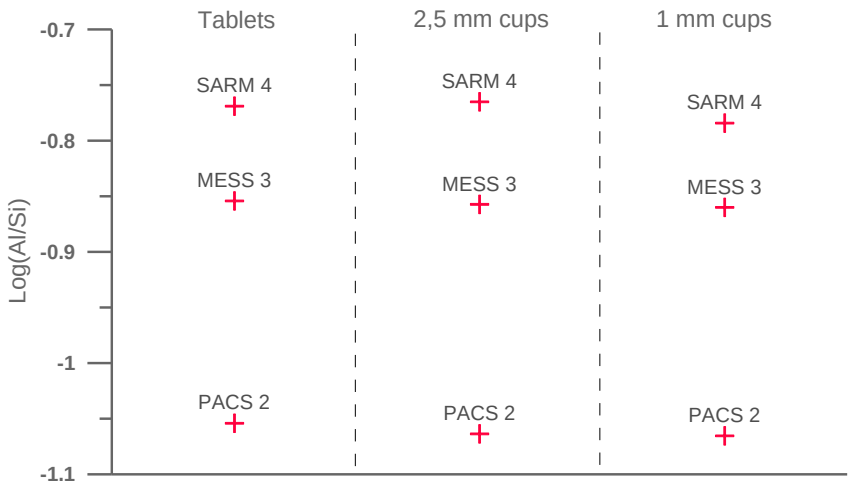

Figure 7. Example of observed differences in the standards SARM 4, MESS 3 and PACS 2 between tablet standards (positions 50-150 mm), 2.5 mm deep cylindrical cups (250-350 mm) and 1 mm deep cylindrical cups (450-550 mm).

The dust was tested for matrix effects. Matrix effects are caused by non-uniform grain size, leading to overestimation of some elements and underestimation of others. The effects are largest when the chemical composition of fine grains differs from that of coarse grains and may influence element counts and elemental ratios. Ground dust was compared to unground dust to test for these effects (fig. 8). Approximately 40 mg of dust was ground in a mortar.

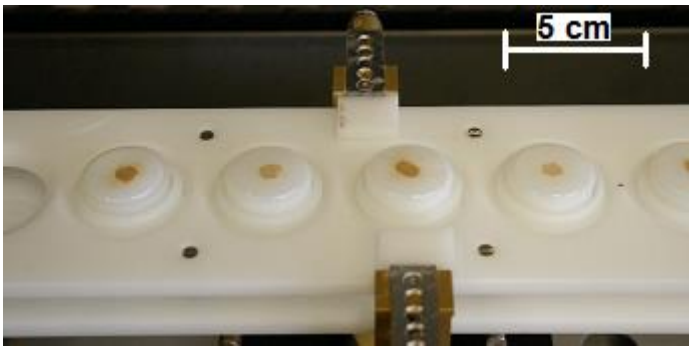

Figure 8. Setup of XRF samples during the matrix effect tests.

Clear grain-size effects could be discerned, as shown in figure 9A. Ground samples showed lower aluminium over silicon ratios, corresponding to the aforementioned matrix effect: penetration depth at 10 Kv is very small, hence large quartz grains (Si rich) were only partly measured whereas clays (Al rich) were fully penetrated. To ensure valid inter-comparison between sampling months it was decided to grind all samples. This study aimed at a qualitative comparison of chemistry between sampling months. Therefore the strongest quality requirement was small variability within a sample (when re-measured or duplicated) compared to the overall variability between sampling months. Re-measurements of both samples and standards showed only slight deviations (fig. 9B&D). Duplicates samples were produced to test for measurement errors that originate from the sample preparation. Results for aluminium over silicon are shown in figure 9C. Duplicate measurements showed consistently lower Al/Si ratios compared to original samples. This was probably caused by another matrix effect: the first samples were pressed into the recess less firmly than subsequent samples. Hence, the duplicates of the first samples were used in the analysis and all subsequent samples were pressed firmly into the recess. For each sample, 50 mg of dust was used. Even at maximum inconsistency of sample preparation that occurred during preparation of the first few samples, the

general pattern in Al/Si was preserved (fig. 9C). The sampling period October-November 2014 was not measured because the amount of dust was insufficient.

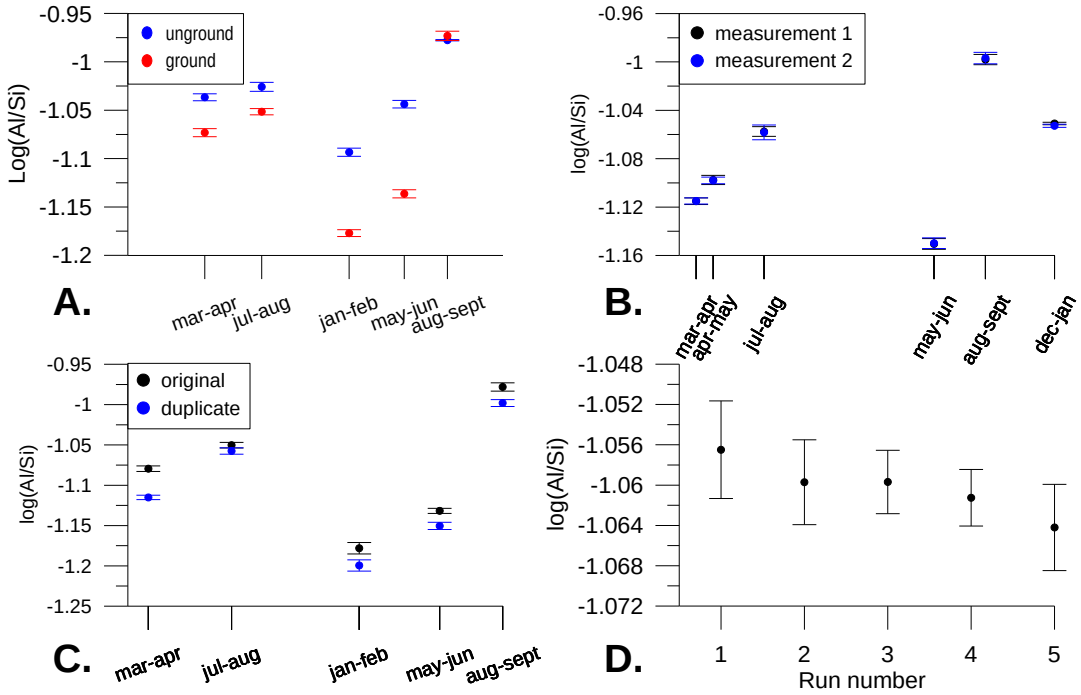

Figure 9. Logarithmic Al/Si ratios. Error bars show relative standard deviation as measured by five iterations of the measurement. A: Matrix effects occur in unground samples, as shown by the large difference between unground and ground samples compared to month to month variability. B: Re-measurements of samples in different runs produce nearly identical results. C: Duplicate samples show the same pattern as the original samples, albeit with systematically lower log(Al/Si) ratio (probably due to matrix effect, see text). D: Low error in PAC 2 standard measured in five different runs.

High magnification imagery using a scanning electron microscope (SEM) and determination of the chemistry of individual particles using energy-dispersive X-ray spectroscopy (EDS) capabilities of the SEM.

A Hitachi 3000 SEM/EDS was used for determination of the chemistry of individual particles as well as for visual inspection of the samples. X-Ray spectra were obtained at an accelerating voltage of 15 kV and an acquisition time of 60 seconds. Samples were stuck on an aluminium sampling stub using double-sided carbon tape. Areas densely packed with grains were identified at 30 x magnification. In such a dense area, a random point was chosen as the centre of a 420 by 280 µ frame (magnification: 400x). All grains that were at least halfway in the frame were measured with EDS point scans using Oxford SwiftED 3000 software. At least three frames were analysed per sample. A separate analysis of the fine (<20 µ) fraction of August-September 2014 was done at higher magnification: once at 3000x and twice at 6000x. The number of grains analysed per frame ranged between 30 (filament was damaged halfway through the run so the measurement was stopped) and 165. The following elements were included in the SEM spectrum model: fluor, sodium, magnesium, aluminium, silicon, phosphorus, sulphur, potassium, calcium, titanium and iron. Carbon and nitrogen were not included because they mainly occurred in the background (especially carbon due to the carbon tape) and in map views no carbonaceous particles were found. Fluor was included to distinguish micas with their characteristic (F, OH) group. Counts of included elements were converted to elemental percentages relative to the total of all included elements. This enabled comparison to mineral elemental formulas. Based on the chemical composition of major minerals in the Sahara (Moreno et al., 2006), a method was developed to assign particles to classes consisting of groups of minerals that are distinguishable by high counts of certain elements. The assignment protocol was based on the

methodology of Deboudt et al. (2010) but criteria used in the current study differed greatly from theirs because Deboudt et al. included carbon and nitrogen. According to Moreno et al. (2006) the most common Saharan minerals are silicates (quartz and diatoms), aluminous clay minerals (kaolinite and illite-sericite) and aluminous silicates (feldspars and dioctahedral smectitic clays). Elemental composition and characteristics of these and other minerals used in the current study are shown in table 2.

Table 2. Some common minerals and characteristics of their elemental formulas used in the particle assignment protocol. Note that the percentages depend on which elements were included in the SEM spectrum model. Pure quartz, for example, should show 100 percent Si because oxygen was not included in the model.

Quartz	$SiO4$	Si: 100%		
Orthoclase	$KAlSi_3O_8$	Si/Al = 3		
Albite	$NaAlSi_3O_8$	Si/Al = 3		
Kaolinite	$Al_2Si_2O_5(OH)_4$	Si/Al = 1		
Illite	$(Al,Mg,Fe)_2(Si,Al)_4O_{10}[(OH)_2,(H_2O)]$	Si/Al = 2/3		
Biotite	$K(Mg,Fe)3(AlSi3O10)(F,OH)2$	Si/Al = 3	F: 15%	(Si+Al): 31%
Muscovite	$KAl_2(AlSi_3O_{10})(F,OH)_2$	Si/Al = 1	F: 22%	
Calcite	$CaCO_3$	Ca: 100%		
Gypsum	$CaSO_4{\cdot}2H_2O$	Ca/S = 1		
Dolomite	$CaMg(CO_3)_2$	Ca/Mg = 1		
Mafic clays, shown: Palygorskite	$(Mg,Al)_2Si_4O_{10}(OH){\cdot}4(H_2O)$	Si/Al = 1		
Iron oxide, shown: Hematite	Fe_2O_3	Fe: 100%		
Sodium chloride	$NaCl$	Na: 100%		

In the assignment protocol dilution of the chemical signature of a grain by surrounding grains was accounted for by lowering the boundaries compared to actual chemical formulas. Grains were assigned using AND OR and IF statements in excel 2013 (table 3). In the silicate criterion, the Si cut-off point was set low to allow for some iron crusting without moving the particle to “ambiguous”. Iron crusting presumably had a large influence due to the shallow penetration depth of the SEM, which is in the order of a few µm. The 0.4 Si/Al cut-off point for alluminosilicates was based on the lowest Si/Al ratio occurring in common alluminosilicates (2/3, illite). The 15 % cut-off point was based on the lowest elemental percentage of Al + Si in the elemental composition of biotite (31%) and allows for some crusting on the particle without moving it to “ambiguous”. The most common iron-

bearing alluminosilicates are illite (Fe/Si = 0.5) and biotite (Fe/Si = 1). Hence the criterion for iron-bearing alluminosilicats was set at Fe/Si >= 0.3. Remaining particles were moved to the class "ambiguous".

Table 3. Particle assignment protocol.

Group	Criterion	Subgroup/mineral	Criterion
Division 1			
Iron oxide	Fe > 50%		
Sodium chloride	Na/Si >= 1 AND Na > 40%		
Mica	F >= 5% AND Si >= 15%		
Carbonate	Ca/Si > 1 AND Ca+Mg > 30% OR Ca+Mg+S > 50%	Gypsum	Ca+Mg+S > 50% AND S/Ca > 0.3
		Dolomite	Mg+Ca > 30% AND S/Ca < 0.3 AND Mg/Ca > 0.3
		Calcites	Remaining carbonates
Division 2			
Silicate	Si/Al >= 5 AND Si > 40 %		
Alluminosilicate	Si/AL >= 0.4 AND Si/Al <5 AND Al+Si > 15%	Iron bearing	Fe/Si >= 0.3
		Non- iron bearing	Remaining alluminosilicates
Ambiguous	non-assigned particles		

Statistical analysis of results of the Mauritanian dust samples

Several characteristics of the Mauritanian dust were tested for correlation to meteorological variables and/or other dust characteristics. Correlations were produced using the rcorr function in the statistical computing programme Rstudio (2015). Where linear relationships were expected, for instance between grain size and chemistry, Pearson's correlation (r_p) was used. If monotonic, non-linear relationships were expected, such as between precipitation and chemistry of the dust, Spearman's correlation (r_s) was used. Results were deemed significant for p-values lower than 0.05 and highly significant for p-values lower than 0.01.

3. Results

3.1. Drifting-trap samples

3.1a. POC, PON and C/N ratios

Particulate organic carbon (POC) and particulate organic nitrogen (PON) settling fluxes at 100, 200 and 400 m depth of the 5 sampling locations together with linear fits are shown in figure 10 and numerically in table 4. For geographical coordinates of the sampling stations see appendix 1. In the following one should bear in mind that the stations were located on an east-west transect at 12° north, M1 being the most eastern and M5 the most western station. M2, however, was situated 13° 45' north, approximately the same longitude as M3. C/N analysis was performed twice on the samples of station M3 and M4a because of unexpected outcomes (fig. 10); (see: discussion). Except if noted, only the duplicate measurements of M3 and M4a are considered in the following section. Accordingly, table 4 only shows the duplicate measurements.

All stations showed attenuation of the POC and PON flux with depth (fig. 10); (table 4). The relative attenuation as shown in table 4 was calculated per 100 m and relative to the flux at 100 m depth. For example, the relative attenuation between 200 and 400 m is $\frac{f_{200}-f_{400}}{f_{100}*2} * 100\%$ where f is the carbon flux and the factor 2 is to correct for the 200 m descent. This attenuation displayed a longitudinal trend: it was significantly stronger at M1, where the POC flux decreased at 27 percent per 100 m from 100 to 400 m depth. Attenuation rate decreased westward and was only 15 percent per 100 m from 100 to 400 m at M5. Nitrogen showed similar diminution between 27 (M1) and 17 percent (M5). Addition information can be gained if we look in more detail at the degradation pattern with depth. At 100-200m depth, M1 showed weaker attenuation than M2, M3 and M4 whereas M5 showed no attenuation. From 200-400 m depth degradation continued unabated at M1 and increased spectacularly at M5, in marked contrast to a decrease in degradation rates at M2, M3 and M4 (fig. 10). Focussing on the initial flux at 100 m depth, a similar trend appeared: the flux was significantly higher at M1, diminished westward but increased again at M5.

Table 4. Carbon and nitrogen fluxes and degradation rates at all stations.

Station	M1	M2	M3*	M4a*	M4b	M5
C at 100 m (mmol/m2/day)	10.29	6.86	3.61	3.31	3.23	5.45
N at 100 m (mmol/m2/day)	1.28	1.09	0.53	0.59	0.51	0.80
Molar C/N at 100 m	8.05	6.30	6.85	5.64	6.35	6.80
Attenuation of C flux per 100m: 100-200 m (%)	30	46	36	30	43	-3
Attenuation of C flux per 100m: 200-400 m (%)	26	13	16	11	6	24
Attenuation of C flux per 100m: 100-400 m (%)	27	24	22	18	18	15
Attenuation of N flux per 100m: 100-200 m (%)	30	61	35	37	45	2
Attenuation of N flux per 100m: 200-400 m (%)	26	10	16	6	7	25
Attenuation of N flux per 100m: 100-400 m (%)	27	27	23	16	20	17

*Note that the duplicate measurement of M3 and M4a are shown. Flux attenuation is expressed as the percentage of attenuation relative to the flux at 100 m depth.

The error between the actual settling flux of POC and PON in the ocean and the flux measured by the drifting traps is unknown. However, the double deployment at M4 provided us with a rough indication of the error during sampling and measurement of the samples. Two drifting traps (M4a and b) were deployed at almost exactly the same location albeit with one day in between. POC deviated by 2 (100 m) to 16 (200m) percent. PON deviated by 10 (100 m) to 26 (400 m) percent (fig. 10). In comparison to this total error, the reported precision of the C/N analysis (0.3%) was negligible

(Sharyn Ossebaar, personal communication, June 16, 2015).

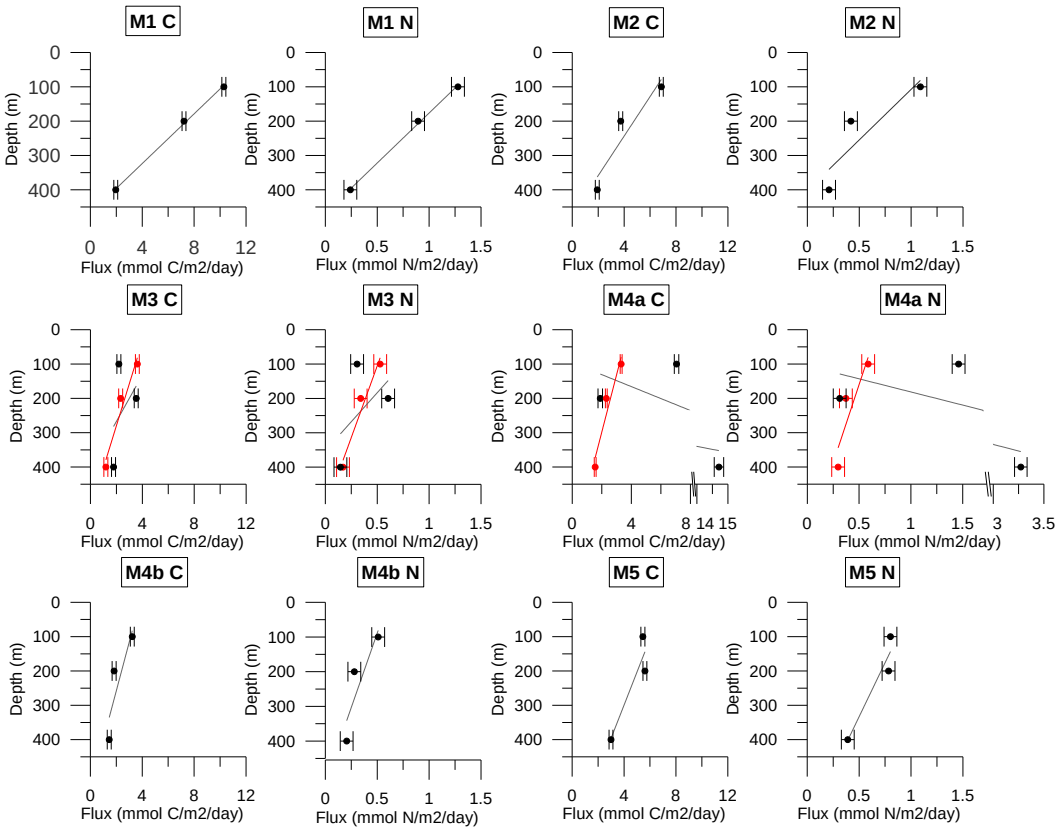

Figure 10. Carbon (C) and nitrogen (N) flux per station with linear fit. Duplicate measurements of M3 and M4a are shown in red. Note departure from a linear trend at M3 and extremely high amounts of carbon and nitrogen at 100 and 400 m at station M4a (note break-axes M4a). Error bars were obtained from the difference between M4a and M4b.

Remarkably, the longitudinal trend in C/N ratio at 100 m depth corresponds to the C flux: C/N ratios were significantly higher at station M1 (8.05), decreased westward to a minimum at station M4 (average 6.00) and increased at station M5 (table 4). In comparison, the widely used Redfield ratio of C/N = 106:16 corresponds to a C/N ratio of 6.625 (Redfield, 1958) and the average C/N ratio of particulate organic matter in the ocean was estimated at 7.4 (Geider and la Roche, 2002). Both these values fall between the maximum and minimum observed at 100 m in the current study. C/N trends with depth are particularly important in the current research because they may provide a qualitative indication of the amount of degradation between sampling depths and hence provide a clue on settling velocity of organic matter. Figure 11 shows C/N ratios of the 5 sampling stations and the duplicate measurements at 100, 200 and 400 m. Again, the difference between M4a and b was used as an indication of error. At M3, the original measurement showed an odd pattern with depth with an extremely high C/N at 400 m (more than twice the Redfield ratio) whereas the second measurement showed a pattern which resembled the pattern observed at the other stations. M4a was also re-measured, resulting in the same pattern as the first measurement and as M4b. Since the secondary C/N analyses presented more credible results both in the C/N analysis (M3) and the C and N flux (M3 and M4a), only the duplicate measurements were considered.

The smallest increase was observed at station M1 and M3, 0.8 and 1.9 units respectively. An increase of this size likely does not exceed the error in this methodology. M2 showed a strong increase in C/N ratio between 100 and 200 m and an intermediate increase from 200 to 400 m. M4b and M5 showed intermediate increase from 100 to 400 m. The fact that the same pattern was observed in measurement 1 and 2 of M4a lends credibility to the observed decrease in C/N ratio from 200 to 400

m. Since M4a and M4b were deployed at the same location, an average of these two stations is interesting (fig. 11). The average shows only a small increase in C/N ratio from 100 to 200 m and a slight decrease from 200 to 400 m.

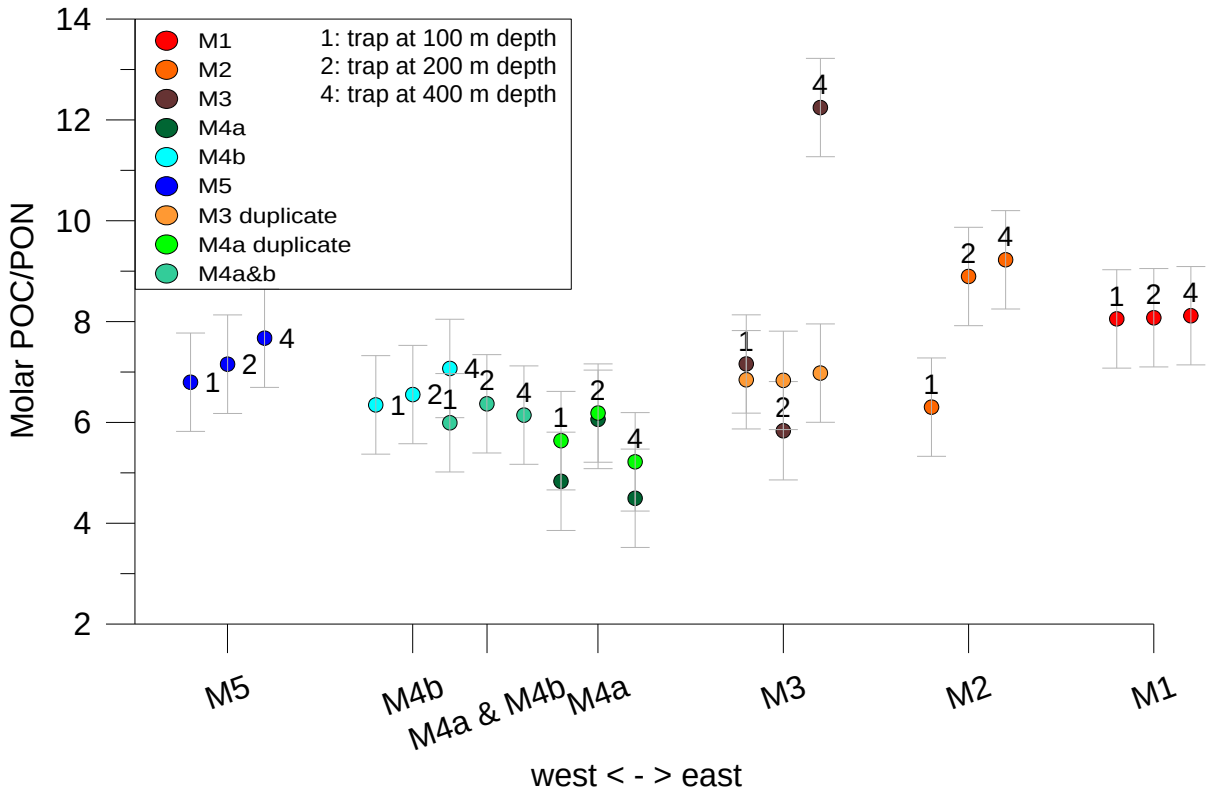

Figure 11. C/N ratios of the filtered material. Labels show the depth divided by 100 m. Duplicate measurements are shown in light green (M4a) and light orange (M3). Note the minimal change with depth at station M1 and the major difference between M3 and its duplicate measurement. Error bars are based on the average difference between the M4a measurements (100, 200 and 400 m) and their duplicate measurements.

3.1b. Gel traps

Gel traps were deployed at station M1, M2, M4a and M5. For convenience, M4a shall be referred to as M4 in this section. Pictures of the gel traps are shown in appendix 4. M1 100 and M1 200 developed an impenetrable layer during deployment and thus could not be used. M1 400 was reasonably clear and particles had penetrated into the gel. The depth to which particles penetrated the gel is presumably linked to their density and settling velocity. Under the camera and with the naked eye it was clear that larger marine snow sank deeper into the gel than smaller flocks. Apart from larger marine snow, zooplankton, shells, faecal pellets and foraminiferal tests also penetrated to the bottom of the gel. First, differences between the sampling stations are discussed based on the gels from 400m depth because this was the only gel available from M1. M1 and M5 contained most material. It was, however, difficult to tell which of the two contained more OM because the type of particles was very different. M2 contained less material and M4 contained very little material. There were a few groups of particles that could be distinguished on the pictures and made up the bulk of the material: marine snow, faecal pellets, zooplankton and foraminifera (fig. 12). A small number of shells was observed, measuring up to 1 mm (fig. 12E). The larger marine snow measured up to 3 mm (fig. 12A&B). Faecal pellets were relative long, up to 4 mm (fig. 12C). The larger zooplankton was 2 to 6 mm long (fig. 12F). The larger foraminifera were around 1 mm in diameter (fig. 12D).

Figure 12. A. Yellowish green large marine snow, ± 3mm diameter: M5 400m. B. Dark green-brown marine snow, ± 2.5 mm wide: M2 100. C. Elongate faecal pellet, ± 1.5 mm: M2 100m. D. Foraminifera, ± 1 mm diameter: M2 100. E. Snail-like shell ± 1 mm diameter: M4 100m. F. Zooplankton ± 6mm: M2 100m.

First, marine snow will be discussed. Marine snow was most abundant at M5 followed by M1, then M2 whereas M4 contained very little marine snow (table 5). There were differences in the size of marine snow. At M1 and M2 the larger fraction of marine snow mainly ranged between 1 and 2 mm. At M4 marine snow was not larger than 1 mm. M5 showed marine snow up to 3 mm. There was a strong difference in the appearance of marine snow between M5 and the other traps. At M5, marine snow was lighter coloured and green to yellowish green. At M1, M2 and M4 it was a darker shade of green-brown of dark brown (fig. 12B). M2 contained the highest amount of faecal pellets, followed by M1 (table 5). M4 contained only a few faecal pellets but they made up a significant fraction of the material. M5 contained almost no faecal pellets. Zooplankton and foraminifera will be discussed for the 100 m traps because they were far more abundant in these traps. Zooplankton was most abundant in the gel of M4, followed by M2 (table 5). M1 and M5 did not contain zooplankton large enough to be identified from the pictures. M2 contained abundant foraminifera in the 100 m trap. Only a few were found in the gel of M5 and none in the other gels.

The vertical trend can be discussed for stations M2, M4 and M5 (table 5) but not M1 because only one gel of this deployment, M1 400, was clear enough to be used in the analysis. The amount of marine snow declined with depth at station M2 and M4. In contrast, M5 400 contained more marine snow than M5 100. Faecal pellets were only abundant enough at M2 to estimate a vertical trend. Their number remained relatively constant with depth. For all traps where zooplankton was observed (M2, M4), the number of zooplankton declined with depth. The number of foraminifera at M2 decreased sharply with depth and they were almost absent at 400 m.

Table 5. The longitudinal and vertical trends in abundance of marine snow, faecal pellets, zooplankton and foraminifera. The relative abundance (longitudinal trend: as compared to the other stations, vertical trend: as compared to the other depths) of a certain type of particle was expressed qualitatively as: abundant (+++), average (++), below average (+), low abundance (-) and not observed (0). Note that particles too small to be identified on the pictures were not included. The longitudinal trend was based on the 400 m traps except where noted (shaded cells, observed at 100 m).

	Marine snow				**Faecal pellets**				**Zooplankton**				**Foraminifera**			
	M1	**M2**	**M4**	**M5**	**M1**	**M2**	**M4**	**M5**	**M1**	**M2**	**M4**	**M5**	**M1**	**M2**	**M4**	**M5**
Longitudinal trend	++	+	-	+++	++	+++	+	-	0	++	+++	0	0	+++	0	-
Vertical trend: 100 m		+++	+++	++		++				+++	+++			+++		
200 m		++	++	+		++				++	++			+		
400 m		+	+	+++		++				+	+			-		

3.2. Mauritanian dust samples

3.2a. Meteorological background situation

Data from the Davis meteorological station at our sampling location showed a distinct yearly wind speed pattern with maxima around spring to early summer (fig. 13A). Wind roses for each sampling month are shown in appendix 7. Average wind direction showed northerly to north-westerly winds throughout most of the year, with the exception of the winters of 2013 and 2015, which showed an increase in easterly winds (fig. 13C). Months with eastern winds displayed significantly lower average wind speeds (r_S=0.475, $p < 0.05$) (fig. 13C). Indeed, only 31% of eastern winds blew faster than 5 m/s, compared to 59% of northern and western winds. Satellite estimated rainfall displayed pronounced peaks in late-summer due to summer-monsoonal rainfall (fig. 13D). The peaks are concurrent with temperature maxima (fig. 13B).

Daily backward trajectories were calculated for 2013-2014 (appendix 7). Although only two years were analysed, a seasonal pattern appeared in the lower tropospheric wind direction. From mid-March to mid-October solely NNW to NNE coastal and western trade winds were observed. Starting from mid-October, (north)-eastern Harmattan winds occurred alongside the coastal and western trades (fig. 14A). Around the turn of the year, these winds even became dominant in the backward trajectories, but their occurrence decreased again towards spring. Summer trajectories at 10 and 5000 m above ground level (AGL) showed coastal and western trade winds in the lower troposphere and eastern winds in the SAL (fig. 14B&C).

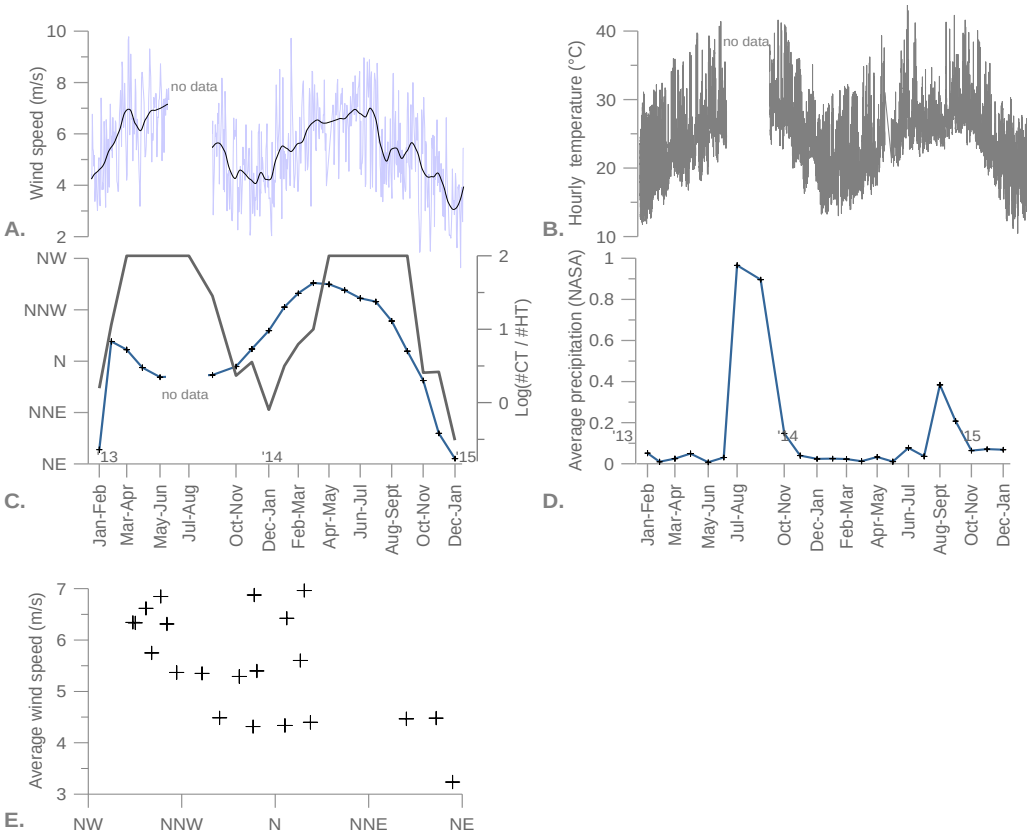

Figure 13. A. Hourly wind speed plotted with a local regression smoothing function in the programme Rstudio. B. Hourly temperature (C°). C. Vector averaged wind direction per sampling month and a logarithmic ratio of the number of coastal and western trade trajectories (northern or western) divided by the number of Harmattan trajectories ((north)-eastern) D. Monthly averaged daily precipitation from Giovanni 4 (NASA), using the dataset TRMM_3B42_daily v7. E. Sampling month averaged wind speed plotted against wind direction with linear fit.

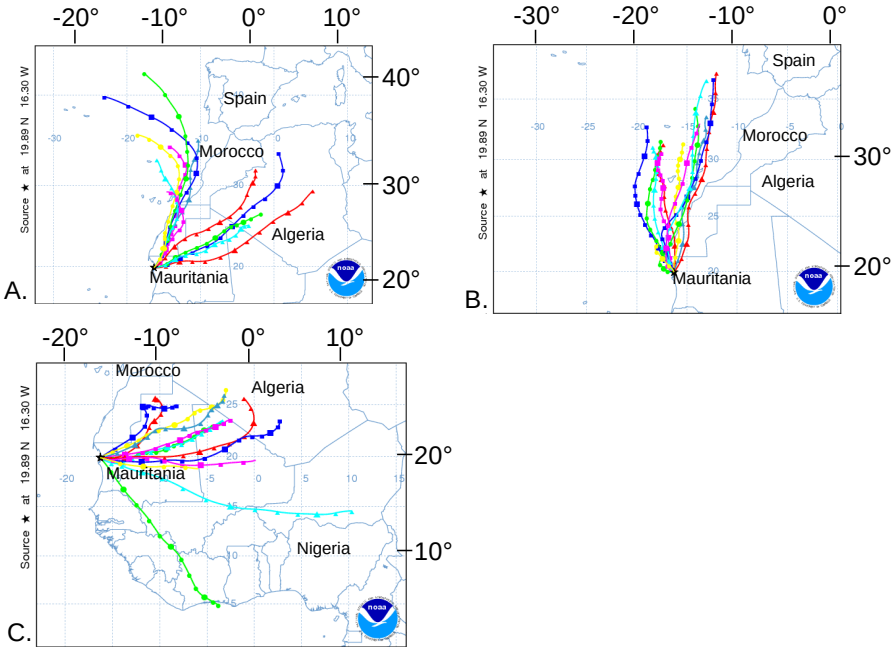

Figure 14. Each picture shows twelve backward trajectories of consecutive days. Each coloured line represents one such backward trajectory starting at noon. Geographical coordinates are in degrees east and degrees north. A. Daily backward trajectories from 20/01/2013 to 01/02/2013, starting at 10 m above ground level (AGL). Both dominant wind directions in the lower atmosphere occurred during this period. B. Daily backward trajectories from 30/06/2013 to 12/07/2013, 10 m AGL. These trajectories only showed coastal trade wind trajectories. C. Daily backward trajectories from 5000 m AGL from 30/06/2013 to 12/07/2013, showing predominantly eastern winds in the Saharan air layer.

3.2b. Dust flux

Some bottles were removed from the analysis based on a strong deviation from the average weight in a sampling month. Bottle 1_1B (mast 1, 90 cm, bottle B) of October-November 2010 was empty. Bottle 1_3B of January-February 2013 was broken. Bottle 1_5B of June-July 2013 was removed because it weighed only 1 mg compared to weights between 15 and 50 mg in the other bottles. Similarly, 1_4A of July-August 2013 was removed because its mass was 17 times smaller than that of the second lightest bottle of that month. Figure 15 shows the dust mass flux as recorded by the MWAC sampler in Mauritania. The average mass of the four bottles per sampling period per sampling height is shown in appendix 6. Mass flux correlated highly significantly to wind speed (r_s = 0.705, $p < 0.01$). March-April 2013 displayed significantly higher mass flux at 500 g/m_2/day. In general, highest mass was observed in spring of 2013 and mid-winter to early summer of 2014. July-August 2013 also showed high mass. The mean dust loading per sampling month showed a very similar pattern despite the influence of wind speed. The two spring maxima displayed monthly averaged dust concentrations of 237 and 170 µg/m^3 respectively. The two fall minima amounted to 6 and 2 µg/m^3 respectively.

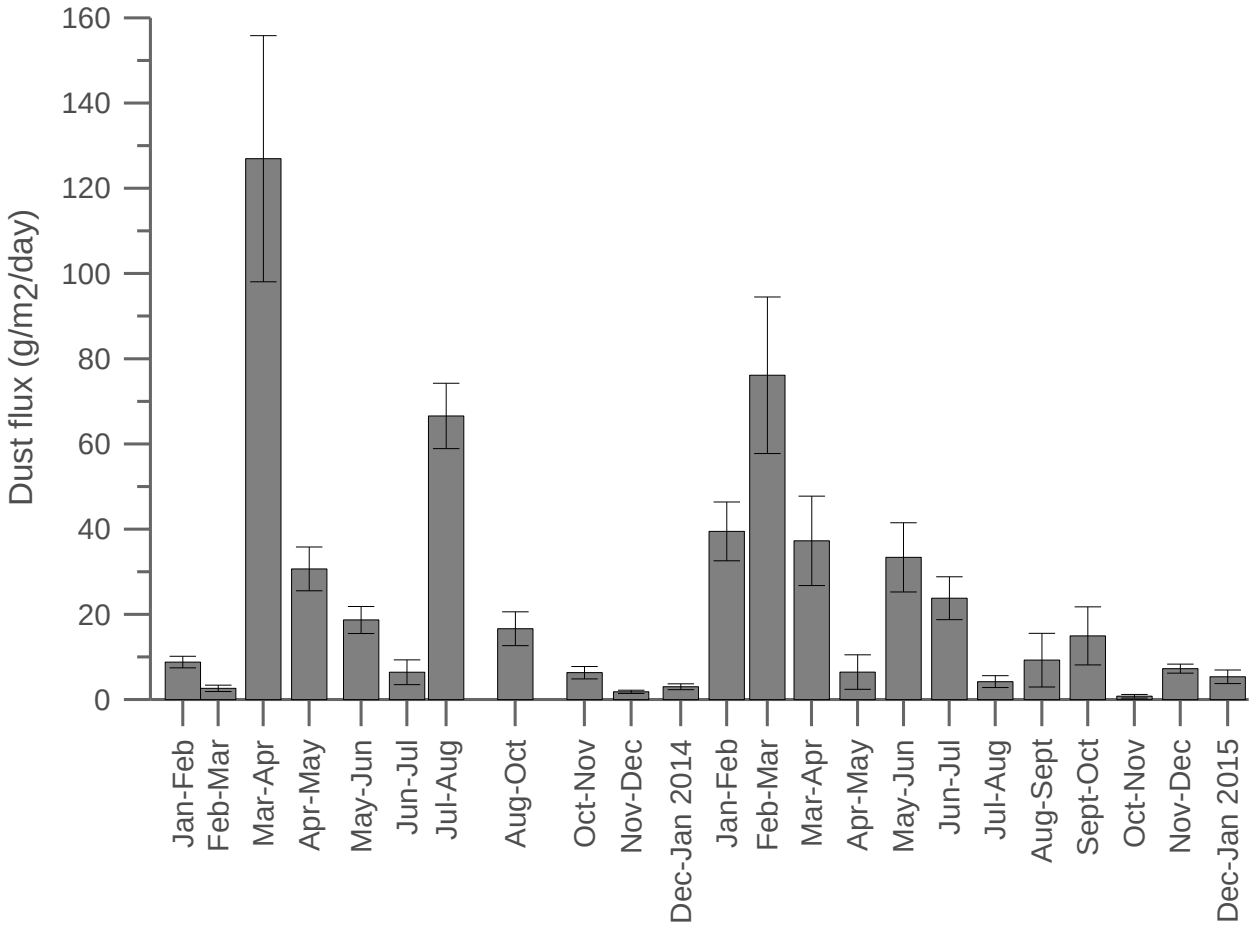

Figure 15. Average daily mass flux of sampling heights 190, 240 and 290 cm (3*4 bottles) with relative standard deviation. The lower two sampling heights were not included (see: discussion).

3.2c. Grain size

The size distributions of the Mauritanian dust displayed a peak between 38 and 66 µm. Generally the peak was narrow and the distributions were negatively skewed with a long tail on the fine-grained side of their distribution (appendix 5). Some distributions showed an additional "coarse shoulder". Good examples are November-December 2013 and April-May 2014 (appendix 5). It is notable that none of the sampling periods shows the coarse shoulder in all of its distributions. Some periods displayed (signs of) a bimodal distribution, with a secondary fine peak around 15 µm, most notably August-September 2014 and to a lesser extent October-November 2013, May-June 2014 and July-August 2014 (appendix 5). In two samples, October-November 2013, 240 cm and August-September, 240 cm, this was the primary peak. In some cases there was strong dissimilarity between the different sampling heights within a sampling period, most notably in August-October 2013, October-November 2013, May-June 2014, November-December 2014 and December 2014- January 2015. In the aforementioned periods, samples from lower heights are invariably coarser than the higher samples (appendix 5). Figure 16 shows average median and modal grain size of the sampling heights 190, 240 and 290 cm. 90 and 140 cm were removed from all analyses due to deviating characteristics of this dust (see discussion). The dust displayed median grain size between 13 and 58 µm. A few periods showed distinctly lower grain size, notably August-October and November-December 2013 and May-June and August-September 2014. The average median grain size of these months was 25 µm, in stark contrast to the average of 41 µm of the remaining months. August-September 2014 displayed an exceptionally low median size of 15 µm. During most of the record, median grain size ranged between 36 and 45 µm. A drop in median and modal grain size in the months August-November 2013 and August-October 2014 co-occurred with increased precipitation. In contrast, the fine-grained dust in May-June 2014 did not coincide with substantial precipitation. Mean, modal and median grain size all displayed negative correlation with precipitation, but only modal grain size correlated significantly at $r_s = -0.43$ ($p < 0.05$). Wind speed and wind direction did not show significant correlation with grain size.

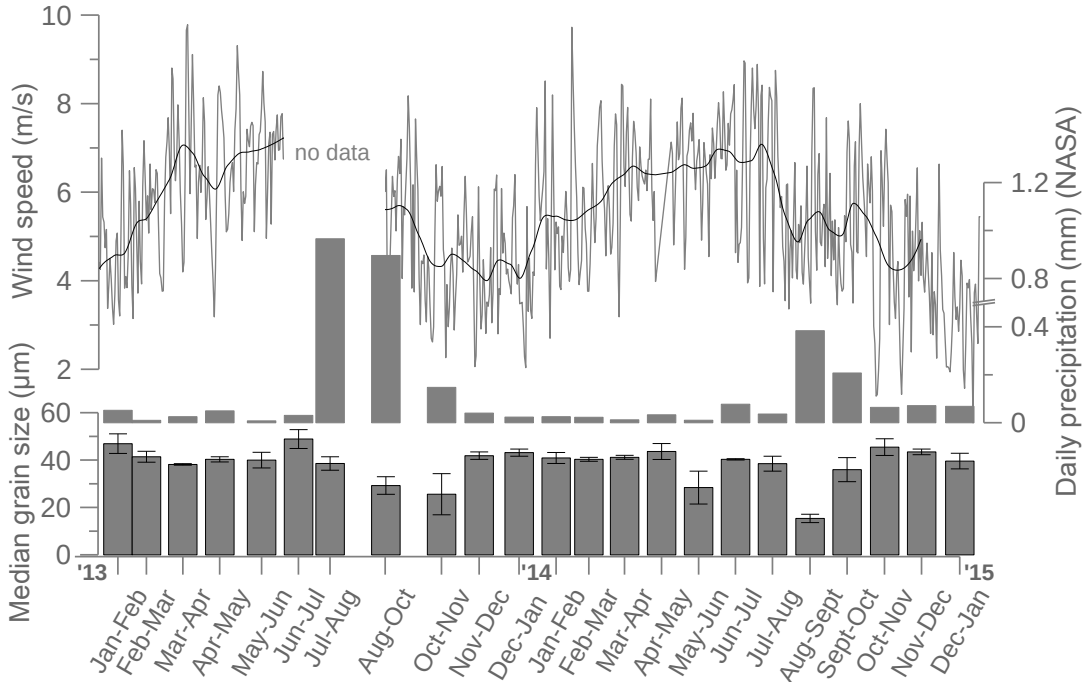

Figure 16. Median grain size (µm) per sampling month. Bottles at 90 and 140 cm have been left out. Error bars depict relative standard deviation. Average daily precipitation and wind speed with a local regression smoothing line were added.

3.2d. Chemical analyses

This section shows the elemental composition of low-level transported Saharan mineral dust. Two complementary methods, ED-XRF and SEM-EDS, were used to determine chemistry of all samples and an estimate of mineralogical composition respectively.

ED-XRF

Results from ED-XRF measurements were plotted as log (element A/element B). Using log ratios, an n-fold change in element A results in the same magnitude of change of the log ratio as an n-fold change in element B, independent of the abundance of A relative to B, making them better suited for evaluation of the chemistry of the samples than regular ratios (Rick Hennekam, personal communication, 15-5-2015). The two major elements Si and Al were plotted as an initial indication of variability in elemental composition of the dust. Presumably, aluminium was enriched in the fine fraction relative to silicon. Such a correlation was observed in the majority of the record except January-February, October-November and November-December of 2013. Only modal grain size correlated significantly to Al/Si ($r = -0.50$, $p < 0.05$), whereas mean and median grain size did not correlate significantly (fig. 17).

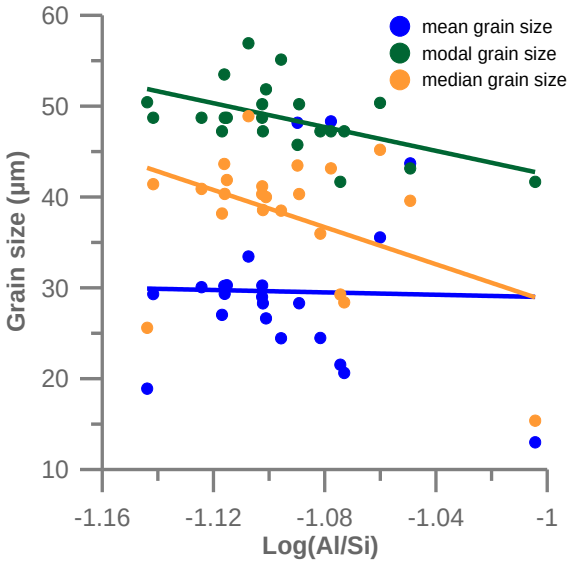

Figure 17. The relationship between grain size variables and logarithmic alumium/silicon ratio with linear fits.

Elements of interest were plotted both as x/Si and x/Al ratios; x being the studied element. The amount of dust in October-November was insufficient for XRF measurement. Bottles at 90 and 140 cm were removed from the analysis due to deviating characteristics of this dust (see discussion). The 240 cm sample of June-July 2014 was removed because it showed extremely high counts for several elements, especially zinc (1.5 times the average) and copper (thrice the average) (fig. 19). The important trace metal nutrients iron, manganese, zinc, copper and nickel (Formenti et al., 2003; Sunda, 2013) were measured. Cobalt was not included in the XRF spectrum analysis because it overlapped with iron. The measured trace metal nutrients are shown in figure 19. Copper and zinc ratios of the omitted sample are also shown. Observed patterns will be described following the order of the graphs from the bottom up. Iron ratios tracked Al/Si ratio very consistently and displayed pronounced peaks in May-June and August September 2014. These peaks were also observed in the other trace metal nutrients. Furthermore, iron ratios showed a broad, unpronounced peak around late summer and fall of 2013 similar to Al/Si. Another characteristic feature was higher concentrations in January-February 2013 and December-January 2014-2015. Nickel did not show clear resemblance to other trace metal nutrients and lacked the pronounced August-September 2014

peak. The strong lows at the beginning and end of our measurement period were similar to those observed in calcium ratios (fig. 21). Manganese ratios were similar to iron, but variability between measurements was large and hence the timing of the peaks was inconclusive. The copper pattern was relatively similar to that of iron and displayed an additional peak in January-February 2014, which also occurred in Ni/Al and to a lesser extent in iron. Zinc showed similar trends but an additional peak was observed in December 2013-January 2014. In short, most trace metal nutrients displayed a pronounced peak in May-June and August-September 2014 and a less pronounced one around late summer and fall of 2013. The peak of May-June 2014 only corresponded to low grain size whereas late summer and fall of 2013 and August-September of 2014 coincided with low grain size and high satellite-estimated precipitation. Two-tailed Pearson's correlation tests showed correlation between several trace metal ratios and grain size. Of the different grain-size characteristics, the median correlates strongest to the ratios. Significant correlations are shown in table 6 and an example is shown in figure 18.

Table 6. Significant ($p < 0.05$) and highly significant ($p < 0.01$) correlations between median grain size and several trace metals. Note that negative correlation coefficients imply increasing ratios with decreasing median grain size.

Ratio	Correlation coefficient (r) with median grain size	p-value
Fe/Si	-0.57	< 0.01
Fe/Al	-0.63	< 0.01
Mn/Si	-0.48	< 0.05
Zn/Si	-0.46	< 0.05
Cu/Si	-0.58	< 0.01
Cu/Al	-0.51	< 0.05
Ni/Si	-0.46	< 0.05

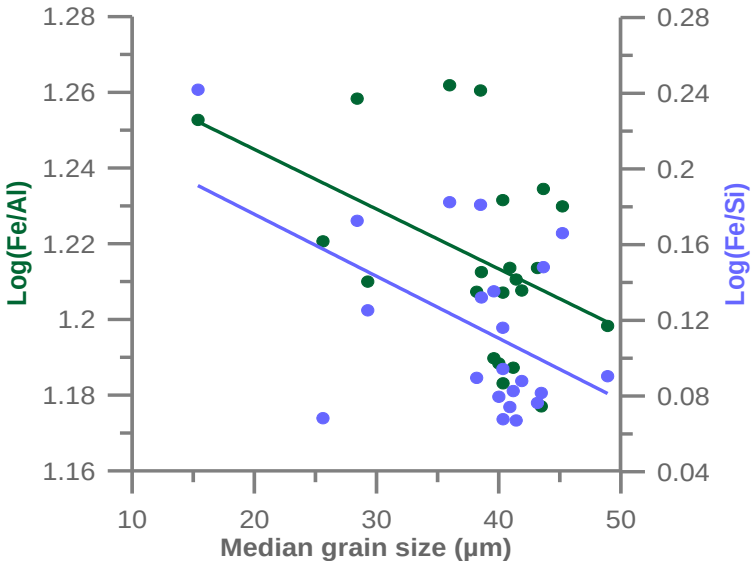

Figure 18. The relationship of logarithmic iron over aluminium and iron over silicon ratios with median grain size is clearly negative.

Al/Si was a predictor of trace metal content as well. It showed significant correlations with: Fe/Si, Fe/Al, Mn/Si, Zn/Si and Cu/Si. There was a strong covariance between the trace metals. The term "convincing correlation" was used here when both the x/Al and x/Si ratio of an element correlated significantly to both the x/Al and x/Si ratio of the other element. This was done to ensure that covariance was not based on trends in aluminium or silicon but rather on mutual trends in the two trace metals. Strongest covariance was observed between nickel and copper: the four possible combinations of the x/Al and x/Si ratios all correlated highly significantly ($p < 0.01$). Strong covariance was also found between iron, zinc and copper. Of the twelve possible correlations, five correlated highly significantly and seven significantly. Nickel nor manganese showed convincing correlation to any of the other trace metals.

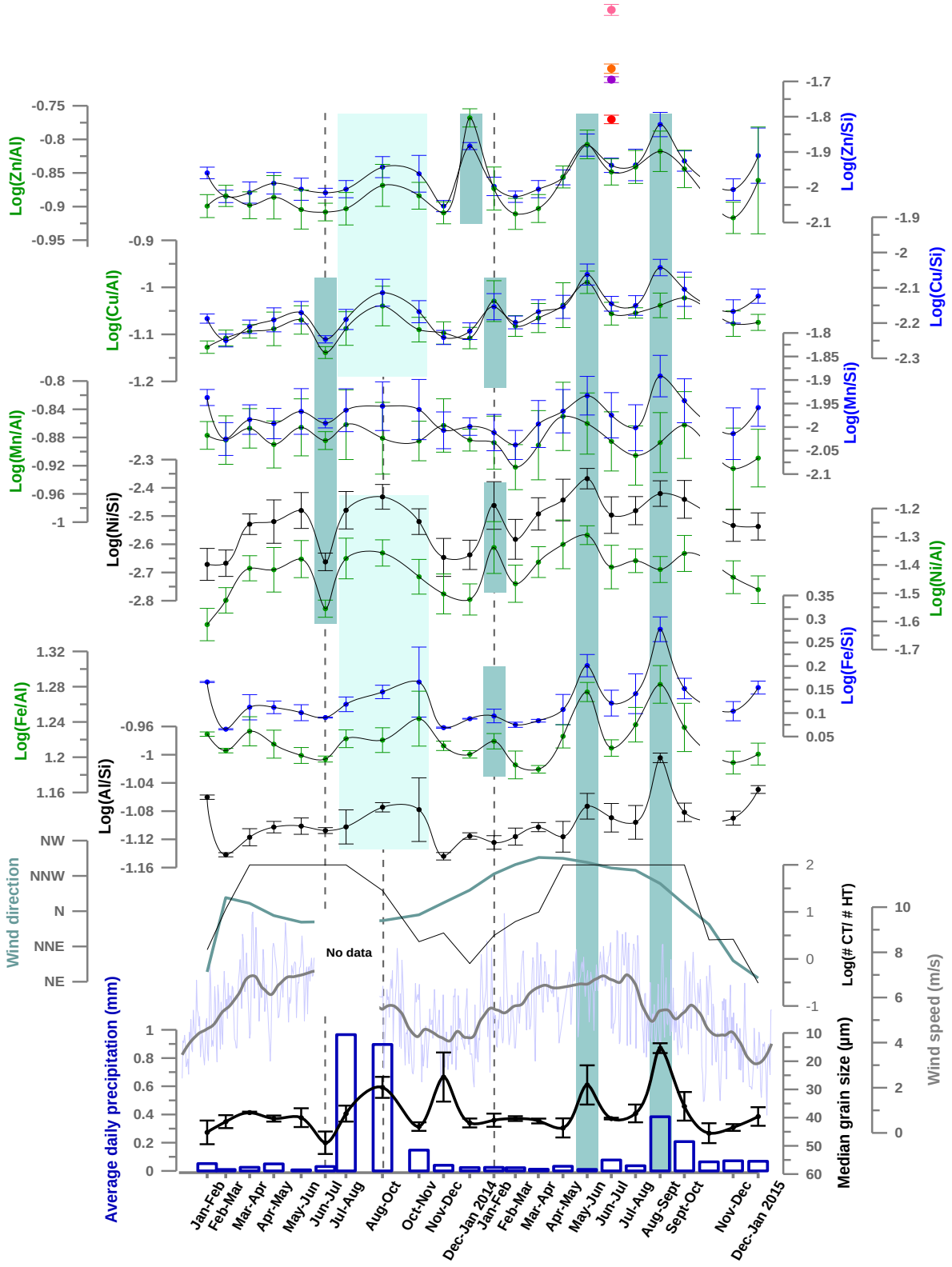

Figure 19. Plot of trace metal nutrient content relative to aluminium and silicon. Logarithmic aluminium over silicon ratio is shown for comparison. Variables that possibly explain shifts in nutrient content were added. These include: Vector averaged wind direction per sampling month, which can be compared to a logarithmic index of the number of coastal trade wind trajectories (north or northwest, CT) divided by the number of Harmattan trajectories (northeast or east, HT) (A logarithmic scale was used for convenient comparison to the vector averaged wind direction). An arbitrary value of 2 was assigned to months without Harmattan winds. Wind speed data are shown in blue, with a local regression smoothing line in grey. The blue bar graph depicts sampling month averaged daily precipitation. Grain size is shown with reversed y-axis so that the peaks (fine-grained) align with peaks in Al/Si. Copper and zinc ratios of the omitted sample 2_3B_201406 are also shown. Red: Cu/Si, orange: Cu/Al, purple: Zn/Si and pink: Zn/Al.

Calcium content may be used to infer the source area of dust (Scheuvens et al., 2013). It showed a very different trend than the trace metals, with pronounced lows at the beginning of 2013 and the end of 2014 (fig. 21). The trend in calcium subtly resembled wind direction, with higher wind speed or more northern/western wind direction corresponding to higher relative concentrations of calcium. Indeed, Ca/Fe correlated highly significantly to vector averaged wind direction ($r = -0.713$, $p < 0.01$), the minus sign implying higher calcium concentration in dust from the north than from the (north)east (fig. 20). The aforementioned peaks in trace metal content and Al/Si of May-June and August-September 2014 and the broad peak centred at Augustus-October 2013 seemed to be super-positioned on the general Ca/Fe trend (fig. 19 & 21).

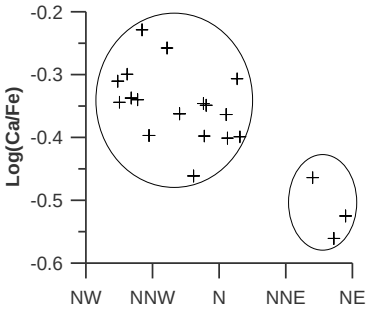

Figure 20. Scatterplot of logarithmic Ca/Fe ratio versus average wind direction.

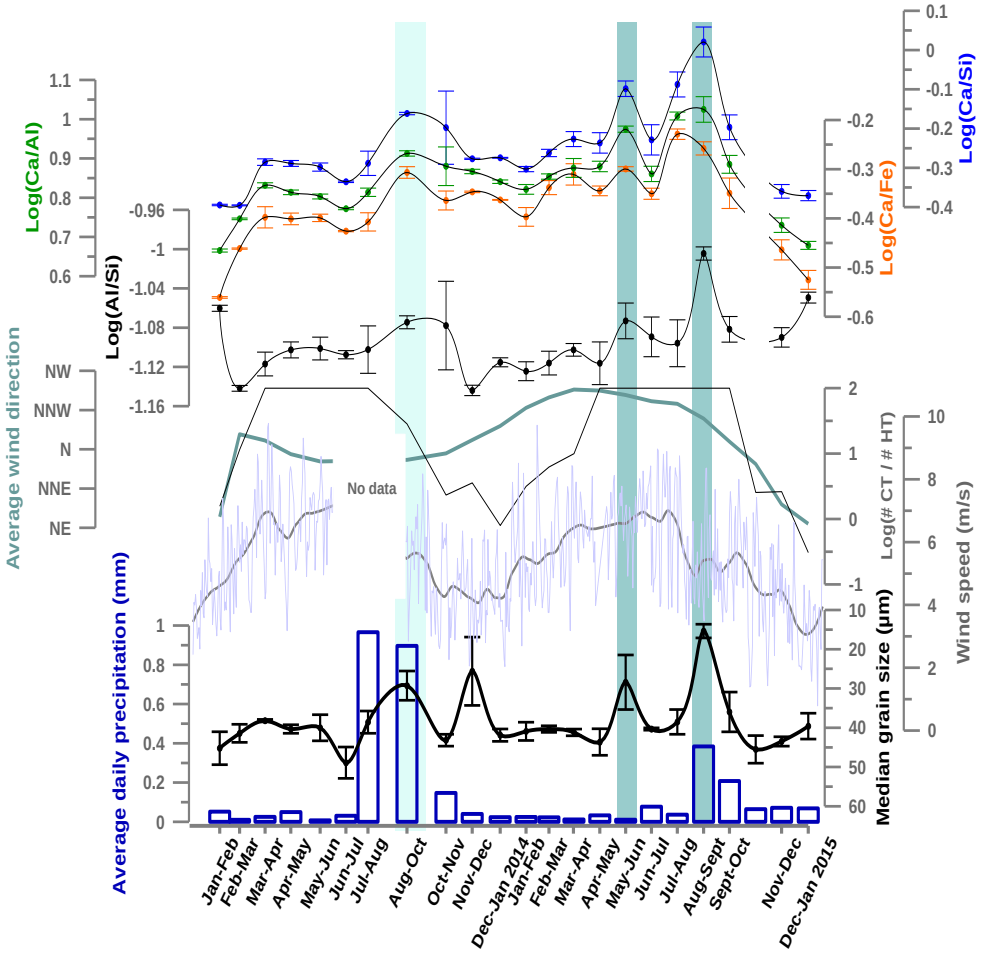

Figure 21. Plot of calcium content relative to aluminium and silicon. Logarithmic aluminium over silicon ratio is shown for comparison. Meteorological variables are the same as in figure 19 except wind speed.

Chemistry of individual particles using energy-dispersive X-ray spectroscopy (EDS) capabilities of the scanning electron microscope (SEM)

Samples for SEM-EDS analysis were selected based on results of the XRF analysis. Two chemically different winter or spring months and two summer months were selected. December 2014- January 2015 was selected for its extremely low calcium over iron ratio and low metal over silicon ratios. It was compared to April-May 2013 because this month showed regular chemistry, mass and grain size. The bimodal sample July-August 2014 was selected because it displayed exceptionally low median grain size and high metal over silicon ratios. Part of the sample was sieved over a 20 µm sieve to separate the finer from the coarser mode for separate analysis. Visual inspection of the samples using the SEM revealed an abundance of aggregates, both large and angular as well as smaller and rounded (fig. 22A&B). Individual particles were mainly angular to sub-rounded (fig. 22C, G&H). The dust samples seemed to consist almost entirely of mineral dust. Incidentally pieces of insect were observed (fig. 22C). Exogenic growth of salts on dust minerals was also observed (fig. 22D). The largest individual particles were micas (fig. 22E). Two diatoms were observed in sample December-January 2015 (fig. 22F). They were most likely freshwater diatoms of the family *Aulacoseiraceae*.

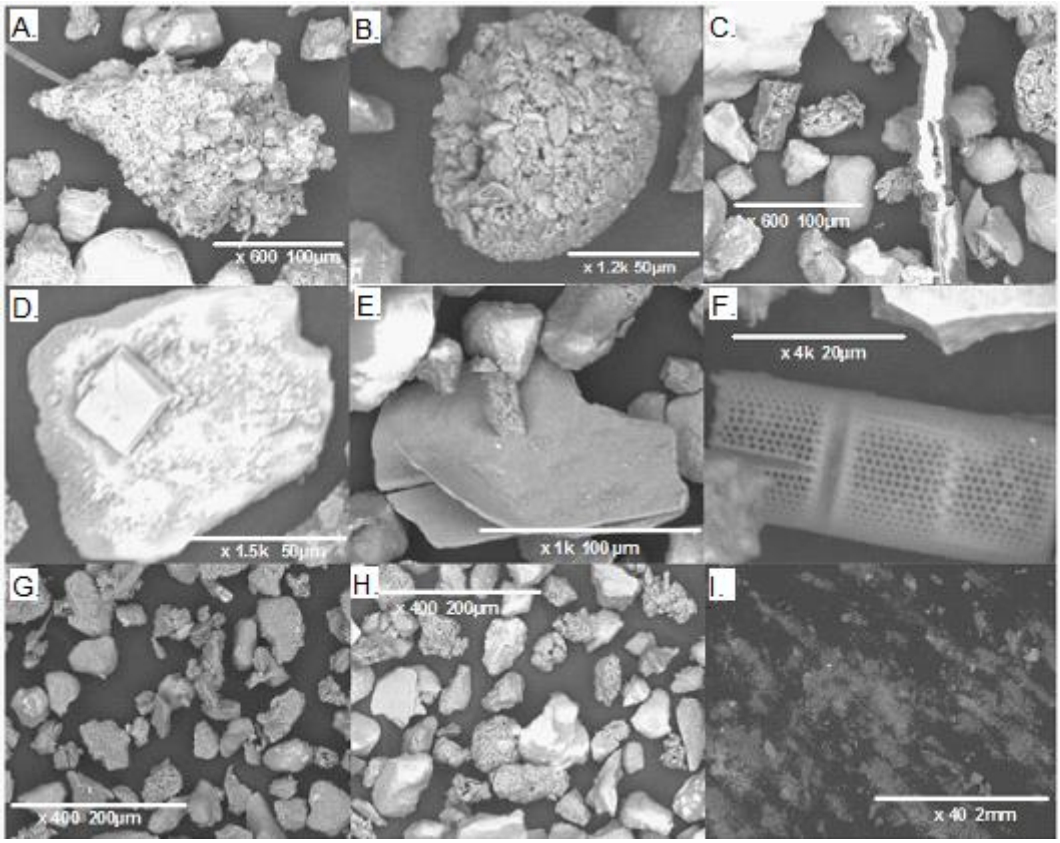

Figure 22. A. Large angular aggregate, presumably formed within the bottle (August-September 2014). B. Rounded aggregate, presumably formed at source area or during transport (August-September 2014). C. Insect's leg (August-September 2014). D. Exogenic growth of NaCl on a dust particle (August-September 2014). E. Mica mineral (December 2014-January 2015). F. Diatom, presumably a member of the Aulacoseiraceae family (December 2014-January 2015). G&H. Two of the frames analysed (August-September 2014 & April-May 2013). I. Overview of the fine fraction sample of August-September 2014.

Chemical analysis of individual particles showed alluminosilicates, silicates (hereafter quartz) and iron bearing alluminosilicates to be the main components of our dust samples (fig. 23). Individual samples could be compared to April-May 2013 because this sample displayed average XRF chemistry, mass and grain size. Equal to the XRF results, August-September 2014 differed most from the reference sample. Mica's were significantly more abundant and quartz and iron bearing alluminosilicates were

less abundant (fig. 23). June-July 2013 was significantly lower in calcite. December-January 2014-2015 was relatively similar to April-May 2013. Particles that were moved to the "ambiguous" class generally showed high iron and high silicon counts. Due to the high occurrence of both elements, these particles did not satisfy the criteria for iron oxides nor silicates. Possibly, these particles consisted of a quartz grain with an iron oxide crust or alternatively certain amphiboles that do not contain aluminium, such as anthophyllite $(Mg,Fe)_7Si_8O_{22}(OH)_2$. As mentioned in the methods section, iron counts of an iron coated particle should be relatively high since the SEM only penetrates to a few µm.

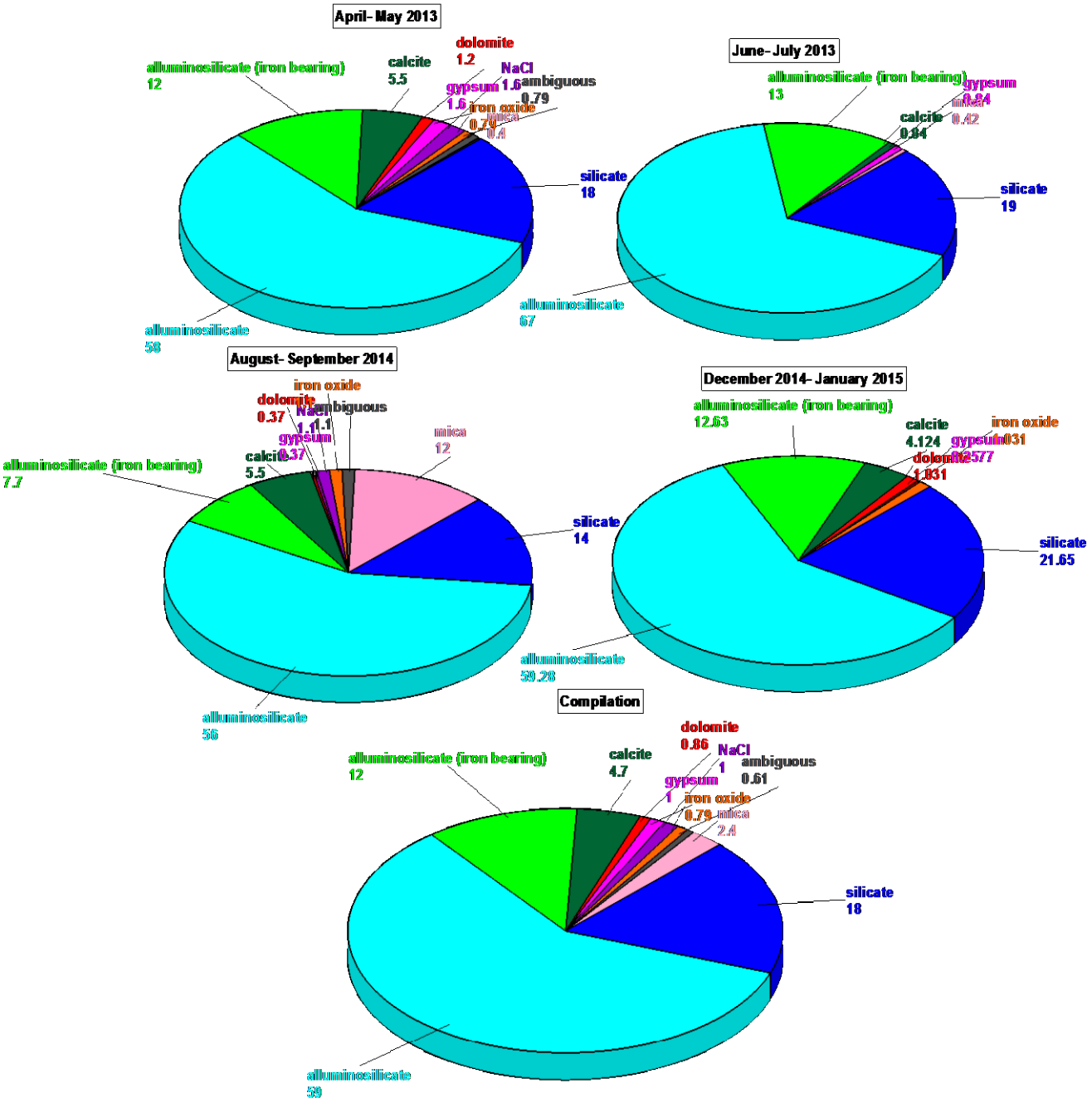

Figure 23. Pie charts showing the relative abundance of mineral classes. Inputs to the compilation were corrected for the mass flux and the total number of grains analysed. Light blue: alluminosilicate; green: alluminosilicate (iron bearing); dark green: calcite; red: dolomite; pink: gypsum; purple: NaCl; orange: iron oxide; grey: ambiguous; salmon pink: mica; dark blue: silicate.

4. Discussion

The current study aimed to improve knowledge of fertilisation and ballasting by Saharan dust. The research consisted of two main sections. First, it focussed on ballasting and fertilisation by a dust event. The research questions were: Does a dust event lead to increased production of organic matter? Can we prove the ballasting hypothesis? In the second part, Mauritanian dust samples were studied to investigate variability in dust flux and characteristics that may influence its fertilisation and ballasting potential. Three questions were central to this work: What are the seasonal trends in flux, chemical and physical characteristics of low-level transported Saharan dust? What may be the influence of these shifts in dust transport and characteristics on phytoplankton production and ballasting? Can we define possible source areas of the dust samples?

Mineral dust is seen as an important source of nutrients for phytoplankton in the open ocean. These dust-supplied nutrients include silicon and the important trace metals iron, manganese, zinc, copper and nickel (Formenti et al., 2003; Sunda, 2013). In meso- and eutrophic waters, as well as under bloom conditions, diatoms tend to dominate. Diatoms require silicon to grow their frustules, but also have higher iron requirements than most phytoplankton (DiTullio et al., 1993). Thus, dust-supplied silicon and iron (and other trace metals) may alleviate nutrient stress and enhance primary productivity in these waters. Indeed, iron or dust enrichment in the oligotrophic open ocean usually results in a community shift from picoplankton (mainly cyanobacteria) to diatom dominated (Chavez et al., 1991; Coale et al., 2002; Duarte et al., 2000). Another cause for iron limitation is nitrogen fixation. This process is very important in the oligotrophic North Atlantic and up to 50 percent of the export production may be supported by nitrogen fixation (Grüber and Sarmiento, 1997). Nitrogen fixers have high iron requirements (Kustka et al., 2002) such that iron may be the ultimate limiting nutrient in oligotrophic waters. Iron and phosphorus were shown to co-limit nitrogen fixation in the oligotrophic North Atlantic (Mills et al., 2004). The above illustrates the major impacts dust may have on the biosphere and carbon cycle of the equatorial North Atlantic and thus why it is important to study the characteristics and the quantity of dust supplied to this area, as well as to investigate the effects of natural dust seedings.

4.1. Evidence from drifting trap and gel trap samples

Before expatiating upon the observed trends in POC, PON and C/N ratios, it is important to consider the validity of the drifting trap methodology and the CN analysis. A decline in POC and PON flux with depth was observed at M1, M2, M4b and M5 (fig. 10). Such a pattern was expected and corresponds to biological remineralisation and solubilisation. In contrast, initial measurements of M3 showed a strong increase from 100 to 200 m depth. M4a showed a decrease from 100 to 200 m and a spectacular increase at 400 m to values significantly higher than observed at M1. Such high values were unexpected for this oligotrophic location. Visually, the filters of the M1 drifting trap were greener and seemed to contain significantly more OM than those of M4a. Furthermore, odd values were also observed in the C/N ratios, especially for M3 400 which showed extremely high C/N ratio compared to the other stations (fig. 11). For this reason, duplicate measurements were made of M3 and M4a. The duplicates showed attenuation with depth and a low flux which tallied more with the expectations for these oligotrophic stations. The difference between the first and secondary measurements casts doubt on the validity of the C/N analysis as performed in the current study. There may be several reasons for the foreign results of the first CN analyses: first, it was decided to use bulk OM for CN analysis. Accordingly, zooplankton was not removed before analysis. A possible drawback is that a single large zooplankton may exert great influence on the amount of POC, PON and the POC to PON ratio. If one filter cut coincidentally contained more zooplankton than the other

this may have caused different total C and N, as well as different C to N ratios. A second possibility is contamination of the samples during preparation for the analysis. However, the gel traps provide validation of the C/N analysis.

When the secondary C/N measurements of M3 and M4a are used, the east-west trend corresponds to the east-west trend in particle flux as observed in the gel traps. This trend is a high flux at M1, a decline westward and an increase again at M5, close to the Caribbean. This trend agrees with the year round pattern of surface production as indicated by chlorophyll (fig. 24). Year-round, chlorophyll concentrations are highest near the North-West African coast and diminish towards the west. They are lowest between approximately 40 and 50 degrees west, where the transect borders the north Atlantic oligotrophic gyre. From there it increases towards the Caribbean but remains significantly lower than in the eastern equatorial Atlantic (Antoine et al., 1996; Feldman and mcClain, 2014). This agrees with the high flux at M1, the minimum at M4 (49° W) and an increase at M5 albeit lower than M1. Antoine et al. showed approximately 1.5 to 2 times larger surface productivity at M1 whereas the current study found more than 3 times larger fluxes at M1 100. Coastal upwelling, which causes high productivity off the north-west African coast, is unlikely to be responsible for the high flux at M1 as horizontal filaments of cold, nutrient-rich upwelling waters have a maximum range up to approximately 19 degrees west (Kostianoy and Zatsepin, 1995). Because a dust storm occurred during deployment of the M1 drifting trap, a likely scenario is that Saharan dust supplied the necessary nutrients to trigger a bloom and the dust to ballast OM, thus enhancing the POC flux. First, possible nutrient supply by Saharan dust will be discussed. The dust storm passed RV. Pelagia from the 11th to the 15th of January and was recorded by on-board dust samplers. Maximum dust flux was measured on the 12th and 13th of January (bachelor project Katarina Wetterauer, 2015); (fig. 25). The event coincided with deployment of the M1 drifting trap, which was deployed at the 13th and recovered the 14th.

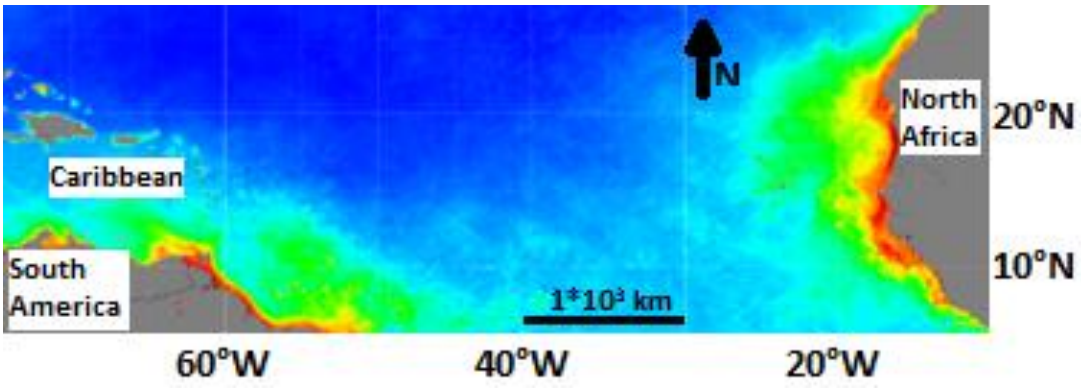

Figure 24. Annual composite of chlorophyll concentration for the equatorial North Atlantic. Dataset: NPP VIIRS chlorophyll concentration with OCI algorithm. Adapted from Feldman and mcClain (2014).

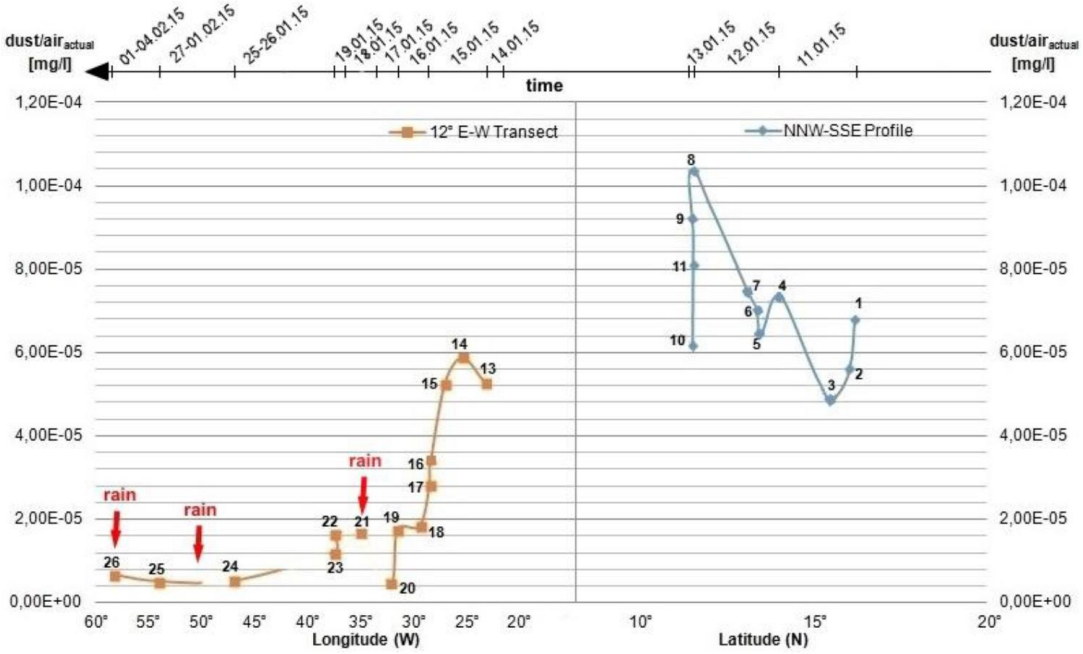

Figure 25. Dust concentration in mg/l along the first leg of the cruise (NNW-SSE from the Cape Verde islands) in blue and along the 12°N transect in orange. Time proceeds from right to left on the top axis. The marks for rain are based on the cruise observations. Adopted from the report of K. Wetterauer, 2015.

A time lag exists between dust addition and phytoplankton response of 2-3 days (Bressac et al., 2013) or 4-8 days (Duarte et al., 2000). In contrast, ballasting may commence immediately (Bressac et al., 2013). Thus, the large carbon and nitrogen flux at M1 may indeed have been caused by (combination of) dust fertilisation and ballasting. In the oligotrophic open ocean, iron or dust enrichment usually results in a community shift from picoplankton (mainly cyanobacteria) to diatom dominated (Chavez et al., 1991; Coale et al., 2002; Duarte et al., 2000) and diatoms are usually limited by silicon (Franz et al, 2012) or iron and are more strongly iron limited than other autotrophs (DiTullio et al., 1993). Saharan dust may supply both these nutrients. The main cyanobacteria prochlorococcus and synechococcus show cellular C/N ratios of 5.7 and 5.4 respectively under P replete conditions and 7.4 and 7.5 respectively under P-limited conditions (Bertilsson et al., 2003). As the p requirement of these cyanobacteria is very low, the ratios most likely tend to the lower end of this spectrum even in open ocean waters (Bertilsson et al., 2003). Trichodesmium in the tropical Atlantic shows a C/N around 5.4 (Sañudo-Wilhelmy et al., 2001). In contrast to these cyanobacteria, diatoms show an average C/N ratio of 8.6 (Brzezinski., 1985). Thus, C/N ratios at M1 suggest a diatom bloom: M1 showed a significantly higher C/N ratio (8.05) than the other stations (5.64 – 6.85).

In contrast to nutrient addition, ballasting by dust presumably operates immediately when dust enters the upper water column and stops soon after the dust storm has passed. Dust is not the only mineral that is reported to have ballasting potential: diatom frustules and calcium carbonate shells were also observed to ballast OM (de la Rocha et al., 2008). Thus, a possible community shift from picoplankton to diatom dominated is itself a factor that may contribute to an increase in settling velocity of the OM and this type of ballasting may last as long as larger phytoplankton is abundant. Three analyses of the current study may provide clues on possible ballasting at M1: the vertical trends in POC and PON flux, the vertical trends in C/N ratio and the gel traps. The vertical trends in POC were especially useful because they could be compared to extensive POC flux datasets. POC profiles from previous work may be used to estimate the efficiency of the downward POC flux, in other words, the steepness of the slope. The flux at 1000 m is used here as an estimate of POC flux to the deep sea. Figure 26 shows a comparison between the DUSTTRAFFIC POC fluxes and datasets

from (a). the oligotrophic subtropical gyre near Hawai and the high-nutrient northwest pacific subarctic gyre (Buesseler et al., 2007) and (b). the Arabian Sea (Lee et al., 1998). The graph shows the best matches with POC flux profiles of the current study. Furthermore, appendix 3 shows a comparison between DUSTTRAFFIC and the northeast Pacific (Martin et al., 1987). Results from the current study were plotted over a graph copied from the article because no raw data were available. All graphs were plotted using power law fits (Martin et al., 1987).

The POC flux observed at M1 does not support the ballasting hypothesis. Not only was the attenuation at M1 considerably larger than the attenuation at the other stations, it was also larger than any of the profiles in any of the three studies to which it was compared. It most likely tends to the least efficient match, which attenuates to approximately 0.4 mmol C/m^2/day at 1000m (fig. 26). The trend at M2 is almost identical to two profiles in the Arabian Sea and one in the northeast pacific. The two Arabian Sea profiles converge to approximately 0.8 mmol C/m^2/day at 1000m (fig. 26). The trends at M3, M4a and M4b were comparable. They displayed weaker attenuation than profiles from the other studies with comparable flux at 100 m. Thus, it seems these sites harboured relatively efficient export of OM. Extrapolating their trend downwards it was estimated that they attenuated to a flux at 1000 m between their least attenuated match and the matches of M2, so between 0.4 and 0.8 mmol C/m^2/day (fig. 26). M5 is more difficult to put into perspective because it showed no attenuation between 100 and 200 m depth which makes its power law fit less accurate. A comparison between M5 and the flux profiles of previous studies tells us that the attenuation at M5 was exceptionally low. This is suggestive of some form of efficient OM export and maybe ballasting. Only the steepest profile with comparable flux at 100 m is similar to M5 and shows 1.4 mmol C/m2/day at 1000 m (fig. 26).

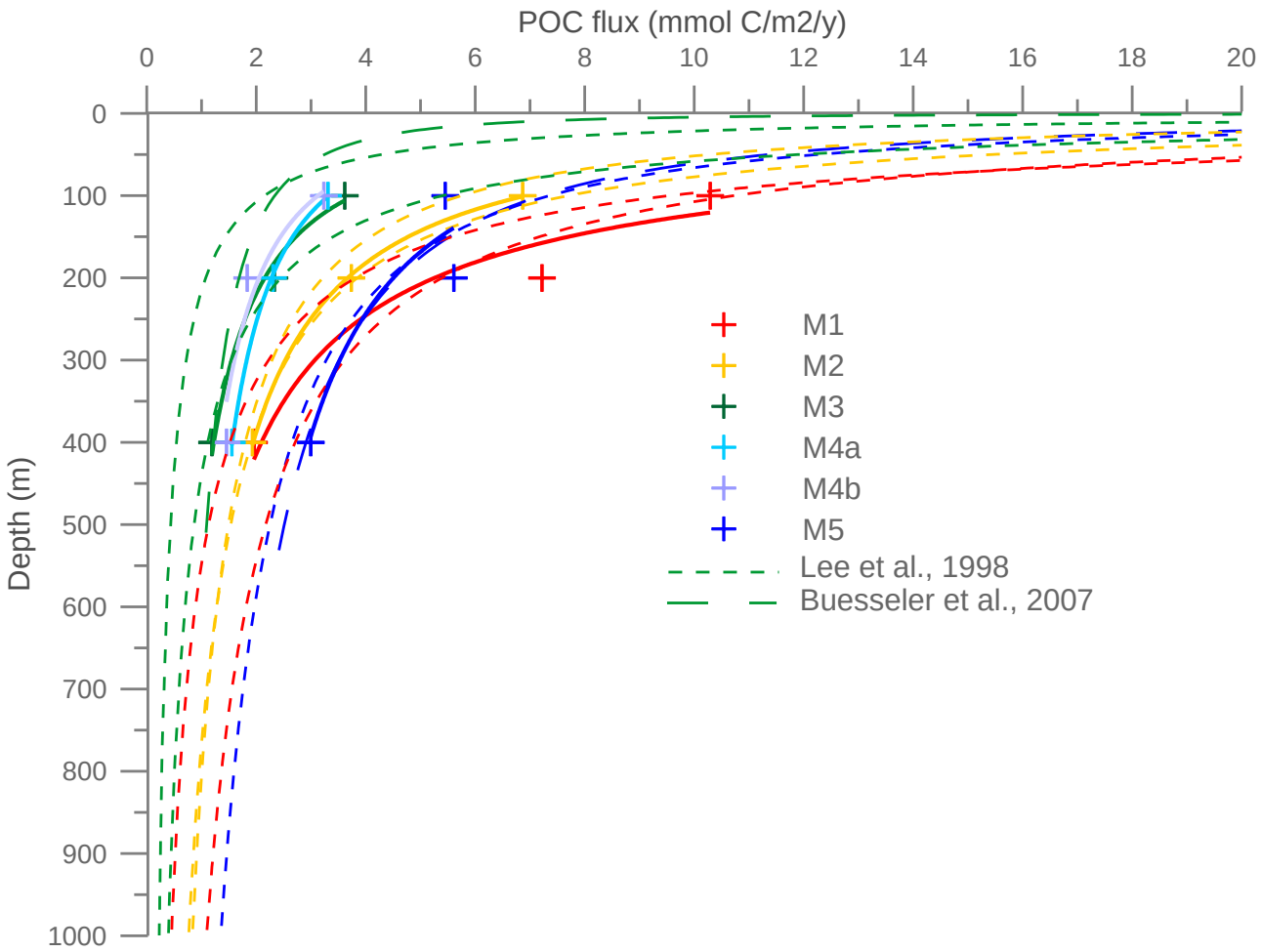

Figure 26. A comparison between DUSTTRAFFIC, Buesseler et al., 2007 and Lee et al., 1998. From the datasets, profiles were selected that resemble DUSTTRAFFIC fluxes the best. Matching profiles are shown in the same colour as the DUSTTRAFFIC station. Power law fits were used for both the DUSTTRAFFIC and the external datasets. Note that M1 400 is hidden underneath the M2 400 data point.

C/N ratios may also provide information on possible ballasting at M1. Nitrogen compounds like proteins are generally more labile and degrade quicker than carbon compounds resulting in increasing C/N ratios with depth if OM settles with low velocity. Such a trend was observed at M2, M4b and M5. In contrast to M4b, M4a displayed substantial decrease in C/N from 200 to 400 m. It is unclear why this decrease was present. Conceptually, ballasting increases settling velocity, hence decreases residence time of organic matter in the upper water column leading to less degradation and hence a C/N profile which shows little change with depth. Such a profile was observed at M1, but also in the second measurement of M3. Ballasting by dust is unlikely at M3 since only background dust concentrations were present during deployment (bachelor project Katarina Wetterauer, 2015). The major difference between the first and second measurement of M3 casts doubt on the validity of the observed C/N ratios but this does not tell us whether the measurement of M1 is reliable since this sample was not re-measured. Also of interest is the difference between M4a and M4b (fig. 11). These traps were deployed at the same location with only 35 hours in between the deployments. The C/N values, as well as the depth profile of C/N are markedly different. This deviation is unlikely to be caused by an error in the C/N measurement itself (the reported precision of the C/N analysis (0.3%) is negligible) so must derive from either an actual difference in the OM that was measured or contamination of the samples or degradation of OM in the samples during the filtering process. Possibly, the small amounts of OM captured on a filter are not enough to accurately describe bulk OM characteristics in the water column (fig. 27).

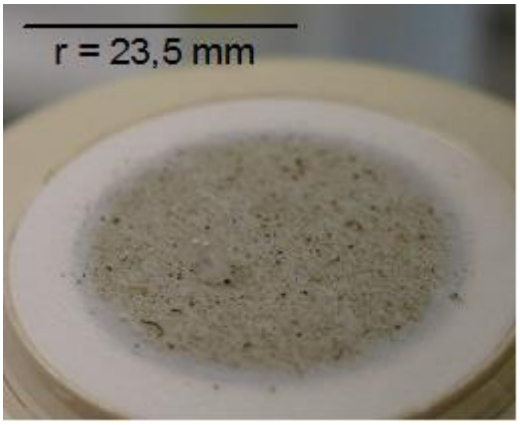

Figure 27. GFF filter (47 mm diameter) with settling matter caught in the tube.

Gel traps provided a third possibility to study possible ballasting at M1. M1 100 and M1 200 developed an impenetrable top layer during deployment and thus could not be used. The reason is probably a reaction between borax salt ($Na_2[B_4O_5(OH)_4]\cdot 8H_2O$) that was used to densify the water in the trap and the medical tissue gel. For no apparent reason M1 400 was clear. All subsequent traps were densified using sea salt (NaCl) which solved the problem. It was postulated that the penetration depth of particles in the gel is related to their settling velocity in the water column. Large marine snow, zooplankton, faecal pellets, foraminiferal tests and miniscule shells all sank to the bottom of the gel. Most finer material, which appeared to be fine marine snow, sank approximately halfway into the gel. This indicates that larger marine snow settles at higher velocity than fine marine snow and hence will undergo less degradation during settling. This observation corresponds to a study from Iversen et al. (2010), who also found higher settling velocities for larger marine snow.

A comparison between the sampling stations, in other words, the longitudinal trend, could only be done for 400 m because M1 100 and 200 were not usable. Interestingly, the trend in rough amounts of OM in the gels was very similar to the longitudinal trend in POC and PON flux at 400 m: high at M1 and M5 and lower in between. Thus, this observation supports the trends that were observed in the results from the C&N analysis. Marine snow made up almost all the material in the M5 trap. The marine snow was also larger at M5 compared to the other stations. What caused the apparently very efficient ballasting (least attenuation of POC flux) and aggregation processes (large marine snow flocks) at M5 is unclear. The abundance of foraminiferal tests at M2 may be explained by a foraminifera bloom. This would help explain why M2 showed such a high OM flux relative to M3 which was deployed only one day later (fig. 10). The foraminiferal tests were not associated with aggregates or visible amounts of OM and thus seem a poor ballasting material. This corresponds to the study of de la Rocha et al. (2007), which found weaker correlation between POC and foraminiferal calcium carbonate flux than between POC and coccolith calcium carbonate flux. Because only one gel was available from M1, it was not possible to observe a vertical trend at M1. Interestingly, the amount of organic matter and marine snow declined at M2, M3 and M4 but not at M5. Here, there was not much difference between 100 and 400 m. M2 contained the highest number of faecal pellets. The number of faecal pellets did not seem to decline with depth, indicating faecal pellets are probably a very efficient pathway to bring organic matter to the deep sea. This observation corresponds to literature (Ploug et al., 2008).

Assembling evidence from the POC and PON flux, the C/N ratio and the gel traps, the case for ballasting by dust at M1 remains unsolved. POC and PON fluxes were actually attenuated at an exceptional rate. This does not tally with ballasting. However, C/N ratios of the M1 trap do correspond to high settling velocity and ballasting. An alternative explanation for this strong attenuation has to do with the timing of the dust event relative to the deployment of M1. Due to the

time lag between dust addition and the biological response, new production probably just started to increase at the time M1 was deployed. As production was continuously growing the downward flux of organic matter, sped up by ballasting, was also growing. An increased export production was first noticed at 100 m and one to three days later at 200 and 400 m since most marine particles settle at approximately 100 m/day or more (Buesseler et al., 2007). Besides M1, station M5 also shows indications of ballasting. Again, the three indices of ballasting do not agree. POC and PON fluxes displayed very weak attenuation and correspondingly, the amount of material in the M5 400 gel was approximately the same as in M5 100, while the other stations showed a decline in the amount of material in the gel traps. In contrast, C/N ratio showed a steady incline with depth which does not correspond to a high settling velocity of OM. Gel traps do support ballasting at M5. They contained a different type of OM and almost all of the OM was aggregated into large marine snow. The marine snow did not contain ballasting materials that were large enough to observe with the camera. It may be that the type of organic matter occurring at M5 is more prone to aggregation or that smaller ballast minerals are responsible for the large aggregates and weak attenuation of the POC and PON flux.

4.2. Mauritanian dust samples

Dust analysed in the current study represents low-layer transported dust almost at the start of its journey over the Atlantic Ocean and before any depositional losses to the ocean. To appreciate the results of the current study, it is important to estimate the significance of dust transported in the trade winds air layer (TWAL) relative to the other main dust transport path: the Saharan air layer (SAL). The TWAL transports dust to the Atlantic year-round (Liu et al, 2008). In winter there is no Saharan air layer and hence the TWAL accounts for all dust transport to the Atlantic (Stuut et al., 2005). The TWAL transports significant amounts of dust as far as 30-40 degrees west (Liu et al., 2008). In summer TWAL transported dust decreases due to weakening of the trade winds and no significant amounts are transported further than 20 degrees west (Chiapello et al., 1995; Liu et al., 2008). SAL transport is at its peak in summer and transports significant amounts of dust across the Atlantic (Prospero et al., 1987). It is also important to know whether the sampling station lies in the zone of maximum dust transport. There is a seasonal latitudinal shift of the zone of maximum dust transport: averaged over the atmospheric column it shifts from 5° N in winter to 20° N in summer over the Atlantic (Moulin et al., 1997). Height resolved profiles of dust occurrence give an indication of the location of the sampling station relative to the zone of maximum dust transport (fig. 28). These profiles were taken east from the sampling station (10°W to 15°E) and hence one should bear in mind that the zone of maximum dust transport is actually located further south once the dust reaches the longitude of the sampling station (16°W). Judging from the dust profiles near ground level, the sampling station lies within the zone of maximum dust transport in summer and winter and near that zone in spring and fall (Liu et al., 2008). However, close to ground level and over North Africa, the winter zone of maximum dust transport is wide and thus Iwik lies in the zone of maximum dust transport in summer and winter and very close to this zone in spring and fall (Liu et al., 2008).

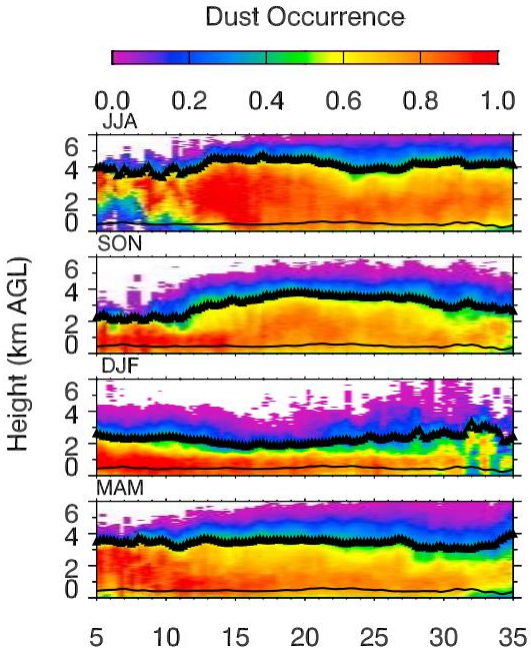

Figure 28. Adopted from Liu et al., 2008. Latitudinal dust occurrence profile from 5 to 35°N, longitudinally averaged from 10°W to 15°E. Dust occurrence is based on the percentage of time in a given period that a data point between the dust layer top and base with 1064 nm attenuated backscattering coefficient is larger than 0.0004/km/sr. (sr = steradian, a unit of the angle in 3-D space). Months are given in letters, e.g. JJA is June, July and August.

The major caveat in the current study is presence of locally produced dust which is not representative for the average characteristics of TWAL transported dust. Indications of locally produced dust were found in higher mass, coarser grain size and different chemistry in the lower bottles (appendix 6). As an example, figure 29 shows mass at the different sampling heights relative to the mean mass of a sampling month. The trend reminds of exponential decay and seems to level off with height, presumably becoming more representative of TWAL dust flux. Therefore, the upper three bottles, which are relatively equal in mass, grain size and chemistry were used in the current study as a representation of TWAL dust characteristics. An average of the upper three heights was preferred over using the highest bottle alone because this would introduce a larger error if one of the bottles did not sample properly. However, the upper three bottles may still contain local dust. Presuming that the ratio of local to non-local dust (not necessarily true) and the composition of local dust (likely) remain constant, trends in flux, grain size and chemistry of the bottles should remain informative about these characteristics of TWAL dust. Local dust in the lowest bottle has not been transported into the bottles by saltation as the lowest bottle of the MWAC sampler (90 cm above ground level) exceeds the maximum height of the saltation layer of approximately 60 cm (Dong and Qian, 2006). Hence, the difference between the lowest one or two bottles and the higher bottles is probably due to vertical inhomogeneity within the dust events that passed Iwik. Closer to ground level the flux is usually higher (Zheng et al., 2004) which may be explained by settling within the dust front and short term suspension of local dust, thereby also explaining coarser grain size and different chemical composition.

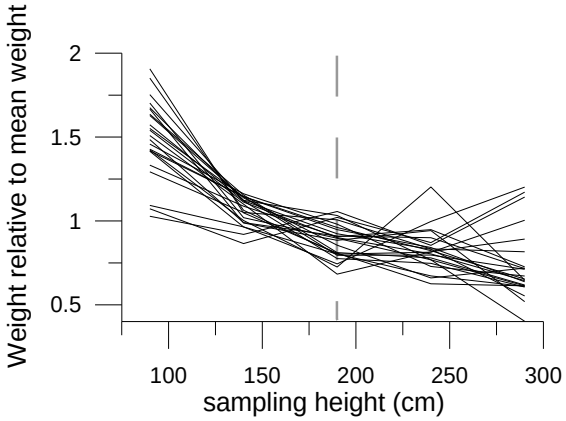

Figure 29. Average mass per sampling height, plotted as deviation from the mean weight of the whole sampling month. All 23 sampling months are shown. The dashed line is set at 190 cm, the minimum sample height of the included samples.

4.2a. Dust flux

Our two-year time series displayed marked seasonal variability in flux. The amount of dust supplied to the ocean is one of the factors determining the magnitude of potential ballasting and fertilising effects. By estimating dust loading, the flux could be compared to dust flux measurements at Sal Island, Cape Verde, which lies at 23° west, 800 kilometer from Iwik along the general dust transport path. The two spring maxima in the current study showed monthly averaged dust concentrations of 237 and 170 µg/m^3 respectively. Three spring maxima measured between 1991 and 1994 at Sal Island, Cape Verde, amounted to 120, 95 and 70 µg/m^3 respectively (Chiapello et al., 1995). The average spring maximum at Sal amounts to approximately 47 percent of the average spring maximum at Iwik. The average dust concentration at Sal during 1992-1994 amounts to approximately 48 percent of the average dust concentration at Iwik during 2013-2014. The foregoing shows that around 50 percent of the low-level transported dust may have been deposited over this short distance. This figure should be interpreted as a rough indication, because the study at Sal Island used a different sampling technique, was carried out almost two decades before the current study and estimated dust concentration from flow rate of the active sampler where the current study used a passive sampler and average wind speed. Furthermore, the sampling station in Sal was posted on top of a 25 m tower located at an altitude of 100 m, which will have greatly reduced local dust in the samples compared to our samples. Upwelling filaments reach to approximately 19° west (Kostianoy and Zatsepin, 1995) so a significant fraction of the dust was deposited where abundant nutrients are already available. If Saharan dust was the only supply of iron to this area, nitrogen fixation and associated primary productivity would benefit from the substantial dust flux. However, north of Mauritania, in the canary basin, upwelled waters are relatively rich in iron from reduction processes in continental margin sediments (Sarthou et al., 2007). If the upwelling waters near the region of the major dust plume are similarly enriched in iron, this means dust iron supply may not be required to support high primary productivity. Ballasting effects, if present, remain important. Outside the area where upwelling filaments are frequent, Saharan dust potentially stimulates nitrogen fixation, triggers phytoplankton blooms and ballasts OM.

The general seasonal trend observed in our dust flux record corresponds to previous work carried out at the Northwest African margin. Highest dust fluxes in the TWAL were usually observed in mid-winter (Chiapello et al., 1995) or early spring (Skonieczny et al., 2013) and lowest fluxes in fall. July-August also showed a substantial dust flux. This was concomitant with high satellite estimated rainfall. Wet deposition can generate significant dust fluxes in summer (Skonieczny et al., 2013) so it may be speculated wet deposition contributed to the high flux. Dust flux showed a highly significant correlation with wind speed. Wind speed at the source is probably a better predictor of dust flux

than wind speed at our sampling station and it should be kept in mind that meteorological data lacked for the summer of 2013. Nevertheless, the correlation shows that wind speed, even at a distance from the source, remains a good predictor of dust flux.

4.2b. Grain size

From the four duplicate samples (two samples per height, two masts) the sample with highest mass was selected. The reasoning behind this being that the sampling bottles should not have collected more dust than the dust that was transported at the sampling height. Thus, bottles containing most material had the highest sampling efficiency, reducing the chance of possible particle selective processes by which some particles did not make it into the bottle or were removed from the bottle through the exit-tube. Grain size remained close to a median of 40 µm or a mode of 50 µm during most of the record. This which is significantly coarser than grain size found at M'Bour, 600 km south of Iwik, where the modal grain size is around 19 µm (Skonieczny et al., 2013). In the study of Skonieczny et al. (2013), particles above 30 µm were sieved out before grain-size analysis, which probably explains a large part of the observed difference. Furthermore, it may be speculated that this difference has to do with the amount of dust that can be generated near the sampling stations. Dust generated at close distance from the sampling station is more likely to have retained its coarse fraction compared to dust from more distant sources. The coastal plain of Mauritania is itself a dust generating area (Skonieczny et al., 2013). In contrast, the area around M'Bour is greener and presumably less prone to wind erosion.

The grain-size methodology used in the current study may also have caused part of the difference. The current study used the least dispersive de-aggregation procedure, thereby retaining strongly bound aggregates. SEM pictures showed abundant rounded aggregates which were likely formed before or during transport and rounded during transport. However, angular aggregates were also present which indicate possible aggregation in the bottle after transport. The latter type of aggregates was a source of some error in the grain-size results, but not many were encountered and it is not certain whether they survived the short de-aggregation treatment. Subsequent runs of the grain-size analysis showed aggregates to primarily be located around the mode and in the coarse tail of the distribution (fig. 30). The aggregates are larger and heavier than the grains of which they consist. Thus, more energy is required to suspend them and keep them aloft. Furthermore, an aggregate has different reflective properties than single grains because it is larger. Thus, inclusion of aggregates in the current study renders the results more representative for the transport processes that took place and the reflective properties of the dust than if the aggregates had been dispersed before grain-size analysis.

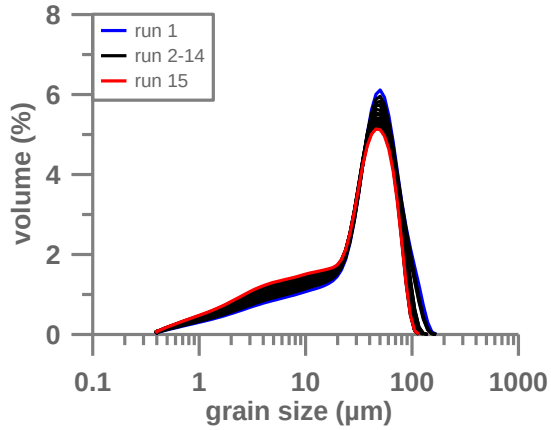

Figure 30. Grain-size distributions at 240 cm height of May-June 2013, showing particle disaggregation during the runs. The graph indicates that aggregates were mainly present around the modal size and in the coarse tail. Run 1 was used in the current study.

The change in grain-size distribution after dust has left the African coast could be derived from a comparison with previous work. Grain-size distributions of three dust events at Cape Verde showed modes around 10 µm with a significant amount of dust above 100 µm (Kandler et al., 2011) and measurements along the coast show modal size between approximately 7 and 20 µm in the vicinity of Iwik (Stuut et al., 2005). Preliminary results of van der Does (DUSTTRAFFIC cruise 2013) of grain size of the terrigenous fraction in sediment traps along a transect at 12° N showed a median size around 10 µm, quartz grains up to approximately 100 µm and micas up to approximately 250 µm as far as 49 degrees west. Thus, the comparison showed that the coarse fraction is lost rapidly after dust leaves the African continent, shifting the median from 40 to approximately 10 µm in less than 1000 km. Furthermore, it shows that part of the extremely large fraction is kept aloft and transported over large distances.

In the current study, the summer monsoon season was defined as mid-June to mid-October with the remainder of the year being assigned to the winter monsoon season. From mid-June to mid-October the ITCZ is found at higher latitudes over Northwest Africa. In these months it lies relatively close to the latitude of our sampling location (20° N) and hence the likelihood of precipitation increases. There was no strong seasonal signal present in the grain-size results, but on average summer monsoon dust was slightly finer (median = 35 µm, standard deviation = 10.5) than that of the winter monsoon (median = 40µ, standard deviation = 5.6). Furthermore, summer monsoon months displayed more mutual variability than winter monsoon months. The strongest departures from the relatively stable grain size in our record were fine-grained, namely August-October and October-November 2013 and May-June and August-September 2014 (fig. 16). In general, finest grain size was attained around late summer to early fall, to which May-June 2014 was an exception (fig. 16). Coarser-than-usual size also occurred in the summer season.

An alternation between two depositional mechanisms is thought to have induced this strong variability in summer. 600 km south of Iwik, in M'Bour, Senegal, grain size was observed to increase during summer (Skonieczny et al., 2013). The authors explained this trend by dry settling from the SAL. Only the coarse fraction has enough settling velocity to reach the surface. Thus, the coarse fraction of SAL dust is mixed with TWAL dust, shifting its size distribution to the right. This process may have caused the coarse distributions of, among others, June-July 2014. In contrast to the study of Skonieczny et al. (2013), many of the late summer months in the current study displayed very fine grain size. In two out of the four most fine-grained periods (August-October 2013 and August-September 2014), significantly finer grain size co-occurred with increased amounts of precipitation. Thus, the explanation may be sought in wet deposition of dust from the SAL. This mechanism was described in the study of Skonieczny et al. (2013). The authors demonstrated that dust was derived from the SAL and brought down by precipitation. In contrast to dry settling, wet settling washes out all dust in the atmosphere below cloud base and dust higher in the atmosphere is on average finer than dust closer to ground level. This high altitude fine dust may be brought down by wet deposition, mix with low-level transported dust and shift the grain-size distribution to the left.

It should be kept in mind that the Iwik dust masts sample horizontally and hence measure transport flux and not deposition flux. However, virga is a common feature over the Sahara. Twenty-eight percent of radar reflectivity profiles over the Sahara show virga (Geerts and Dejene, 2005). Essentially, virga is rainfall that does not reach the ground because it evaporates in the dry air below cloud base. Dust settling with precipitation may be released during evaporation of the droplets and continue on its horizontal trajectory, albeit at a lower level. Moreover, because wet-deposited dust is relatively fine-grained, it is likely to be re-suspended when the soil dries. The finest grained month in our record, August-September 2014, showed strongest evidence of wet deposition: it displayed a

bimodal distribution with peaks at 15 and 40 µm (fig. 31). The fine peak at 15 µm may be interpreted as the characteristic modal grain size of wet deposited dust in this area. Indeed, it corresponds very well to the 14 µm modal size of the wet deposition event described by Skonieczny et al. (2013). The coarse peak is similar to the average modal grain size in our study.

The remaining two exceptionally fine-grained samples (November-December 2013 and May-June 2014) did not co-occur with increased amounts of precipitation and thus another explanation has to be speculated upon. They may also have been caused by wet deposition, as only minute amounts of rainfall can already trigger significant wet deposition (Löye-pilot et al., 1989). Alternatively, the fine grain-size distribution of November-December 2013 may have been caused by low wind speed. The yearly minimum in wind speed overlaps with this period and only very little dust was deposited in the sampling bottle. However, other periods with low wind speed, for example December 2014 -January 2015 and other periods with low dust flux, for example October-November 2014, do not show fine grain size (fig. 15 & 16). Another factor that may be responsible for finer-grained samples is a longer average trajectory from the source to Iwik. In May-June 2014 and many other summer sampling periods, backward trajectories indicate winds overpassed the sea on their coastal trajectory and only crossed land again shortly before arrival in Iwik (appendix 7). Thus, there was no chance for uptake of dust from areas nearby Iwik, causing a longer average transport path, and as coarse grains are deposited preferentially during transport, finer grain-size distributions.

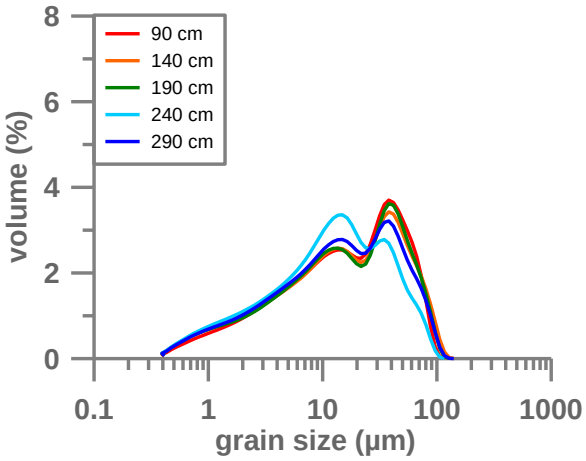

Figure 31. Grain-size distributions of August-September 2014.

4.2c. Chemical analyses

The main objectives of the chemical analyses were 1) to infer possible sources area and 2) to observe fluctuations in chemical composition of Saharan dust and essential trace metals in particular and to infer the variable(s) driving these fluctuations.

Inferred source areas

Three wind systems dominate dust lofting and transport in northwest Africa and transport dust from separate source areas (fig. 32). In the northwest Sahara, shallow coastal trade winds carry dust from the coastal plains in Western Sahara and the Atlas Mountains (Stuut et al., 2005). The latter dust source probably mainly consists of alluvial fan deposits at the foot of the Anti-Atlas Mountains (Scheuvens et al., 2013). Harmattan winds are also an expression of the trade winds. They increase in intensity during boreal winter and carry dust from the central Sahara (Stuut et al., 2005). Two of the main dust sources worldwide lie on its path: The Bodélé depression and an area stretching from mid-Mauritania in an ENE direction to the Hoggar Massif (hereafter West- North African Source (WNAS) (Moreno et al., 2006; Scheuvens et al., 2013). In summer, dust is also injected into the SAL and

transported westward at mid-tropospheric levels (Stuut et al., 2005). The Bodélé depression is the largest contributor to SAL transported dust (Koren et al., 2006). It is clear that dust from the SAL makes up the majority of the dust deposited in the western equatorial Atlantic during summer. However, in the eastern equatorial Atlantic, the two trade wind systems compete with SAL transport and it is unclear which wind system dominates dust supply. In winter there is no SAL transport and only the two trade wind systems transport dust to the Atlantic.

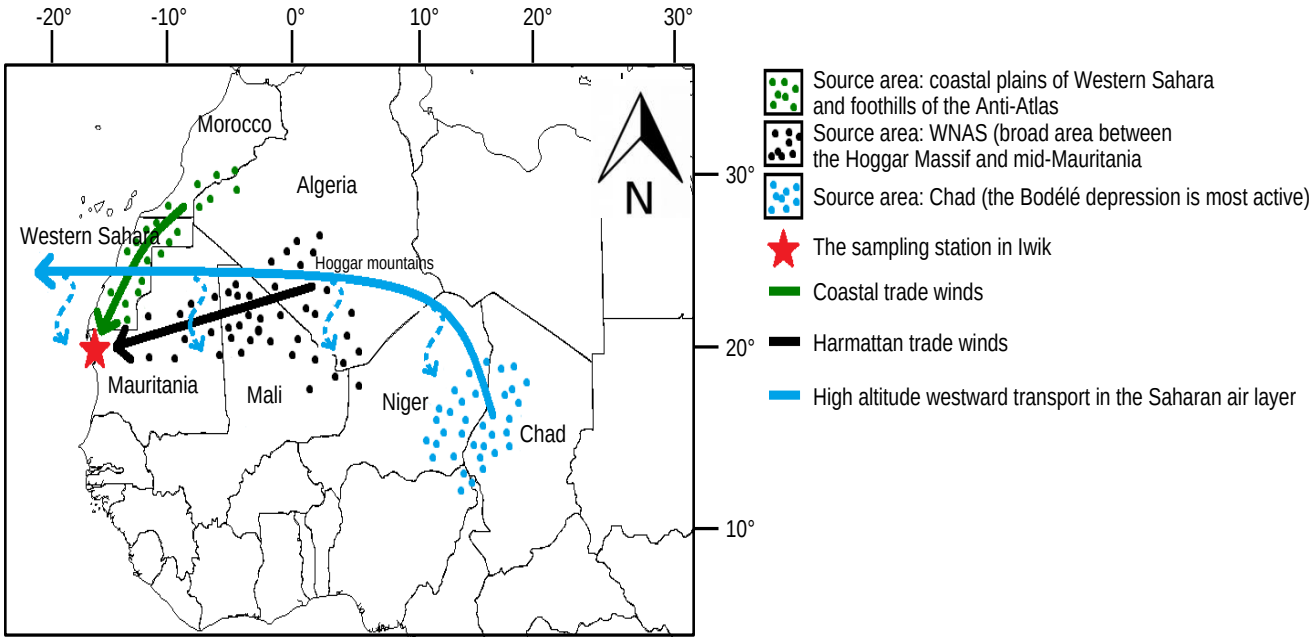

Figure 32. Most likely source areas and transport pathways of dust to Iwik. Major dust transport trajectories are after Stuut et al. (2005). The broken blue lines depict dry or wet deposition from the SAL. General source areas of the dust were based on Scheuvens et al., 2013 and Moreno et al., 2006. Latitude and longitude are given in °N and °E respectively. The base map was obtained from: https://commons.wikimedia.org/wiki/File:World_map_blank_black_lines_4500px.gif.

Calcium over iron ratios are considered the most useful bulk compositional source area tracer for North-African dust (Scheuvens et al., 2013) and may be helpful in answering which wind system dominates dust deposition to the eastern part of the equatorial Atlantic. The coastal plains of Western Sahara and sediments derived from the Anti-Atlas region are strongly enriched in calcium (Scheuvens et al., 2013). The WNAS generally shows very low Ca content, except for one sample from the study of Washington et al., 2009 (Scheuvens et al., 2013). The Bodélé depression shows varying calcium content which is generally lower than that of the coastal plains of Western Sahara and the Anti-Atlas foothills, but some areas show very high calcium content (Abouchami et al., 2013; Scheuvens et al., 2013).

From this background information one expects high Ca/Fe ratios in dust transported by the coastal trade winds (coastal plains and Anti-Atlas region), low Ca/Fe ratios in Harmattan-transported dust (WNAS) and intermediate Ca/Fe ratios in SAL transported dust (Bodélé & WNAS). The interplay between wind direction and Ca/Fe ratio agrees well to these expectations: Ca/Fe ratios correlated highly significantly to wind direction as measured by the on-site meteorological station ($r = -0.713$, $p < 0.01$), such that northern winds were concomitant with high Ca/Fe ratios and (north)eastern winds with low Ca/Fe ratios (fig. 20). A ratio of the number of coastal trade wind trajectories (north or northwest) divided by the number of Harmattan trajectories (northeast or east) as counted from the daily backward trajectories (appendix 7) also relates to the Ca/Fe ratio, although coastal trades were more dominant in the winter of 2013-2014 than would be expected from the Ca/Fe ratio (fig. 21). Despite the good agreement, it should be kept in mind that our data are based on average dust

composition over one month. From backward trajectories and meteorological data alone one cannot deduce the exact timing of dust supply. In other words, it is possible that the majority of the dust was supplied from a wind direction that was not the dominant wind direction in that month.

In the winters of 2012-2013 (January-February) and 2014-2015 (November-January), very low Ca/Fe ratios were attained concomitant with eastern backward trajectories and wind direction. This indicates that the Harmattan trade winds had a major influence on dust transport and that the WNAS area was an important source area. However, the month December 2013-January 2014 does not conform: both wind direction and backward trajectories showed eastern winds; Ca/Fe ratios, however, were average. Possibly, this dust was mainly derived from areas nearby Iwik. This makes sense if the coastal plains of Mauritania are similarly enriched in calcium as the coastal plains of Western Sahara. In the remainder of the record, backward trajectories and wind direction predominantly showed winds derived from the north. These are the coastal trade winds. Ca/Fe ratios are higher in this period and thus confirm a northern source. Consequently, the most likely source areas for the summer samples are the coastal plains of Western Sahara and the foothills of the Anti-Atlas.

Three sampling periods (August-October 2013, May-June 2014 and August-September 2014) displayed even higher Ca/Fe ratios, indicating yet another source area may have contributed. As discussed in the grain-size section, at least the two late-summer sampling periods showed signs of wet deposition of SAL transported dust. Previous work both rejects and supports this hypothesis: Scheuvens et al. (2013) showed that Ca/Fe ratios are generally low in the region supplying dust to the SAL. However, some areas in the bodelé depression, a major source area for SAL dust, contain deposits enriched in calcium (Abouchami et al., 2013). Interestingly, chemical analysis using the SEM showed an abundance of mica's in August-September 2014. This result has to be treated with caution: Fluor, on which the mica assignment is based, is a very light element and partly overlaps with oxygen in the EDS spectrum, which may cause error. However, the difference is large: August-September 2014 saw 12 percent of the measured grains assigned to the mica group, compared to less than 0.5 percent in the other measured samples. From a conceptual point of view, it is likely that the percentage of the platy mica minerals in dust increases with transport distance and transport height because they have lower settling velocities. Indeed, mica's amount to up to 50 percent in Cape Verdian dust and even 60 percent across the Atlantic at Barbados and Miami (Glaccum and Prospero, 1980). Thus, the high amount of micas in August-September 2014 may be explained by wet deposition from the Saharan Air layer. Future research would benefit from on-site measurements of haziness or other dust loading estimates to determine the exact timing of dust events. If the timing of dust events is known, focused research of backward trajectories and meteorological circumstances will reveal more on source areas and possible wet deposition.

Essential trace metal content

The essential trace metals were plotted as x/Si and x/Al ratios; x being the studied element (fig. 19). Because aluminium is enriched in the fine fraction relative to silicon, and these elements together make up a significant fraction of the dust, they were expected to show opposing fluctuations in abundance. Thus, if both the x/Si and the x/Al ratio of a certain element show the same trends, these trends are likely caused by the element of interest. The important trace metals iron, manganese, zinc, copper and nickel co-varied strongly (fig. 19): their x/Si and x/Al (x being the studied element) correlated highly significantly or significantly, indicating that the majority of the trends was dictated by the element of interest and not variability in Si or Al. Nickel and especially manganese displayed weaker covariance. However, standard deviations of nickel and manganese ratios indicate that their signal to noise ratio is low (fig. 19). Over almost the entire record all x/Si and x/Al ratios shifted in

tandem. Only one sampling period, January-February 2013, and only two elements, zinc and copper, remain inconclusive as their x/Si and x/Al ratio disagreed. Because trace metals showed strong covariance, their general trend is discussed first, followed by their mutual differences. Median grain size correlated strongly to most trace metal ratios and future studies can possibly use median grain size as a rough indication of trace metal content if the chemical composition is not measured. Presumably, the grain size dependence of trace metal content is caused by the fact that clays and iron(hydr-)oxides, which are generally fine grained, are richer in trace metals than coarse grained feldspars and quartz. Focusing on iron, Iron (hydr-)oxides consist of around 60-80 percent iron (by weight), clays between 0 and 25 percent whereas feldspars consist of less than one percent iron (Journet et al., 2008). The percentage of iron in iron-coated quartz was not found in literature.

In the foregoing, August-October 2013, August-September 2014 and possibly also May-June 2014 were linked to wet deposition. August-September 2014 has very likely been influenced by wet deposition. SEM-EDS measurements showed that wet-deposited dust was strongly enriched in micas, which are rich in iron: biotite contains up to 27 % iron by weight and muscovite around 3 % by weight (Häggström, 1969; Herbillon, 1976). This may explain why fine-grained and wet-deposited dust is richer in trace metals. As such, the clay- and mica-rich wet deposited dust is also likely more beneficial to phytoplankton growth and primary production than dry deposited dust. In addition, wet deposition has the advantage that photochemical reduction in more acidic cloud waters and precipitation may leach iron and other metals from the dust, further increasing the bioavailability of the metals (Gao et al., 2003). Especially Fe and to a lesser extent Mn, Cu and Zn also increased in January-February 2013 and December-January 2015. In contrast to the other peaks in trace metal content, these peaks were not accompanied by fine grain size, so another explanation must be sought. In the foregoing it was shown that these periods were strongly influenced by (north)eastern Harmattan transported dust in contrast to the remainder of the record which was more influenced by northern coastal trades. Moreno et al. (2006) showed that dust from the Hoggar Massif, east-northeast of Iwik and on the path of the Harmattan trades, is rich in trace metals relative to the other areas they studied. This may explain the non-grain size related increase in trace metals during these periods. In these kind of source area assessments it should be kept in mind that we are limited by the sparse distribution of dust and/or sediment samples in the Sahara region and that although we have knowledge of the wind trajectories, it is unsure which source area(s) along such a trajectory actually contributed to the dust flux. A few strong fluctuations in several trace metals remain poorly understood. November-December 2013 showed exceptionally fine grain size which was not reflected in high Al/Si nor high trace metal content. It is unclear which mineral(s) made up the fine fraction in this month. Furthermore, Fe, Ni and Cu displayed a peak in January-February 2014 and Zn in December 2013- January 2014. These peaks were not related to a shift in grain size, Al/Si nor wind direction.

The response of trace metal content of the dust load to shifting wind direction and wet deposition holds important implications for the relationship between dust and phytoplankton growth now and under future climate change. Although the amount of dust supplied to the ocean is the main factor determining the amounts of trace metals reaching the ocean, apparently wet deposition, source area and/or source distance should also be considered. Interactions between these factors complicate scenarios for future nutrient supply by dust. For example, average wind speed may increase and cause higher dust fluxes from the Sahara. However, it is possible that different source areas contribute to this dust flux due to the change in wind regime, which may either counteract or enhance the effect of increased dust flux. Alternatively, precipitation may increase over the Sahara region, causing soil stabilisation and therefore reduced dust flux. Under the changed rainfall regime, wet deposition may become the dominant mechanism of dust deposition, partly counteracting the

effect of a reduced dust flux. The above examples show that the dust flux, source areas and precipitation regime may all change under future climate change and their effects may interact in complex ways to influence the amounts of bioavailable trace metals supplied to the equatorial Atlantic.

Synthesis and future perspectives

Year round a zone of high productivity extends further from north-west Africa than could be expected if upwelling filaments were the sole nutrient supply (Antoine et al., 1996; Feldman and mcClain, 2014; Kostianoy and Zatsepin, 1995). Saharan dust may be the missing link, supplying trace metals further westward over the tropical Atlantic than do the upwelling waters, thereby stimulating primary productivity. The current study supports but does not provide unambiguous evidence for dust fertilisation under a natural dust event in the tropical north Atlantic. Indications were found of a phytoplankton bloom following a dust event south of the Cape Verde islands, at 12°N, 23°W. During the dust event, higher fluxes of carbon and nitrogen were recorded, as well as a different carbon to nitrogen ratio, suggestive of a diatom bloom. There were also indications of ballasting taking place during the dust event: the corresponding drifting trap showed invariable carbon to nitrogen ratio from 100 to 400 m depth, suggesting no substantial degradation took place and therefore that the particles settled at a higher velocity. However, the dissimilar carbon to nitrogen ratios from primary and secondary C/N analysis casts doubt on the validity of these results and the suitability of the C/N ratio to determine settling velocity. Furthermore, bulk carbon and nitrogen of the filters contradict the conclusions drawn from the carbon to nitrogen ratio because they showed strong attenuation at station M1, implying rapid degradation of the organic matter. The deviating outcomes from C/N analysis and especially the carbon to nitrogen ratio demonstrate that multiple runs of C/N analysis per sample are necessary in future work. Possibly the results could be validated further using a ratio of degraded pigments (phaeopigments) to fresh pigments (e.g. chlorophyll a) as indication of the amount of OM degradation that took place. Another improvement would be to collect duplicate samples for microscopic analysis of ballasting. Future work should aim to estimate the relative importance of dust as a ballasting agent compared to biogenic ballast materials such as diatom frustules. More specific, it should derive approximate equations for the amount of ballasting taking place depending on the concentration of dust and/or biogenic ballast material and organic matter in the upper water column. Additionally, video analysis of aggregates in the upper water column in a dust-frequented area may provide the high temporal resolution necessary to proof or refute the dust ballasting hypothesis.

The second part of the current research provided valuable information on the flux and characteristics of dust and their seasonal variability. A comparison between the dust flux measured in the current study and that found by Chiapello et al., 1995, it became clear that the dust flux diminishes quickly in the westward direction: approximately 50 percent was lost over only 800 km of open ocean. This has important implications for dust as a nutrient source for the tropical Atlantic: close to Northwest Africa, where most of the dust is deposited, upwelling waters form a competing source of nutrients. A graph of this concept of competition between nutrient sources is shown in figure 33.

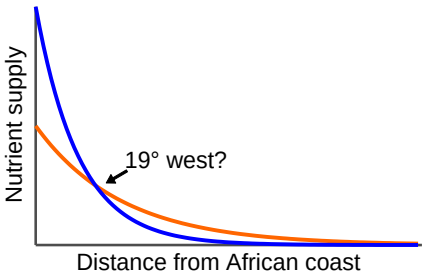

Figure 33. Hypothetical amounts of nutrients supplied by dust (orange) and upwelling filaments (blue). At 19° west no more upwelling filaments were found (Kostianoy and Zatsepin, 1995).

Outside the range of upwelling filaments, trace metals released from dust that was deposited into the surface ocean may stimulate phytoplankton growth. The actual fertilising effect of dust may depend on: 1. the settling flux of dust into the ocean; 2. the trace metal deficiency of the phytoplankton community; 3. the extent to which trace metals are leached from the dust so they become bio-available. Using these assertions as a guideline, two seasons seem to have most potential for dust fertilisation. Around late winter/spring a spring bloom occurs: chlorophyll is at a maximum concentration and extent off the coast of Northwest Africa (fig. 34). Diatoms tend to be a major group in spring blooms and they may become severely iron limited as the bloom progresses, especially if there is no resupply of iron by upwelling filaments. To recap, diatoms are more iron limited than other phytoplankton groups (DiTullio et al., 1993) and concurrently seem to respond well to iron addition (Chavez et al., 1991; Coale et al., 2002; Duarte et al., 2000). The late winter/spring season is also the season in which we recorded highest dust fluxes at Iwik, Mauritania. Taken together, this implies dust fertilisation may be especially significant in this season.

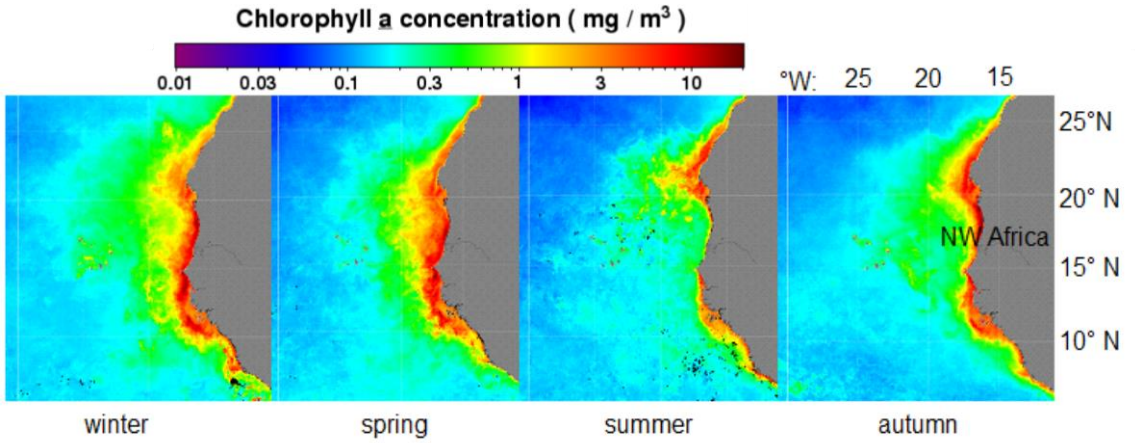

Figure 34. Satellite derived chlorophyll concentration over the north-eastern tropical Atlantic. Dataset: NPP VIIRS chlorophyll concentration, OCI algorithm. Adapted from Feldman and Macclain (2014).

Interestingly, the current study found that finer-grained dust contained relatively more trace metals than coarse-grained dust. This fine-grained and trace metal rich dust mainly arrived during late summer and was presumably related to wet deposition. During wet deposition dust is pre-leached, enhancing bioavailability of the trace metals (Gao et al., 2003). Moreover, the finer grains have a higher surface to volume ratio. Conceptually this should enhance the dissolution rate per unit mass. From the foregoing, it seems that the dust has highest fertilisation potential per unit mass during late summer wet deposition. Coincidentally, this is also the season during which phytoplankton attain the strongest deficiency in trace metals: after the spring blooms, the nutrient stock is depleted and it remains low until deep winter mixing resupplies nutrients from below. During late summer the sea surface temperature and light conditions are favourable to phytoplankton growth. Thus, iron and other trace metals released from dust particles may enhance iron limited nitrogen fixation, causing a

resupply of the nitrogen stock which may help sustaining high primary productivity during this low-nutrient season.

In order to make full use of the current results on quantity and quality of the Saharan dust supply, future work in mesocosm experiments should aim to quantitatively describe the response of phytoplankton growth to different quantities of dust supply as well as dust with different trace metal concentrations. Such work is complex, but if linked to the quantity and quality of the Saharan dust flux it would provide us with estimates of the magnitude of dust-stimulated phytoplankton growth. The current study outlines that it may be more difficult to predict future changes in the magnitude of this process than previously asserted: the demonstrated influence of source area and wet deposition on the amounts of bioavailable trace elements shows that the response of dust-stimulation of phytoplankton growth to future climate change is not solely a function of the change in dust flux.

5. Conclusions

During cruise 64PE395 a dust event occurred, providing an opportunity to study the effect of a natural dust seeding on phytoplankton in the north-eastern equatorial Atlantic. During the dust event exceptionally high carbon and nitrogen fluxes of settling organic matter were measured in the upper 400 m of the water column (trap M1). The trap recorded a 1.5 to 3 times larger settling flux than the other traps. Gel traps also showed that M1 contained a larger amount of organic matter than the other traps. In addition, the high C/N ratio at M1 corresponds to a diatom dominated phytoplankton community, indicative of a bloom. Therefore, it is likely but not uncircumstantial that a dust storm, passing RV Pelagia before and during deployment of M1, caused a phytoplankton bloom through addition of trace metals.

The case for ballasting by Saharan dust at M1 remained ambiguous: at M1, the uniform C/N ratio with depth indicates little degradation took place which supports the ballasting hypothesis. However, the strong flux attenuation of POC and PON discredit the ballasting hypothesis. An alternative explanation for the strong attenuation is that the timing of the dust event and the following bloom rather than degradation caused the vertical pattern. Compared to vertical flux trends in literature, M5, were no substantial dust flux was present, showed exceptional preservation of flux and large marine snow, indicating that other materials may or processes may be equally or more effective as dust at aggregation and ballasting of organic matter. The remaining ambiguity around ballasting in the current study indicates future work needs validation of C/N ratios by other measurements, for example analysis of the ratio of degraded pigments to fresh pigments in the drifting traps. Such work was initialised during the current study but could not be realised within the given time frame. The initial results indicate this method is promising, but detection of the degraded pigments was not possible in the smallest samples. An interesting side result of the current study is that foraminiferal tests are not an efficient ballasting material. The tests observed at M2 showed no aggregation to organic matter whatsoever.

The current study presented dust characteristics from a sampling station that lies within the zone of maximum low-level dust transport during the majority of the year. Concurrent to previous work, highest dust fluxes occurred in late-winter to spring and lowest fluxes in late-fall to early winter. Substantial dust flux was also observed in one summer month which was attributed to wet deposition. Dust flux showed highly significant correlation to wind speed, indicating wind speed is a good predictor of dust flux. A comparison of our results with dust flux measurements at Sal Island, Cape Verde (Chiapello et al., 1995), showed that roughly half of the dust flux is deposited in an area where nutrient and iron rich upwelling filaments are common and thus does not stimulate phytoplankton growth significantly (but may ballast organic matter).

The average median grain size was approximately 40 µm and the average modal grain size was 50 µm, significantly coarser than dust 600 km south of Iwik (19 µm, Skonieczny et al., 2013). However, this difference may solely have been caused by the decision of the authors to sieve off all grains above 30 µm. By comparing the modal grain size of the current study to that of previous work downwind of Iwik, the current study showed that the coarse fraction is lost rapidly after dust leaves the African continent, shifting the modal grain size from approximately 50 to 10 µm in only 100-800 km (Kandler et al., 2011; Stuut et al., 2005). On average, summer monsoon dust was slightly finer (median = 35 µm, standard deviation = 10.5) than that of the winter monsoon (median = 40µ, standard deviation = 5.6) and showed more mutual variability, presumably due to inmixing of both dry (coarse) and wet (fine) deposited dust from the Saharan air layer. The current study showed that aggregates are abundant in mineral dust and shift the grain-size distribution. In future work, climate

modellers should take into account that many of the current studies use rigorous disaggregation procedures before measurement and hence slightly underestimate effective grain size during dust transport. The effect of grain size on the ballasting potential of dust remained unclear, but conceptually, grains should be coarse enough to act as an anchor for organic matter, but fine enough to allow enough time in the mixed layer to form aggregates with organic matter. Future work on residence time of different grain-size fractions in the upper water column could be combined with grain-size distributions like the ones produced in the current study to solve this question.

The current study combined calcium over iron ratios, backward trajectories and vector averaged wind direction to estimate from which source area the dust originated. In the second half of the winter of 2012-2013 (sampling started in January 2013) and the first half of the winter of 2014-2015 (the last sample was from December-January 2014-2015), dust was predominantly transported by the (north)-eastern Harmattan trade winds from the calcium depleted western North African source, an area stretching from mid-Mauritania in an east-northeast direction to the Hoggar Massif. In summer, the main sources probably lay north of Iwik. Both the coastal plains of Western Sahara and alluvial fan deposits at the foot of the Anti-Atlas Mountains were likely sources (Scheuvens et al., 2013; Stuut et al., 2005). This dust was presumably mixed with alternating dry and wet deposition from the Saharan air layer. Wet deposition was characterised by high amounts of mica minerals. Interestingly, the trace metal content of dust seemed to be influenced by the source area. Trace metal content showed peaks in January-February 2013 and December-January 2015 that were not related to grain size or wet deposition. These periods were strongly influenced by (north)-eastern Harmattan transported dust in contrast to the remainder of the record which was more influenced by northern coastal trades. This effect of source area on trace metal content is another pathway through which future changes in wind regime over the Sahara region may affect phytoplankton growth in the equatorial Atlantic.

The current study revealed a qualitative relationship between concentrations of biologically important trace metals and grain size, with finer grain size corresponding to dust enriched in trace metals. Median grain size showed the best correlations. Future work may derive quantitative relationships between median grain size and several trace metal nutrients using quantitative chemical analysis. Such relationships are valuable because grain size is a characteristic that is measured more frequently than chemistry. Furthermore, the current study showed strong covariance between the trace metals. This holds an important implication for future studies: the trace metal abundance in a sample may be estimated by quantitatively measuring only one trace metal (most likely iron, as it has the highest concentration), as long as approximate quantitative relationships between the different essential trace metals are known. Wet deposition showed increased trace metal content compared to dry deposited dust. This result shows an alternative pathway through which future changes in the rainfall regime may affect the amount of trace metals supplied to the equatorial Atlantic and therefore the growth of phytoplankton therein.

Aggregating information from mass flux, grain size, trace metal content and previous work, it became apparent that Saharan dust may be specifically important in two seasons. In late winter or spring, the dust fluxes are very high. Concurrently, severely iron limited diatom spring blooms are commonplace and may benefit substantially from the high dust flux (DiTullio et al., 1993). In summer, wet deposition is frequent and wet-deposited dust is rich in trace metals of which the bioavailability is higher due to pre-leaching. Furthermore, the nutrient stock is low in this season whereas other growing conditions (light, temperature) are beneficial. By relieving iron stress in the nitrogen fixing community, this especially trace metal rich dust may prolong the growing season. The current study showed that prediction of future dust-stimulation is complicated by the fact that dust-stimulated

phytoplankton growth is not only a function of dust flux, but also of source area and the contribution of wet deposition relative to that of dry deposition to dust settling fluxes.

6. References

1. Abouchami, W., Näthe, K., Kumar, A., Galer, S. J., Jochum, K. P., Williams, E. ..... and Andreae, M. O. (2013). Geochemical and isotopic characterization of the Bodélé Depression dust source and implications for transatlantic dust transport to the Amazon Basin. *Earth and Planetary Science Letters*, 380, 112-123.

2. Air resources laboratory [online]. Available at: Ready.arl.noaa.gov [Accessed may 2015].

3. Antoine, D., André, J-M., Morel, A. (1996). Oceanic primary production. Estimation at global scale from satellite (coastal zone color scanner) chlorophyll. *Global biogeochemical cycles*, 10 (1), 57-69.

4. Bertilsson, S., Berglund, O., Karl, D.M. and Chisholm, S.W. Elemental composition of marine Prochlorococcus and Synechococcus: Implications for the ecological stoichiometry of the sea. *Limnology and oceanography*, 48(5), 1721-1731.

5. Blain, S., Guieu, C., Claustre, H., Leblanc, K., Moutin, t., Quéguiner, B., ... and Sarthou, G. (2004). Availability of iron and major nutrients for phytoplankton in the northeast Atlantic Ocean. *Limnology and Oceanography,* 49(6), 2095-2104.

6. Blain, S., Quéguiner, B., Armand, L., Belviso, S., Bombled, B., Bopp, L., ... and Wagener, T. (2007). *Effect of natural iron fertilization on carbon sequestration in the Southern Ocean*. Nature, 446, 1070-1074.

7. Bressac, M., Guieu, C., Doxaran, D., Bourrin, F., Desboeufs, K., Leblond, N. and Ridame, C. (2013). Quantification of the Lithogenic Carbon Pump Following a Dust Deposition Event. *Biogeosciences Discussions*, 10(8), 13639-13677.

8. Brzezinski, M. (1985). The Si:C:N ratio of marine diatoms: interspecific variability and the effect of some environmental variables. *Journal of Phycology*, 21(3), 347-357.

9. Buesseler, K. O., Lamborg, C. H., Boyd, P. W., Lam, P. J., Trull, T. W., Bidigare, R. R., ... and Wilson, S. (2007). Revisiting carbon flux through the ocean's twilight zone. *Science*, 316(5824), 567-570.

10. Chavez, F., Buck, K., Coale, K., Martin, J., Ditullio, G., Welschmeyer, N., Jacobson, A. and Barber, R. (1991). Growth rates, grazing, sinking, and iron limitation of equatorial Pacific phytoplankton. *Limnology and Oceanography*, 36(8), 1816-1833.

11. Chiapello, I., Bergametti, G., Gomes, L., Chatenet, B., Dulac, F., Pimenta, J. and Suares, E. (1995). An additional low layer transport of Sahelian and Saharan dust over the north-eastern Tropical Atlantic. *Geophysical Research Letters*, 22(23), 3191-3194.

12. De la Rocha, C. and Passow, U. (2007). Factors influencing the sinking of POC and the efficiency of the biological carbon pump. *Deep Sea Research Part II: Topical Studies in Oceanography*, 54(5), 639-658.

13. De La Rocha, C. L., Nowald, N. and Passow, U. (2008). Interactions between diatom aggregates, minerals, particulate organic carbon, and dissolved organic matter: Further implications for the ballast hypothesis. *Global Biogeochemical Cycles*, *22*(4).

14. Deboudt, K., Flament, P., Choël, M., Gloter, A., Sobanska, S. and Colliex, C. (2010). Mixing state of aerosols and direct observation of carbonaceous and marine coatings on African dust by individual particle analysis. *J. Geophys. Res.: Atmospheres (1984-2012)*, 115(D24), 1-14.

15. DiTullio, G. R., Hutchins, D. A. and Bruland, K. W. (1993). Interaction of iron and major nutrients controls phytoplankton growth and species composition in the tropical North Pacific Ocean. Limnology and Oceanography, 38(3), 495-508.

16. Does, M. van der, (6-16-2015). Preliminary results of grain-size analyses of the terrigenous fraction collected in buoy M4, at 1200 and 3500 m depth. DUSTTRAFFIC cruise 2013.

17. Dong, Z. and Qian, G. (2006). Characterizing the height profile of the flux of wind-eroded sediment. *Environmental Geology*, 51(5), 835-845.

18. Duarte, C., Agustí, S. and Agawin, N. (2000). Response of a Mediterranean phytoplankton community to increased nutrient inputs:a mesocosm experiment. *Marine Ecology Progress Series*, 195, 61-70.

19. Feldman, G., McClain, C. (2014). Ocean Color Web, NPP VIIRS chlorophyll concentration, OCI algorithm, NASA Goddard Space Flight Center. Eds. Kuring, N., Bailey, S. [accessed 20-9-2015]. http://oceancolor.gsfc.nasa.gov/

20. Formenti, P., Elbert, W., Maenhaut, W., Haywood, J. and Andreae, M.O. (2003). Chemical composition of mineral dust aerosol during the Saharan dust experiment (SHADE) airborne campaign in the Cape Verde region, september 2000. *Journal of geophysical research: Atmospheres (1984-2012)*, 108 (D18), 3.1- 3.15.

21. Franz, J., Krahmann, G., Lavik, G., Grasse, P., Dittmar, T. and Riebesell, U. (2012). Dynamics and stoichiometry of nutrients and phytoplankton in waters influenced by the oxygen minimum zone in the eastern tropical Pacific. *Deep sea research*, 62, 20-31.

22. Gao, Y., Fan, S. M., and Sarmiento, J. L. (2003). Aeolian iron input to the ocean through precipitation scavenging: A modeling perspective and its implication for natural iron fertilization in the ocean. *Journal of Geophysical Research: Atmospheres,* 108(D7).

23. Geerts, B. and Dejene, T. (2005). Regional and Diurnal Variability of the Vertical Structure of Precipitation Systems in Africa Based on Spaceborne Radar Data. *Journal of Climate*, 18(7), 893-916.

24. Geider, R. and La Roche, J. (2002). Redfield revisited: variability of C: N: P in marine microalgae and its biochemical basis. *European Journal of Phycology*, 37(1), 1-17.

25. Giovanni [online]. Available at: http://giovanni.gsfc.nasa.gov/giovanni/ [Accessed 15 may 2015]. Precipitation dataset: TRMM_3B42_daily v7.

26. Glaccum, R.A. and Prospero, J.M. (1980). Saharan aerosols over the tropical north Atlantic – mineralogy. *Marine geology*, 37 (3-4), 295-321.

27. Goossens, D., Offer, Z. and London, G. (2000). Wind tunnel and field calibration of five aeolian sand traps. *Geomorphology*, 35(3-4), 233-252.

28. Gruber, N., and Sarmiento, J. L. (1997). Global patterns of marine nitrogen fixation and denitrification. *Global Biogeochemical Cycles*, 11(2), 235-266.

29. Gyan, K., Henry, W., Lacaille, S., Laloo, A., Lamsee-Ebanks, C., McKay, S., ... and Monteil, M.A. (2005). African dust clouds are associated with increased paediatric asthma accident and emergency admissions on the Caribbean island of Trinidad. *Int J Biometeorol*, 49, 371-376.

30. Häggström, L., Wäppling, R. and Annersten, H. (1969). Mössbauer study of iron-rich biotites. Chemical physics letters, 4 (3), 107-108.

31. Herbillon, A.J., Mestdagh, M. M., Vielvoye, L. and Derouane, E.G. (1976). Iron in kaolinite with special reference to kaolinite from tropical soils. *Clay minerals*, 11, 201-220.

32. Iversen, M. H., Nowald, N., Ploug. H., Jackson, G.A. and Fischer, G. (2010). High resolution profiles of vertical particulate organic matter export off Cape Blanc, Mauritania: Degradation processes and ballasting effects. *Deep Sea Research Part I: Oceanographic Research Papers*, 57.6 (2010): 771-784.

33. Journet, E., Desboeufs, K.V., Caquineau, S. and Colin, J.L., 2008. Mineralogy as a critical factor of dust iron solubility. *Geophysical Research Letters,* 35, art. no. L07805.

34. Kandler, K., Schütz, L., Jäckel, S., Lieke, K., Emmel, C., Müller-ebert, D., …… and Weinbruch, S. (2011). Ground-based off-line aerosol measurements at Praia, Cape Verde, during the Saharan Mineral Dust Experiment: microphysical properties and mineralogy. *Tellus B*, 63(4), 459-474.

35. Koren, I., Kaufman, Y., Washington, R., Todd, M., Rudich, Y., Martins, J. and Rosenfeld, D. (2006). The Bodélé depression: a single spot in the Sahara that provides most of the mineral dust to the Amazon forest. *Environmental research letters*, 1(1), article no. 014005.

36. Kostianoy, A.G. and Zatsepin, A.G. (1995). The West African coastal upwelling filaments and cross-frontal water exchange conditioned by them. *Journal of marine systems,* 7, 349-359.

37. Kustka, A., Carpenter, E. J. and Sañudo-Wilhelmy, S. A. (2002). Iron and marine nitrogen fixation: progress and future directions. *Research in Microbiology*, 153(5), 255-262.

38. Lee, C., Murray, D. W., Barber, R. T., Buesseler, K. O., Dymond, J., Hedges, J. I., ... and Wakeham, S. G. (1998). Particulate organic carbon fluxes: compilation of results from the 1995 US JGOFS Arabian Sea Process Study by the Arabian Sea Carbon Flux Group. *Deep-Sea Research Part II*, 45(10-11), 2489-2501.

39. Loÿe-Pilot, M. D., Martin, J. M., and Morelli, J. (1989). Atmospheric input of particulate matter and inorganic nitrogen to the northwestern Mediterranean. *Water pollution research*, 13, 368-376.

40. Liu, D., Wang, Z., Liu, Z., Winker, D. and Trepte, C. (2008). A height resolved global view of dust aerosols from the first year CALIPSO lidar measurements. *Journal of geophysical research: Atmospheres (1984-2012)*, 113(D16), 1-15.

41. Martin, J.H., Knauer, G.A., Karl, D.M. and Broenkow, W.W. (1987). VERTEX: carbon cycling in the northeast pacific. *Deep sea research*, 34(2), 267-285.

42. Martin, J. H. (1990). Glacial-interglacial CO_2 change: the iron hypothesis. *Paleoceanography*, 5(1), 1-13.

43. McDonnell, A.M.P. and Buesseler, K.O. (2010). Variability in the average sinking velocity of particles. *Limnology and oceanography*, 55(5), 2085-2096.

44. Mills, M. M., Ridame, C., Davey, M., La Roche, J. and Geider, R. J. (2004). Iron and phosphorus co-limit nitrogen fixation in the eastern tropical North Atlantic. *Nature*, 429, 292–294.

45. Moore, C. M., Mills, M.M., Langlois, R., Milne, A., Achterberg, E.P., La Roche, J. and Geider, R.J. (2008). Relative influence of nitrogen and phosphorus availability on phytoplankton physiology and productivity in the oligotrophic sub-tropical north Atlantic ocean. *Limnology and oceanography*, 53 (1), 291-305.

46. Moreno, T., Querol, X., Castillo, S., Alastuey, A., Cuevas, E., Herrmann, L., ... and Gibbons, W. (2006). Geochemical variations in aeolian mineral particles from the Sahara–Sahel Dust Corridor. *Chemosphere*, 65(2), 261-270.

47. Moulin, C., Lambert, C., Dulac, F. and Dayan, U. (1997). Control of atmospheric export of dust from north Africa by the north Atlantic oscillation. *Nature*, 387, 691- 694.

48. Müller, P.J. (1977). C/N ratios in pacific deep-sea sediments: Effect of inorganic ammonium and organic nitrogen compounds sorbed by clays. *Geochimica et Cosmochimica Acta*, 41, 765-776.

49. Neuer, S., Ratmeyer, V., Davenport, R., Fischer, G. and Wefer, G. (1997). Deep water particle flux in the Canary Island region: seasonal trends in relation to long-term satellite derived pigment data and lateral sources. Deep Sea Research Part I: Oceanographic Research Papers, 44(8), 1451-1466.

50. Neuer, S., Torres-Padrón, M.E., Gelado-Caballero, D., Rueda, M.J., Hernández-brito, J., Davenport, R. and Wefer, G. (2004). Dust deposition pulses to the eastern Subtropical North Atlantic gyre: Does ocean's biogeochemistry respond? *Global biogeochemical cycles*, 18(4), 1-10.

51. Ploug, H., Iversen, M. H. and Fischer, G. (2008). Ballast, sinking velocity, and apparent diffusivity within marine snow and zooplankton fecal pellets: Implications for substrate turnover by attached bacteria. *Limnology and oceanography*, 53 (5), 1878-1886.

52. Prospero, J.M., Nees, R.T. and Uematsu, M. (1987). Deposition rate of particulate and dissolved aluminum derived from saharan dust in precipitation at Miami, Florida. *Journal of geophysical research*, 92 (D12), 14723-14731.

53. Redfield, A. C. (1958). The biological control of chemical factors in the environment. *American scientist*, 230A-221.

54. Sañudo-Wilhelmy, S.A., Kustka, A.B., Gobler, C.J., Hutchins, D.A., Yang, M., Lwiza, K., ... and Carpenter, E.J. Phosphorus limitation of nitrogen fixation by trichodesmium in the central Atlantic ocean. *Letters to nature,* 411, 66-69.

55. Sarthou, G., Baker, A. R., Kramer, J., Laan, P., Laës, A., Ussher, S., ….. and Blain, S. (2007). Influence of atmospheric inputs on the iron distribution in the subtropical North-East Atlantic Ocean. *Marine Chemistry*, 104(3), 186-202.

56. Scheuvens, D., Schütz, L., Kandler, K., Ebert, M. and Weinbruch, S. (2013). Bulk composition of northern African dust and its source sediments - a compilation. *Earth-Science Reviews*, 116, 170-194.

57. Skonieczny, C., Bory, A., Bout-Roumazeilles, V., Abouchami, W., Galer, S., Crosta, X., Diallo, A. and Ndiaye, T. (2013). A three-year time series of mineral dust deposits on the West African margin: Sedimentological and geochemical signatures and implications for interpretation of marine paleo-dust records. *Earth and Planetary Science Letters*, 364, 145-156.

58. Slingo, A., Ackerman, T.P., Allan, R.P., Kassianov, E.I., McFarlane, S.A., Robinson, G.J., ... and Dewitte, S. (2006). Observations of the impact of a major Saharan dust storm on the atmospheric radiation balance. *Geophysical research letters*, 33(24), 1-5.

59. Stuut, J-B., Zabel, M., Ratmeyer, V., Helmke, P., Schefuß, E., Lavik, G. and Schneider, R. (2005). Provenance of present-day eolian dust collected off NW Africa. *Journal of geophysical research: Atmospheres*, 110 (D4).

60. Sunda, W.G. (2013). Trace metal interactions with marine phytoplankton. *Biological oceanography*, 6, 411-442.

61. Torres-Padrón, M. E., Gelado-Caballero, M. D., Collado-Sánchez, C., Siruela-Matos, V. F., Cardona-Castellano, P. J., and Hernández-Brito, J. J. (2002). Variability of dust inputs to the CANIGO zone. *Deep Sea Research Part II: Topical Studies in Oceanography*, 49(17), 3455-3464.

62. Verardo, D., Froelich, P. and McIntyre, A. (1990). Determination of organic carbon and nitrogen in marine sediments using the Carlo Erba NA-1500 analyzer. *Deep Sea Research Part A. Oceanographic Research Papers*, 37(1), 157-165.

63. Washington, R., Bouet, C., Cautenet, G., Mackenzie, E., Ashpole, I., Engelstaedter, S., ... and Tegen, I. (2009). Dust as a tipping element: the Bodélé Depression, Chad. *Proceedings of the National Academy of Sciences*, 106(49), 20564-20571.

64. Yu, H., Chin, M., Yuan, T., Bian, H., Remer, L.A., Prospero, J.M., ... and Zhao, C. (2015). The fertilizing role of African dust in the Amazon rainforest: a first multiyear assessment based on CALIPSO LIDAR observations. *Geophysical research letters*, 42(6), 1984-1991.

65. Zheng, X., He, L. and Wu, J. (2004). Vertical profiles of mass flux for windblown sand movement at steady state. *Journal of geophysical research: Solid Earth (1978-2012)*, 109(B1).

7. Appendix

7.1. Drifting trap stations list

Trap	Date	Time (UTC)	Lat (N)	Long (W)
M1	13-jan-15	04:40	11° 59.51634'	23° 0.46152'
M1	14-jan-15	04:33	11° 59.5665'	23° 1.84488'
M2	19-jan-15	05:37	13° 48.28248'	37° 49.66632'
M2	20-jan-15	05:58	13° 42.90114'	37° 50.691'
M3	20-jan-15	17:04	12° 18.81396'	38° 46.34556'
M3	22-jan-15	13:18	12° 18.42888'	38° 48.11862'
M4a	27-jan-15	06:12	11° 56.403'	49° 5.15598'
M4a	28-jan-15	05:41	11° 54.01002'	49° 7.74072'
M4b	28-jan-15	17:29	12° 2.23932'	49° 14.17248'
M4b	29-jan-15	14:54	11° 58.90086'	49° 15.98184'
M5	2-feb-15	09:29	11° 59.73264'	56° 6.76716'
M5	3-feb-15	11:42	11° 58.24416'	56° 6.64608'

7.2. Dust sampling periods

Year	Month	Start	End	Mid-date	Number of days
2013	Jan-Feb	1/27/2013	2/15/2013	2/5/2013	19.00
2013	Feb-Mar	2/15/2013	3/15/2013	3/1/2013	28.00
2013	Mar-Apr	3/15/2013	4/16/2013	3/31/2013	32.00
2013	Apr-May	4/16/2013	5/15/2013	4/30/2013	29.00
2013	May-Jun	5/15/2013	6/24/2013	6/4/2013	40.00
2013	Jun-Jul	6/24/2013	7/15/2013	7/4/2013	21.00
2013	Jul-Aug	7/15/2013	8/15/2013	7/30/2013	31.00
2013	Aug-Oct	8/15/2013	10/15/2013	9/14/2013	61.00
2013	Oct-Nov	10/15/2013	11/15/2013	10/30/2013	31.00
2013	Nov-Dec	11/15/2013	12/16/2013	11/30/2013	31.00
2013/2014	Dec-Jan	12/16/2013	1/20/2014	1/2/2014	35.00
2014	Jan-Feb	1/20/2014	2/15/2014	2/2/2014	26.00
2014	Feb-Mar	2/15/2014	3/15/2014	3/1/2014	28.00
2014	Mar-Apr	3/15/2014	4/15/2014	3/30/2014	31.00
2014	Apr-May	4/15/2014	5/15/2014	4/30/2014	30.00
2014	May-Jun	5/15/2014	6/15/2014	5/30/2014	31.00
2014	Jun-Jul	6/15/2014	7/15/2014	6/30/2014	30.00
2014	Jul-Aug	7/15/2014	8/15/2014	7/30/2014	31.00
2014	Aug-Sept	8/15/2014	9/15/2014	8/30/2014	31.00
2014	Sept-Oct	9/15/2014	10/15/2014	9/30/2014	30.00
2014	Oct-Nov	10/15/2014	11/16/2014	10/31/2014	32.00
2014	Nov-Dec	11/16/2014	12/15/2014	11/30/2014	29.00
2014/2015	Dec-Jan	12/15/2014	1/18/2015	1/1/2015	34.00

7.3. A comparison between DUSTTRAFFIC POC flux and results from Martin et al. (1986).

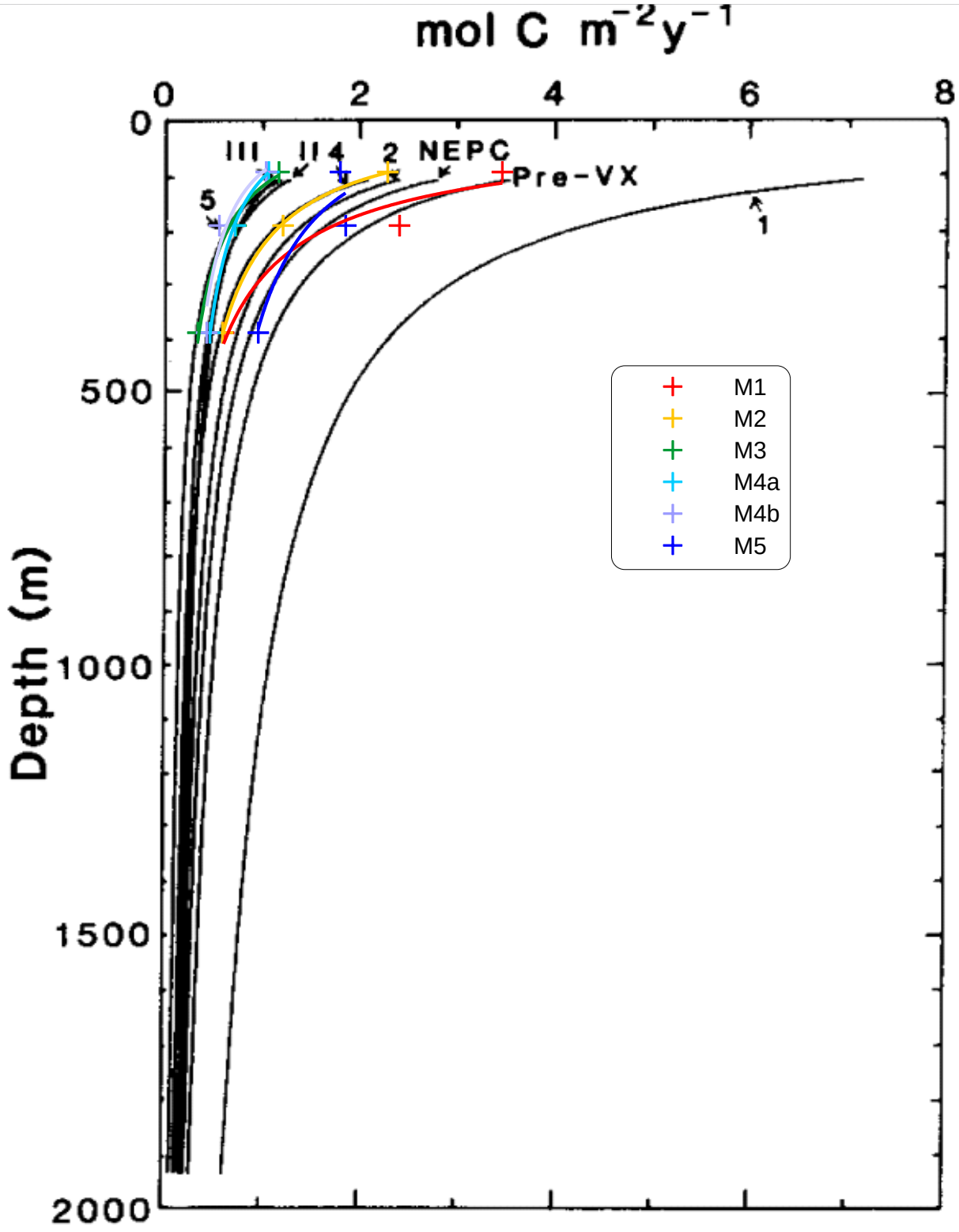

7.4. Gel trap photography

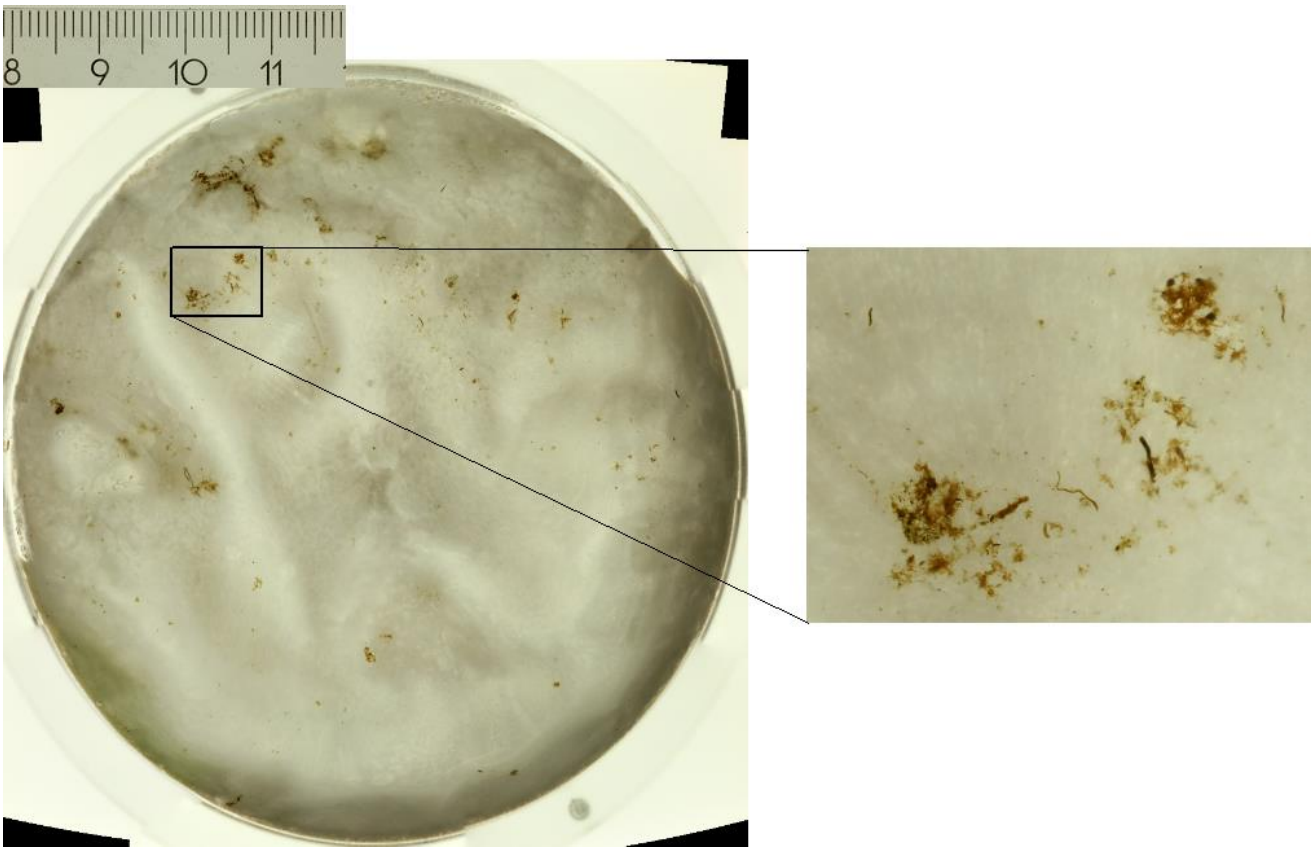

M1 100 with white precipitation on the gel and close-up of marine snow and faecal pellets

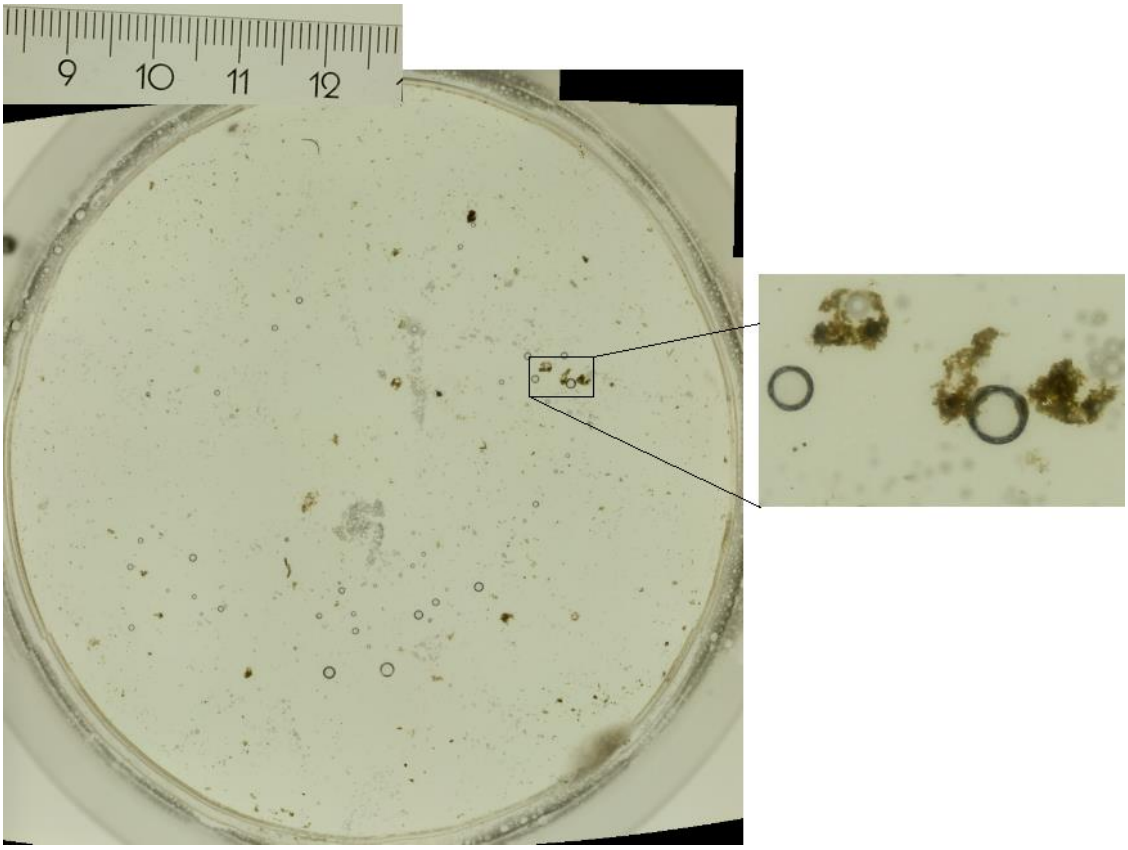

M1 400 with close-up of marine snow

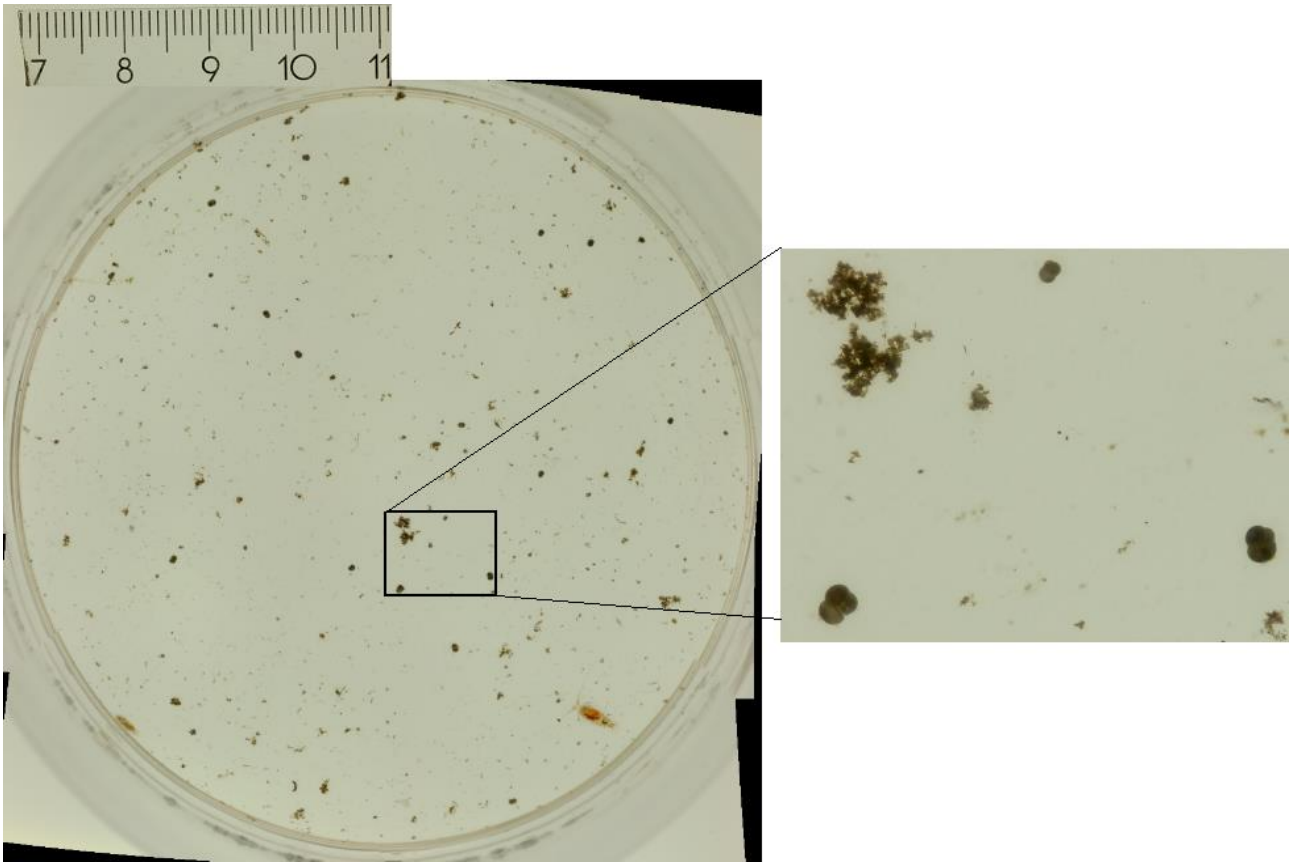

M2 100 with close-up of marine snow and foraminifera

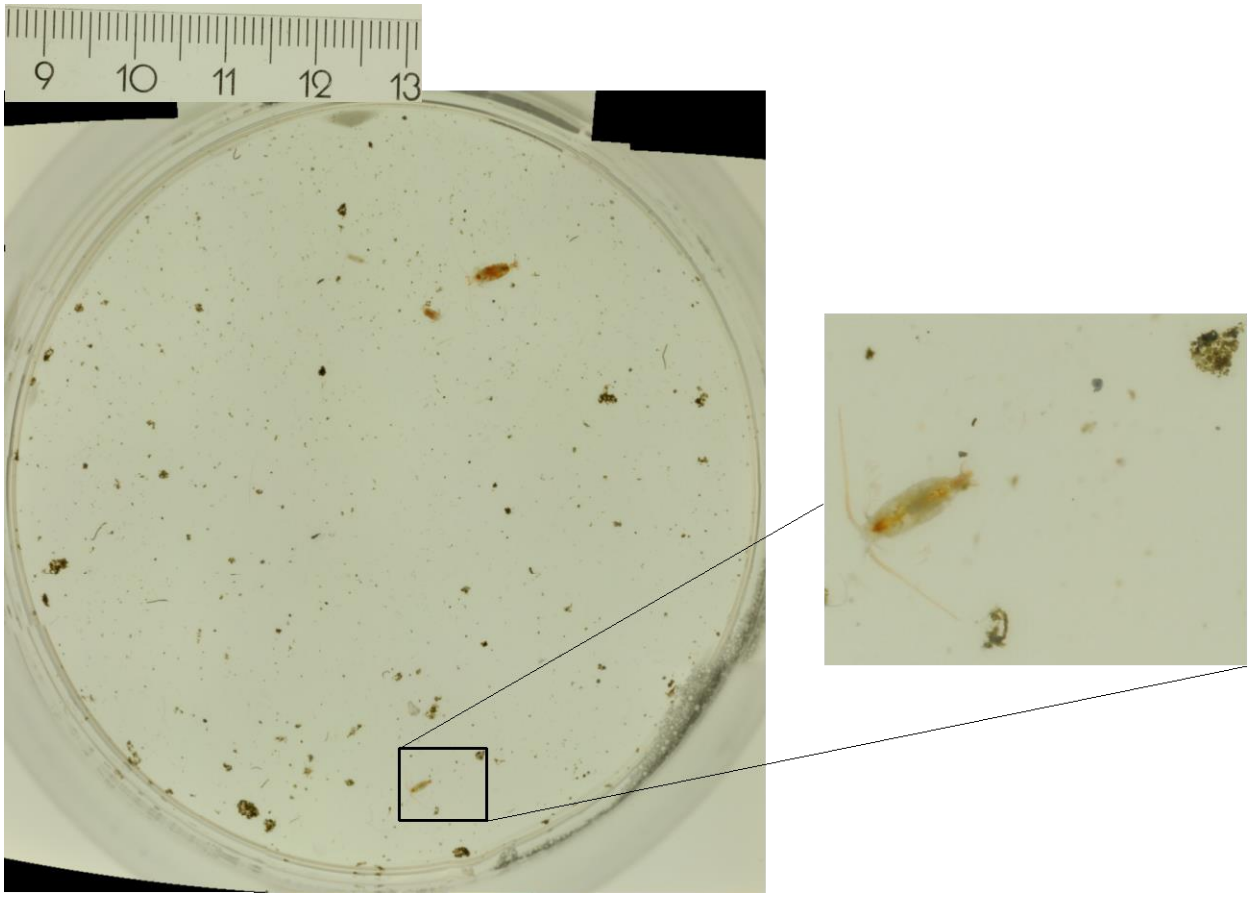

M2 200 with close-up of copepod and marine snow

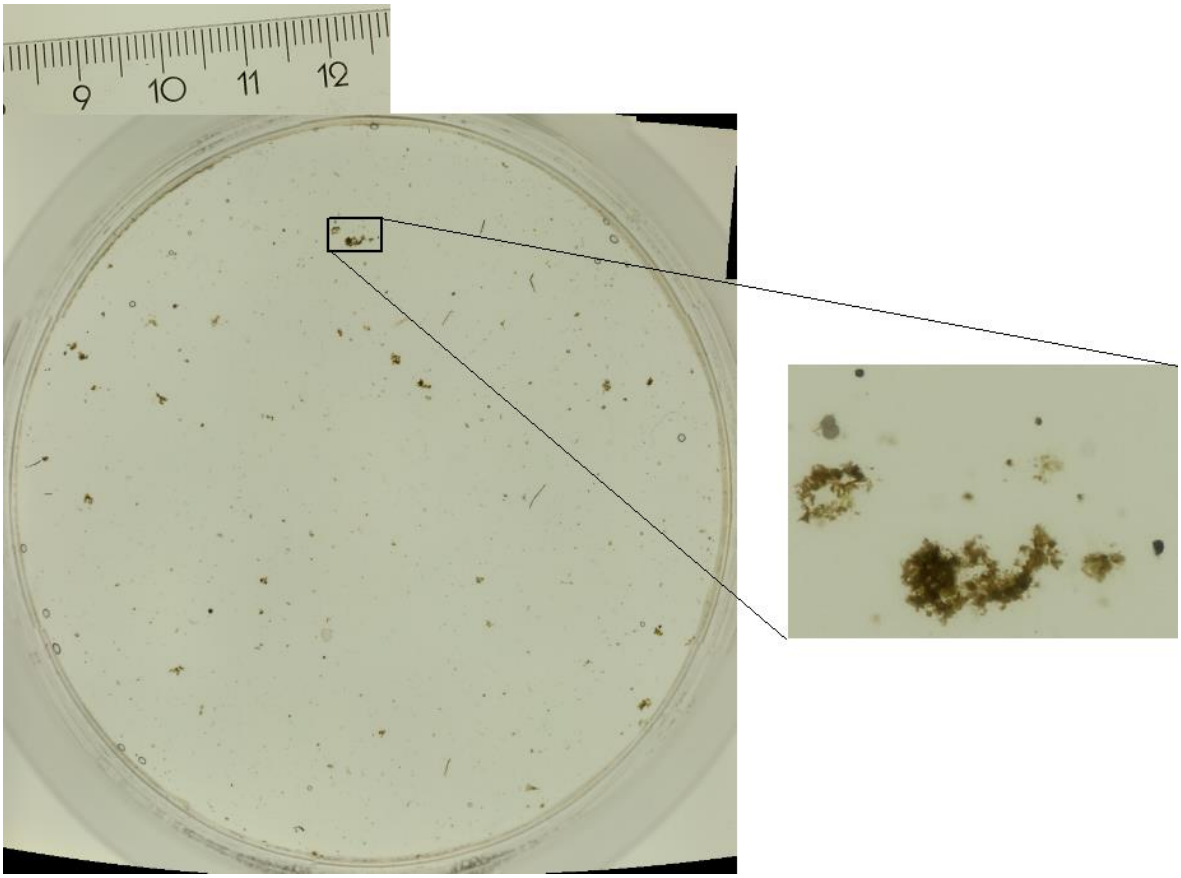

M2 400 with close-up of marine snow and foraminifer

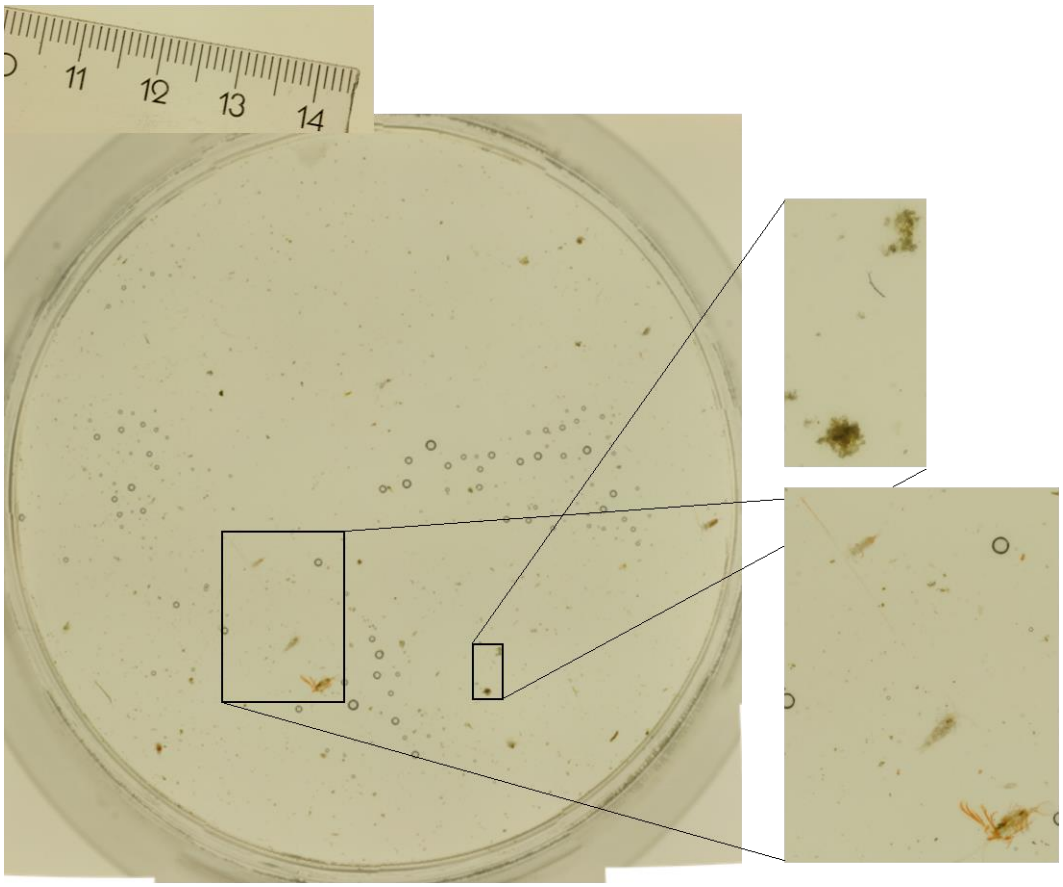

M4 100 with close-ups of marine snow and zooplankton

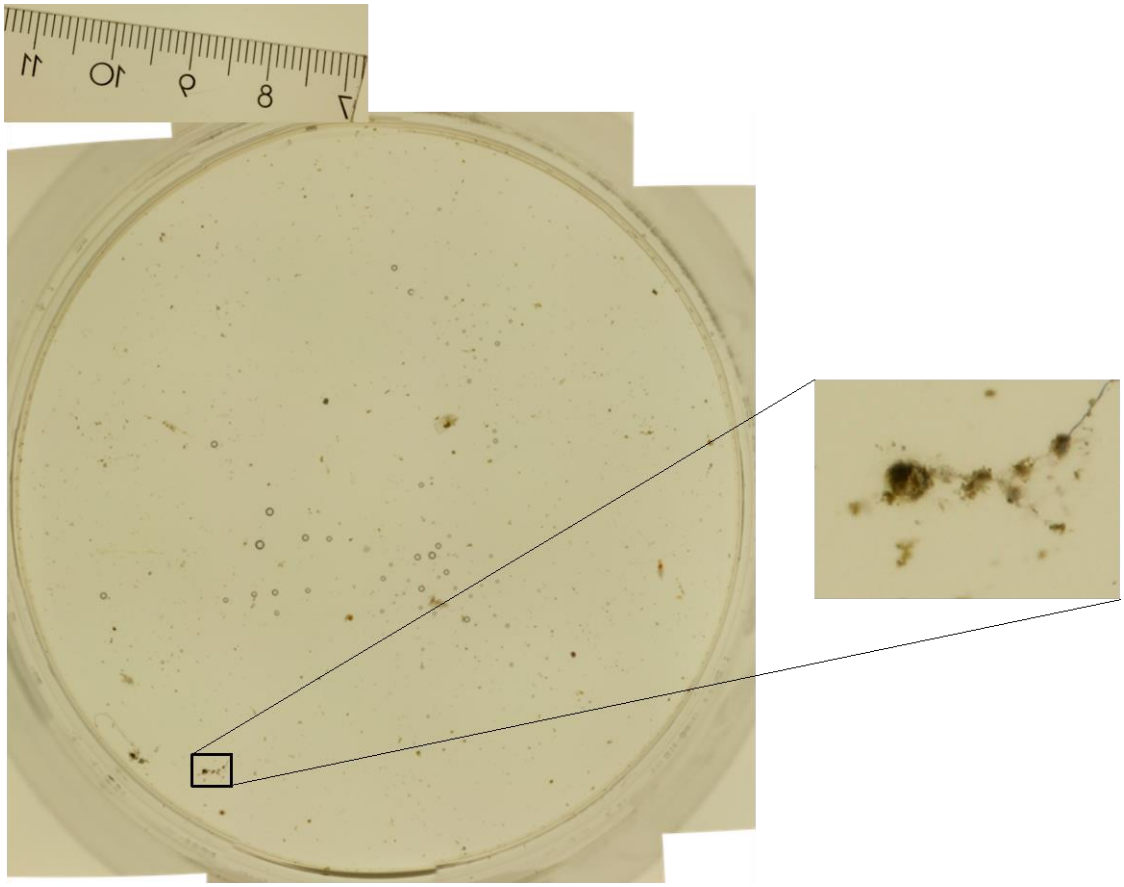

M4 200 with close-up of marine snow

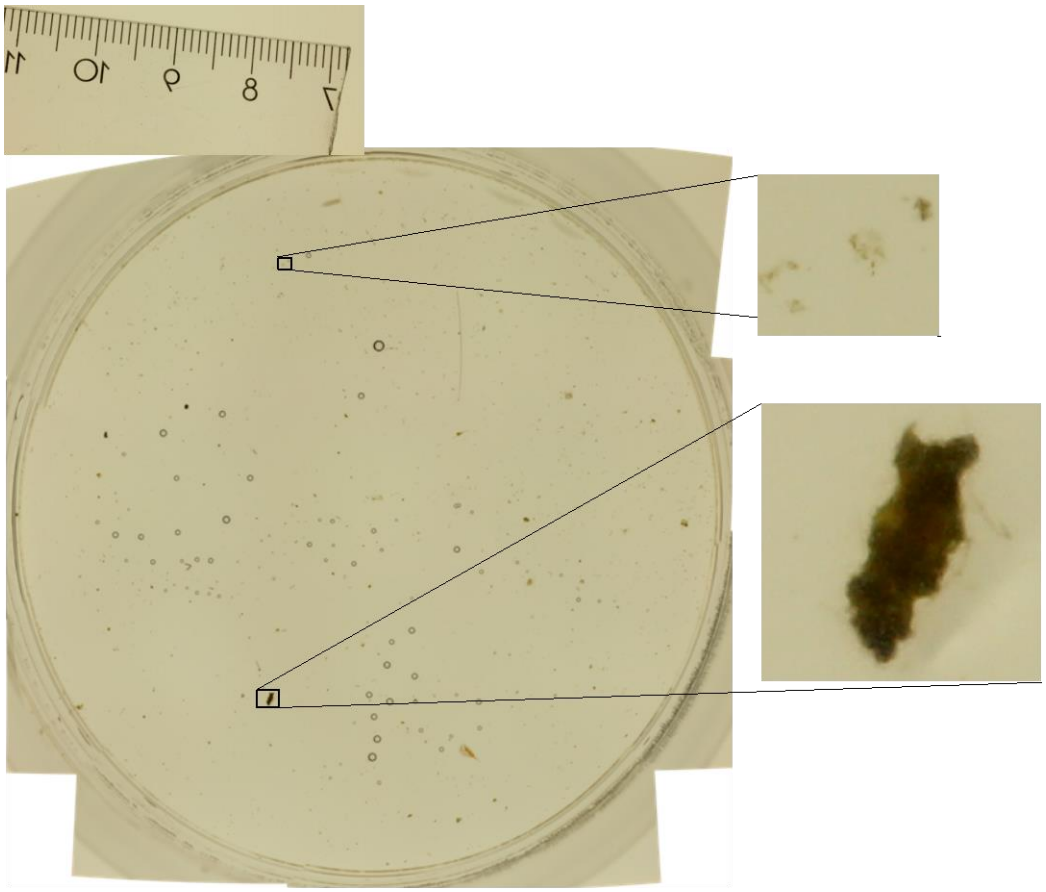

M4 400 with close-up of small marine snow and large faecal pellet (?)

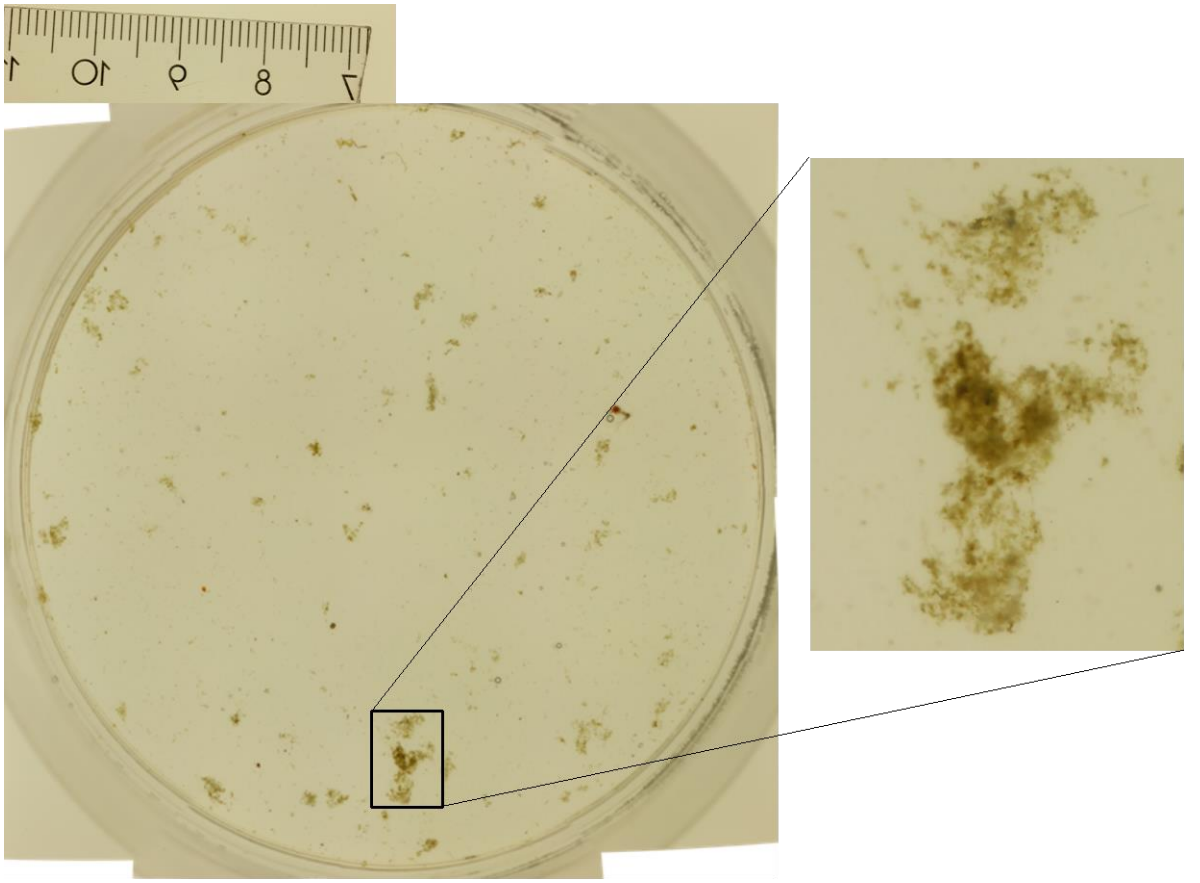

M5 100 with close-up of large marine snow flocks

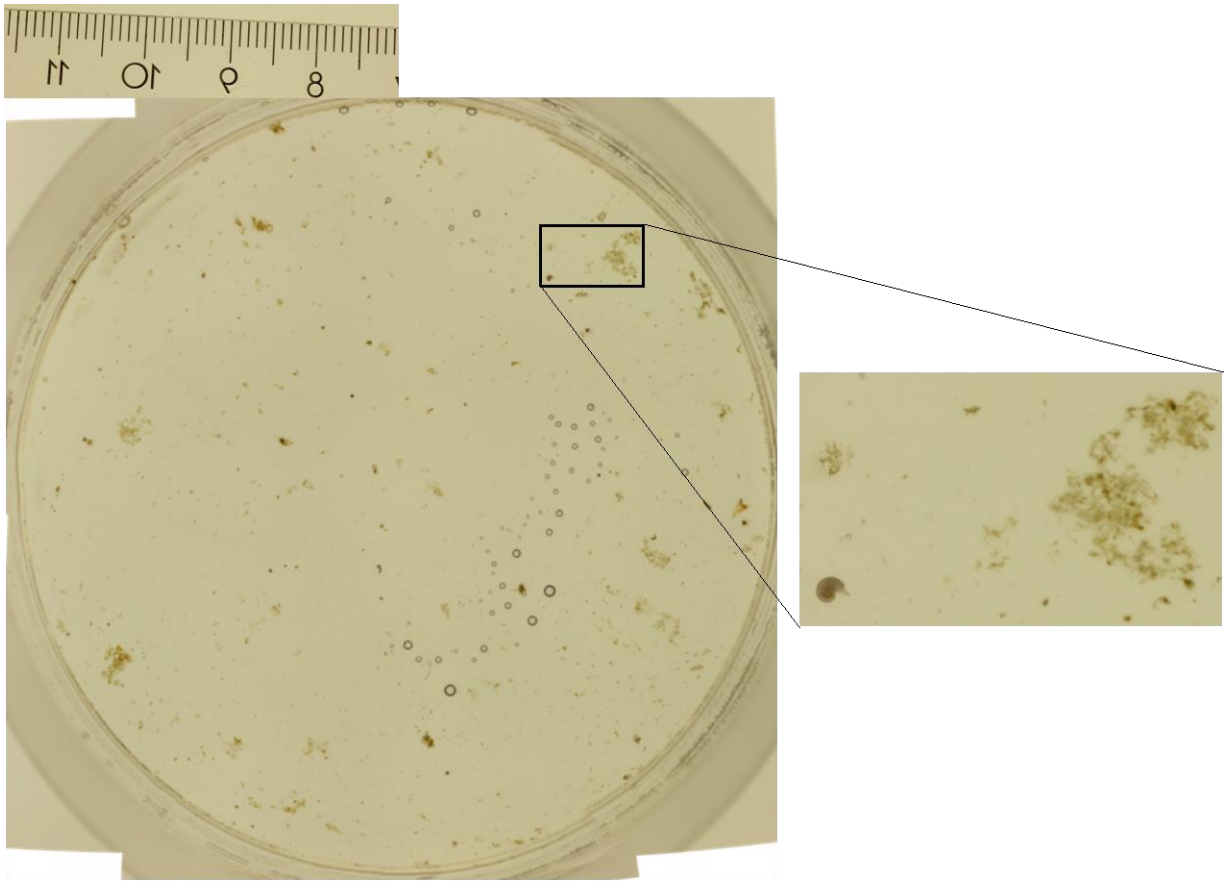

M5 200 with close-up of large marine snow and small snail

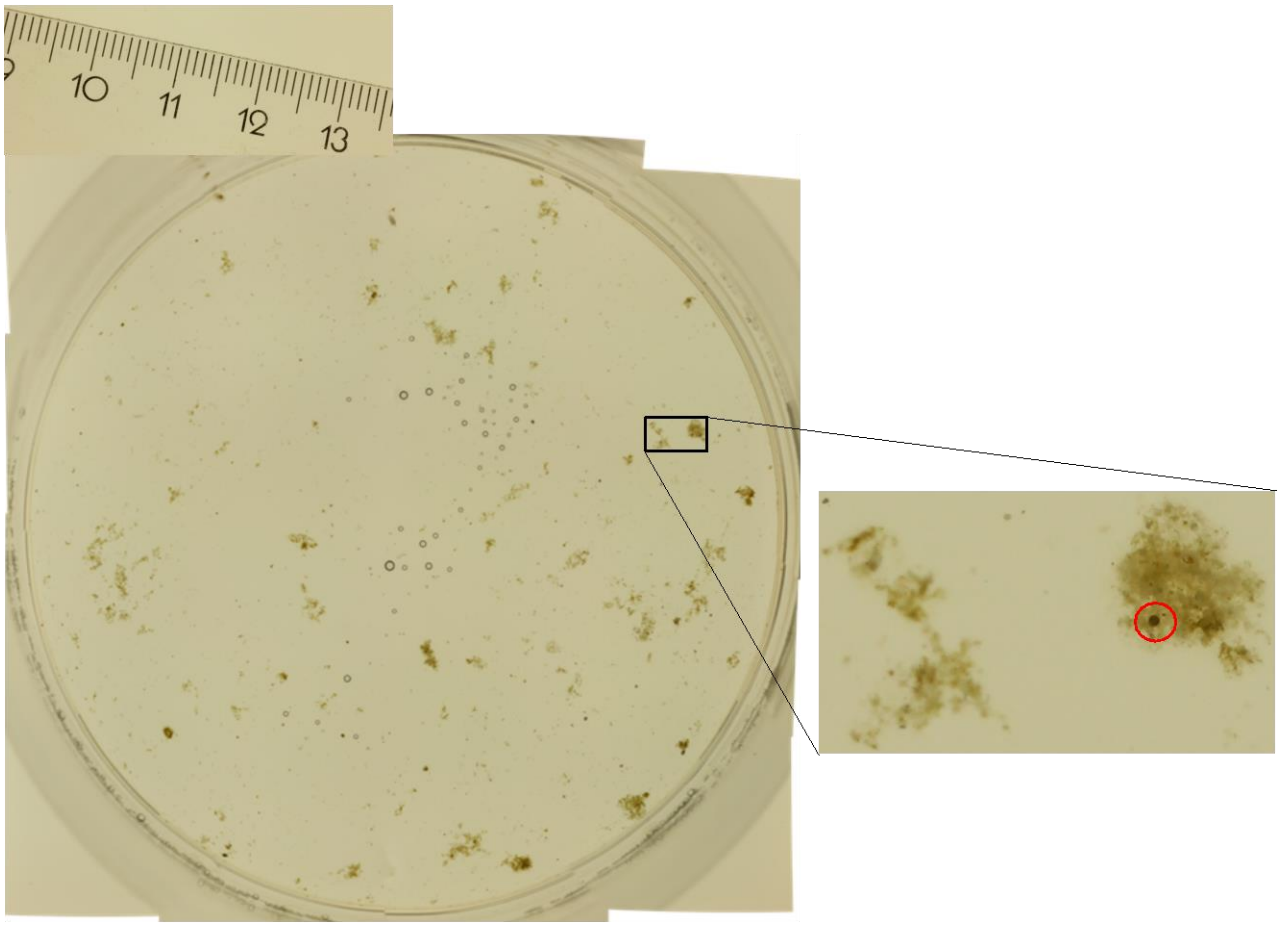

M5 400 with close-up of large marine snow with possible ballasting agent (unidentified)

7.5. Grain size

7.5a. Distributions of 2013

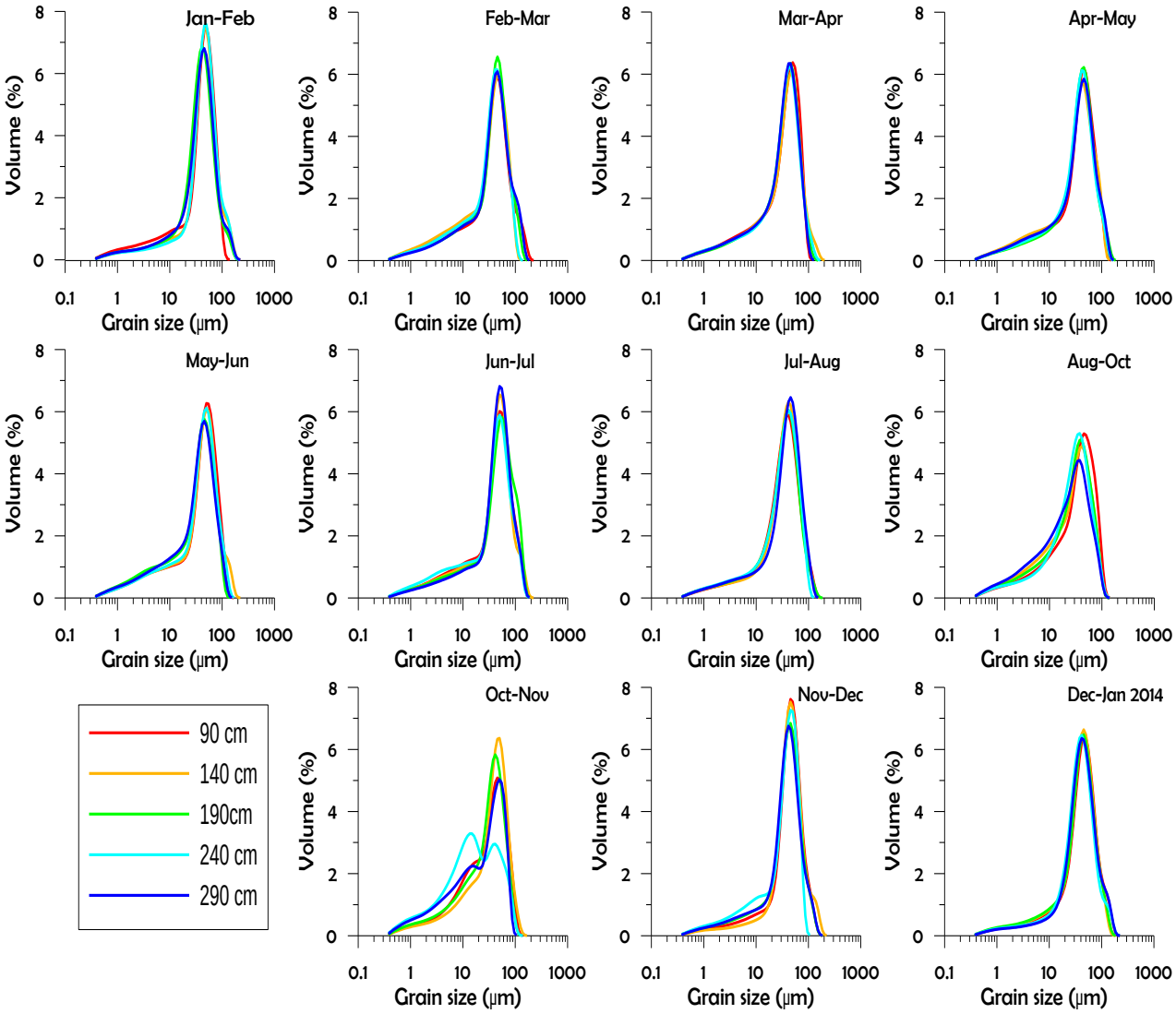

7.5b. Distributions of 2014

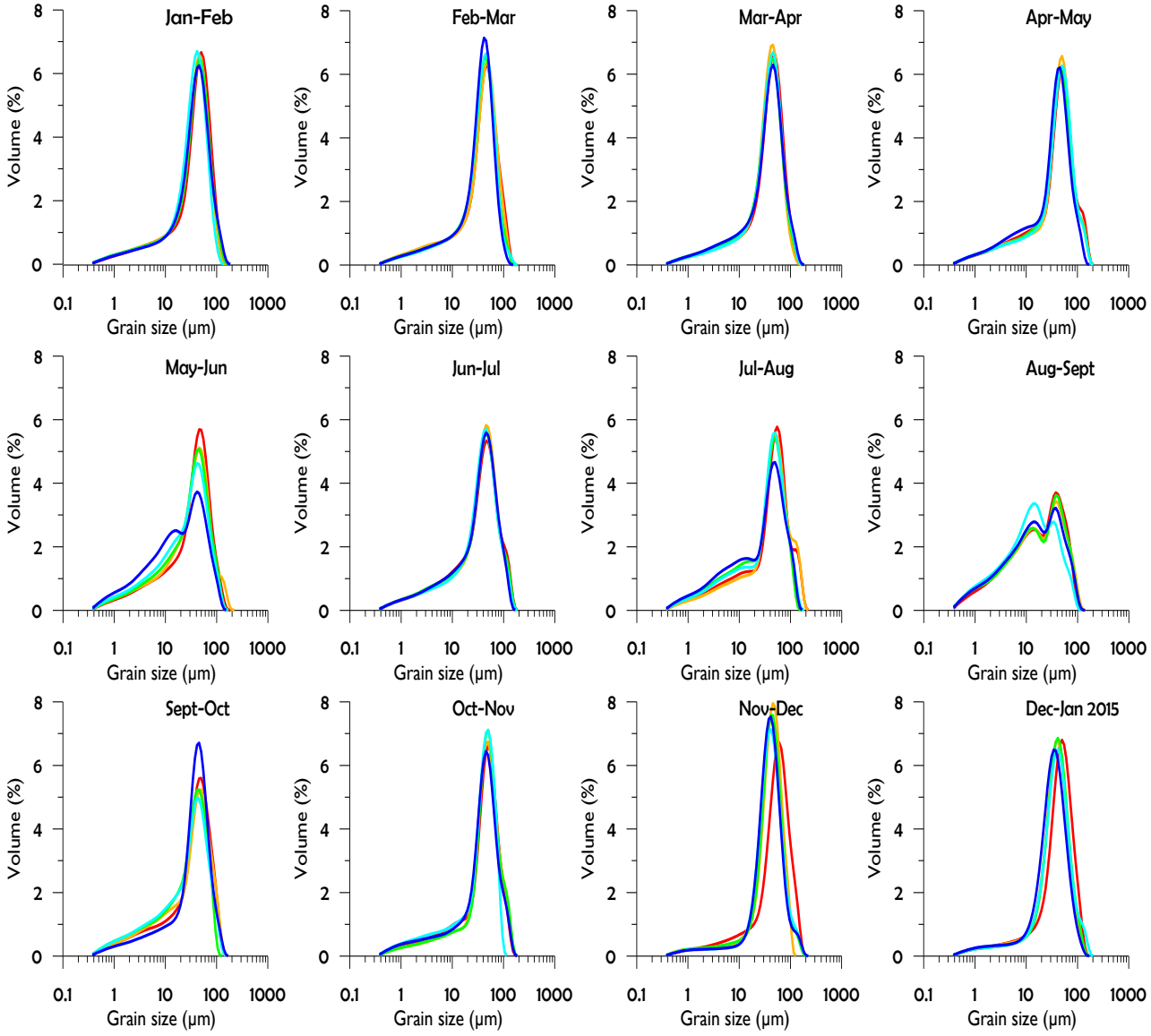

7.6. Locally produced dust in the lower bottles: chemistry, grain-size and mass flux.

Different variables are shown here per sampling height. Note of caution: in both XRF plots some heights miss a few data points because these heights could not be measured. If two samples of different heights were mixed to obtain a sufficient amount, the data point is depicted as the lowest of the two heights.

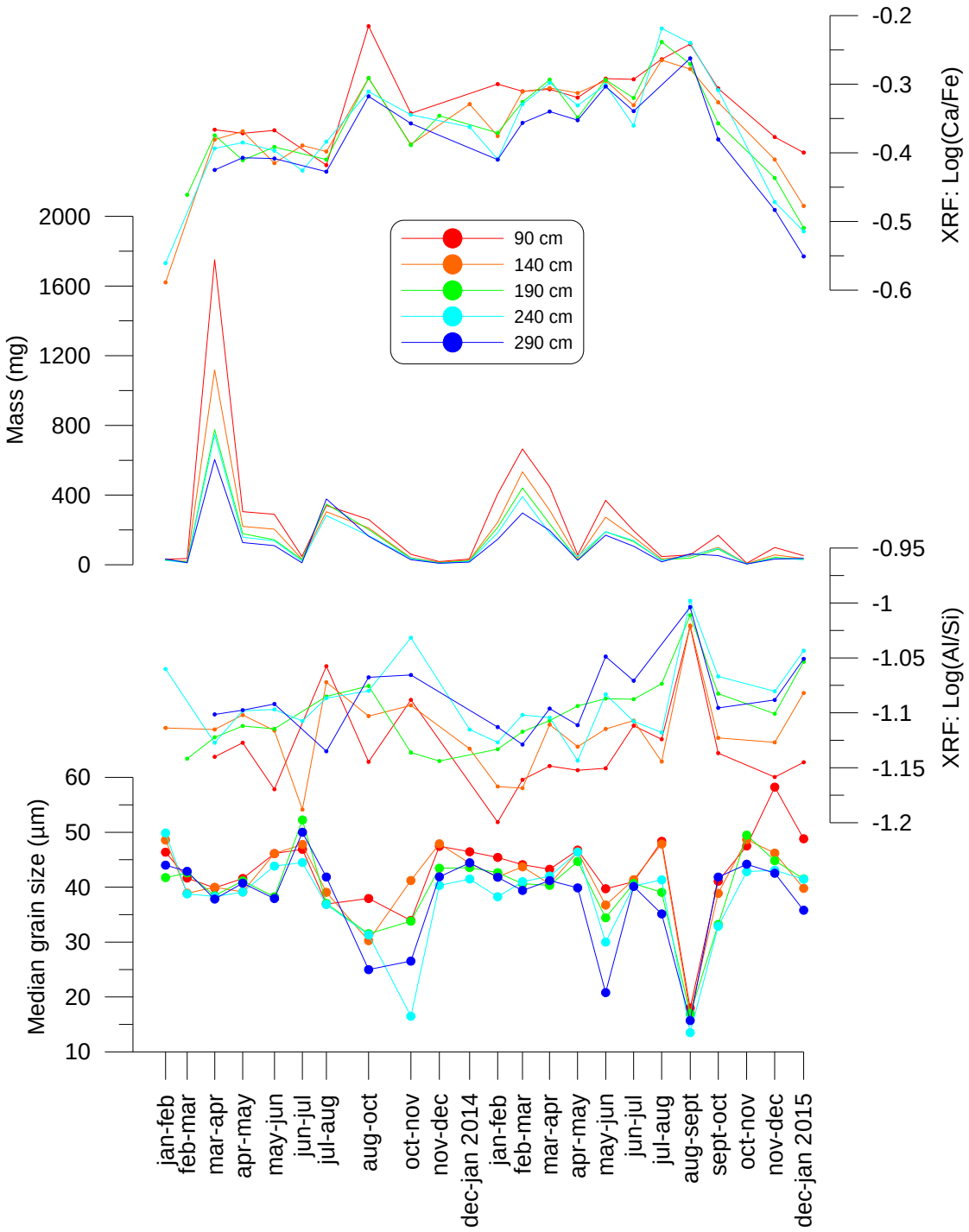

7.7. NOAA HYSPLIT backward trajectories and wind roses from the sampling station

Backward trajectories end at 12:00 UTC each day. Each coloured line represents one such backward trajectory.

January-February 2013

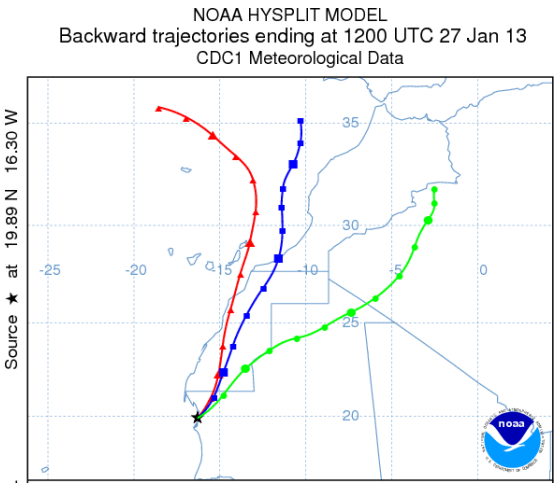

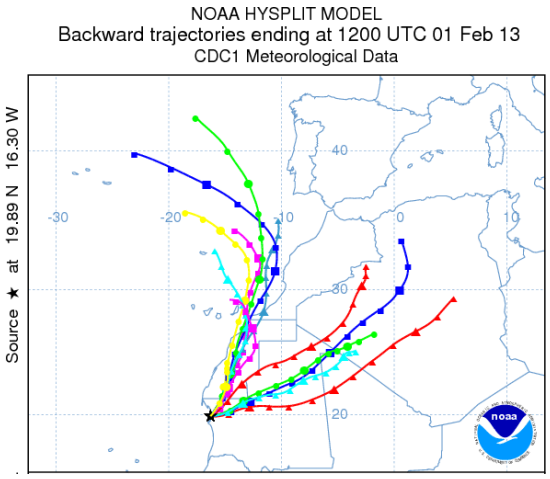

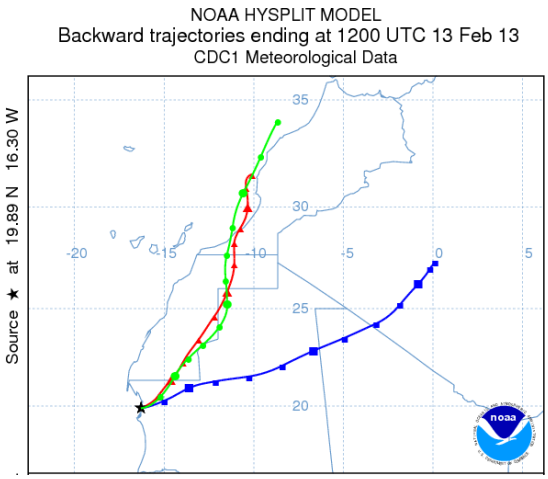

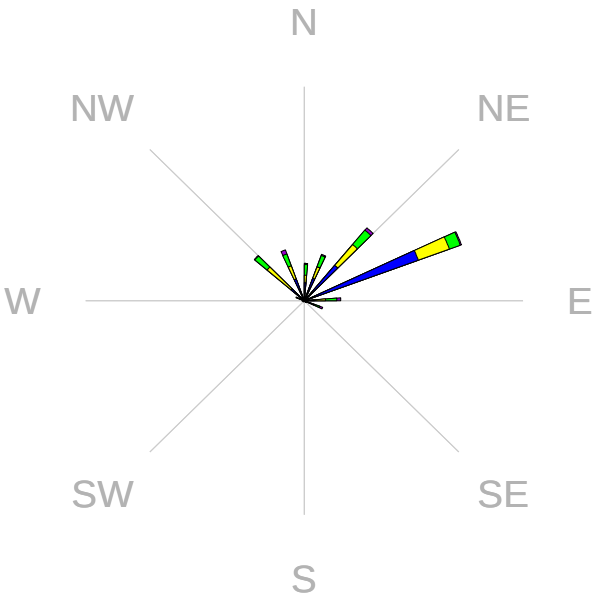

wind speed (m/s)

- <=4
- >4 - 6
- >6 - 8
- >8 - 12
- >12

February-March 2013

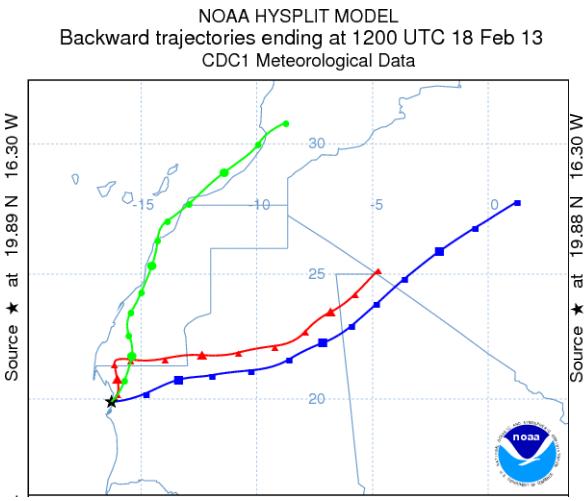

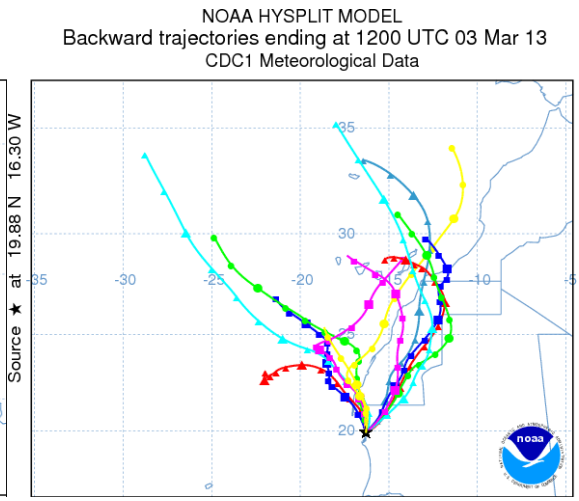

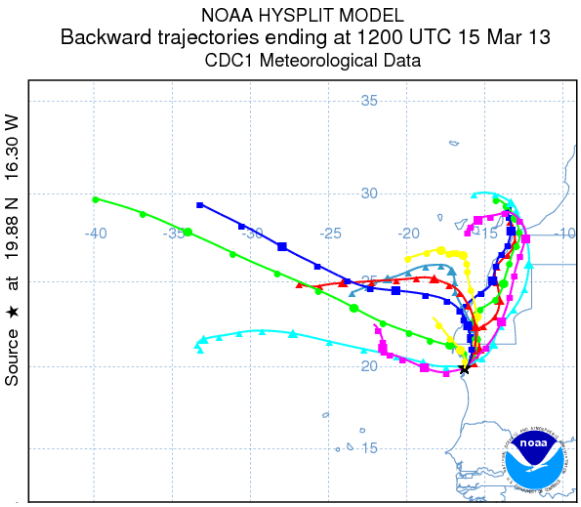

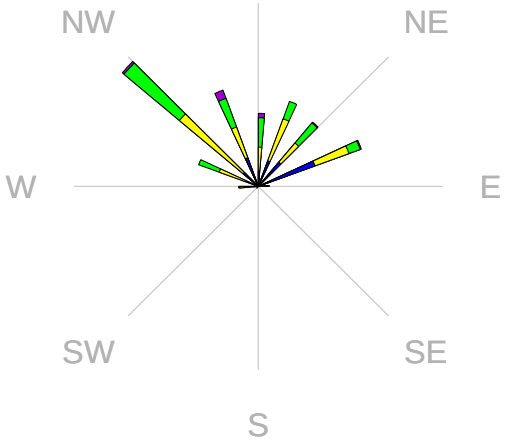

March-April 2013

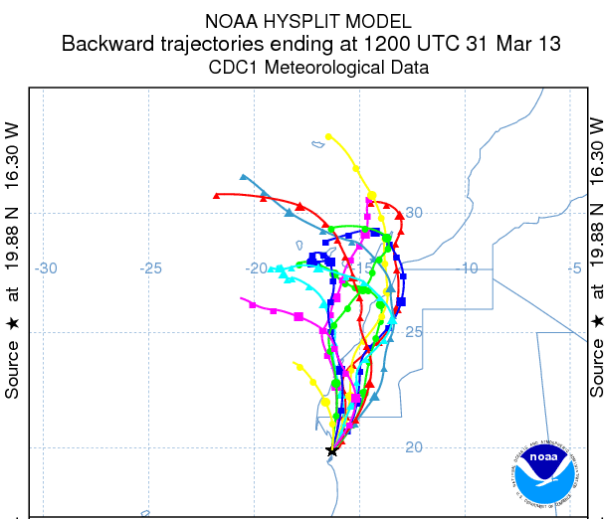

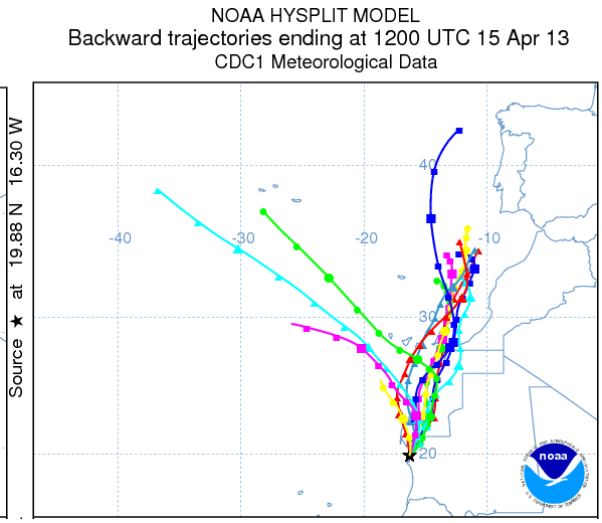

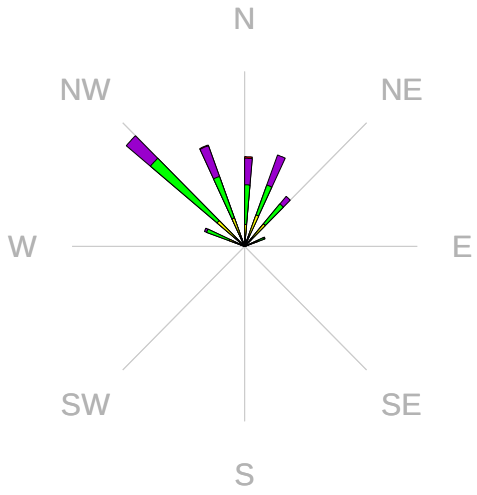

April-May 2013

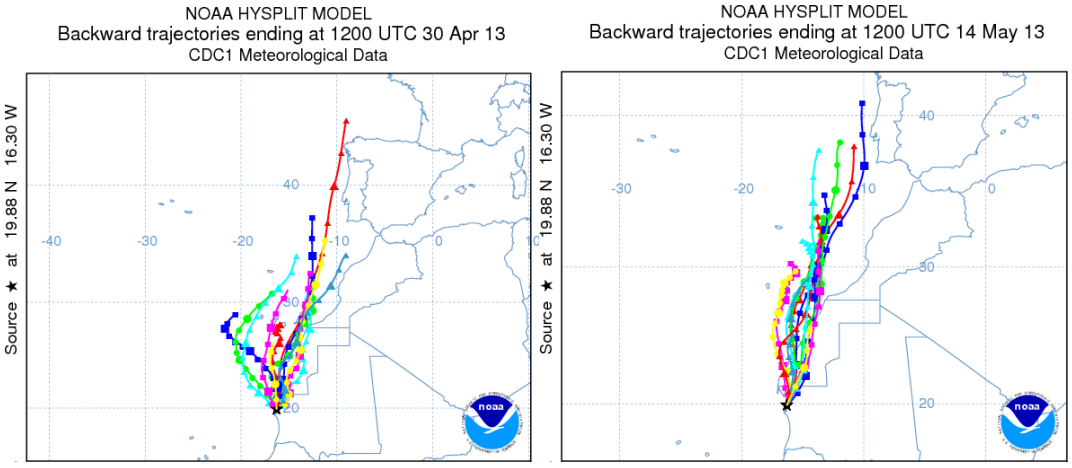

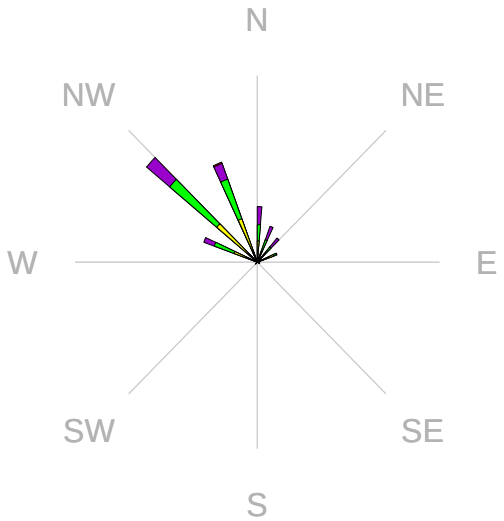

May-June 2013

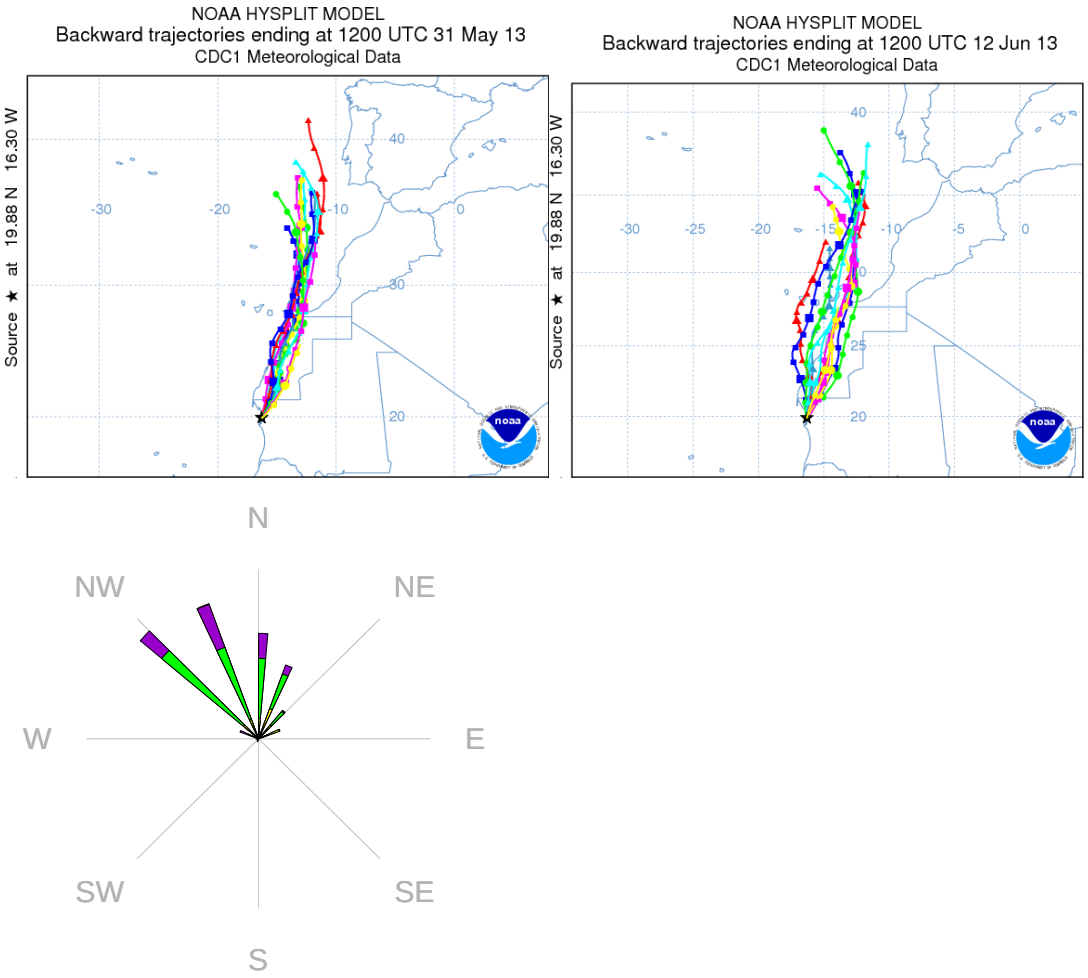

June-July 2013

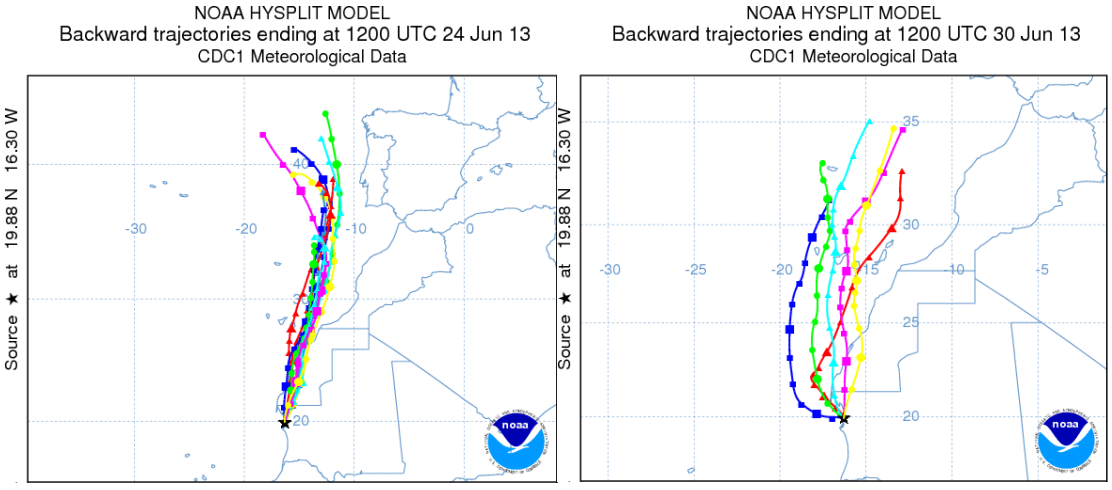

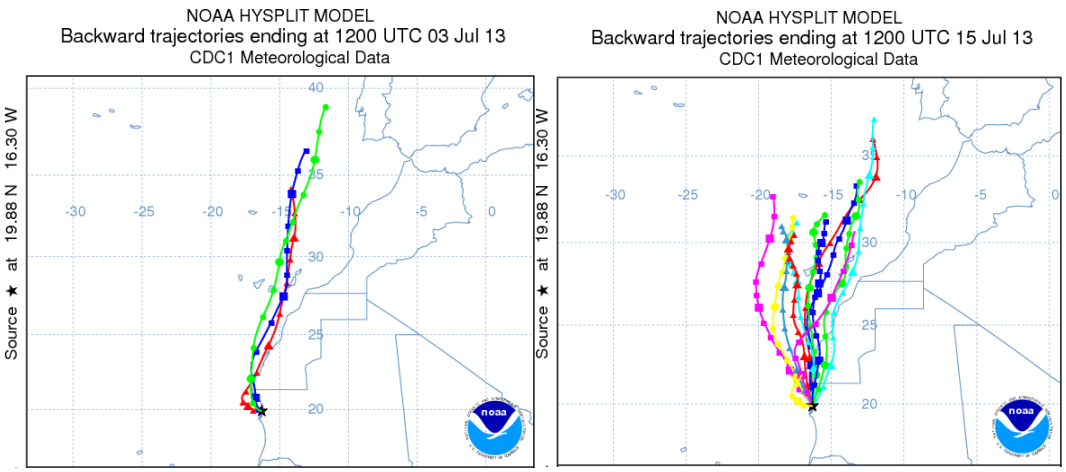

No meteorological data available from the sampling site.

July-August 2013

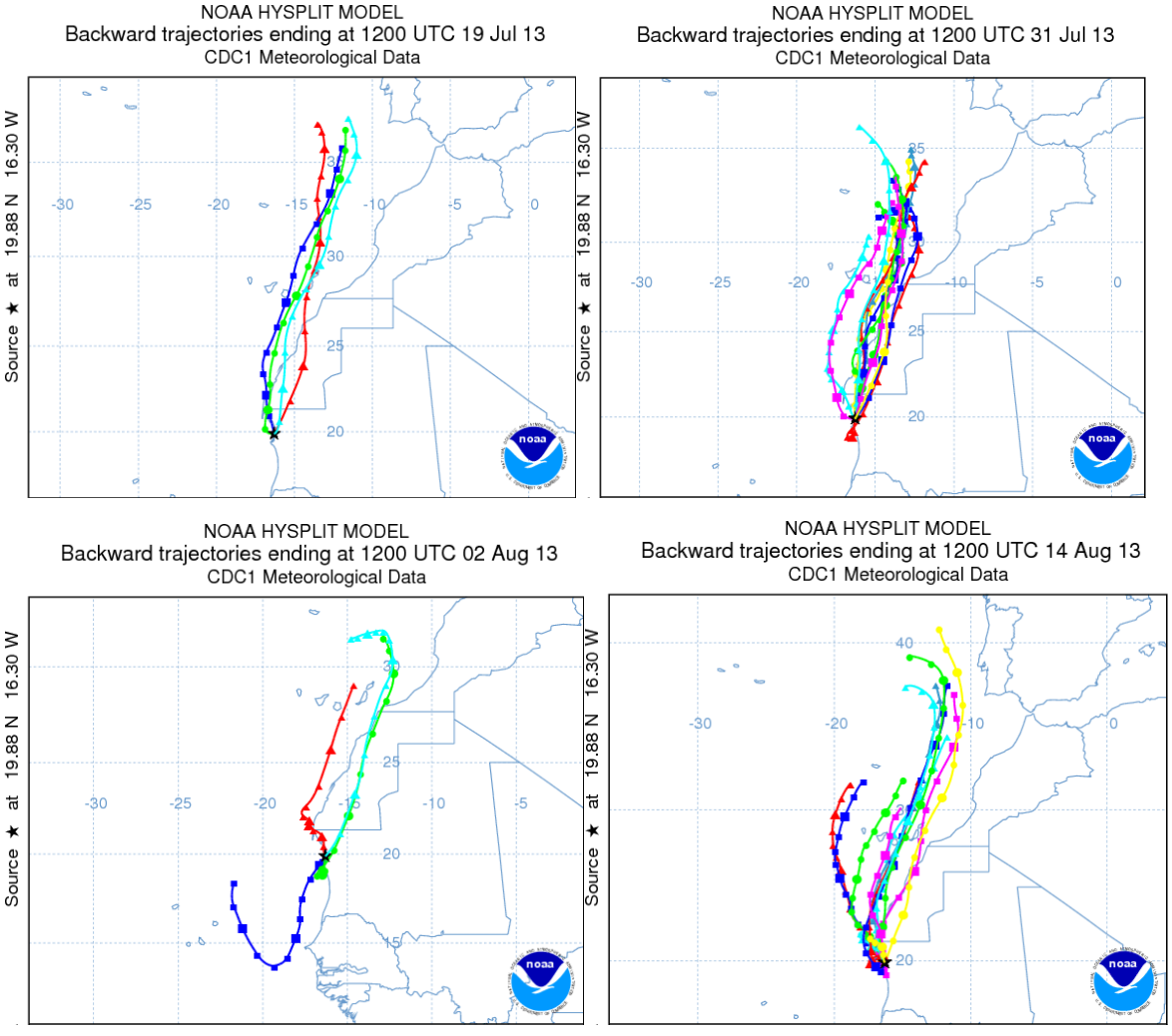

No meteorological data available from the sampling site.

August-October 2013

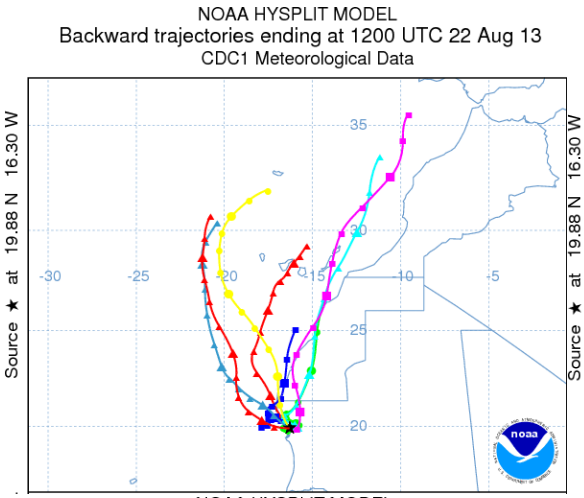

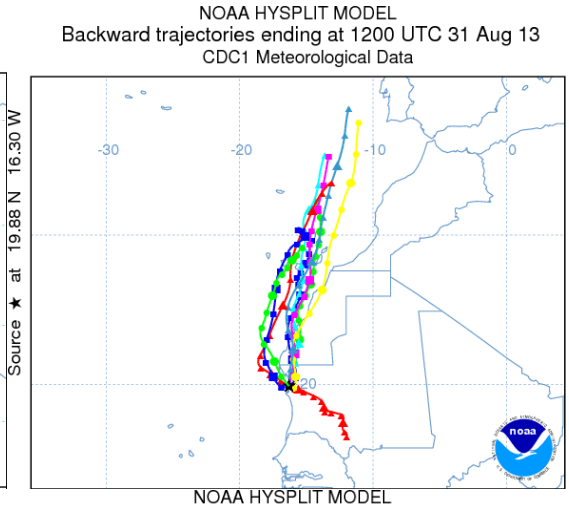

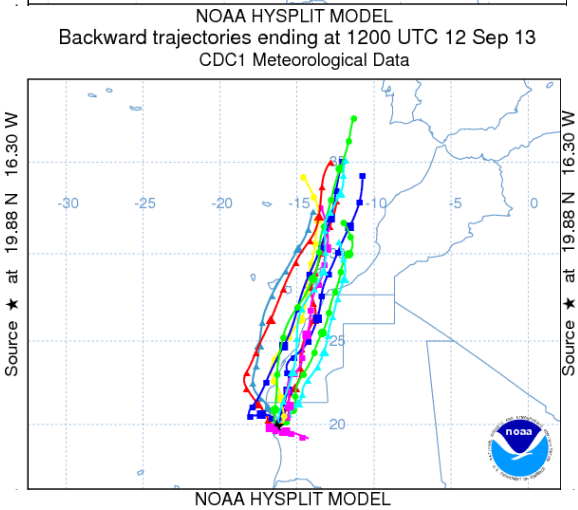

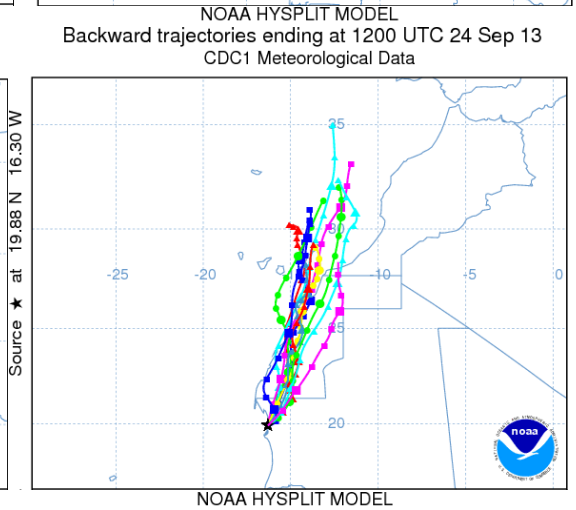

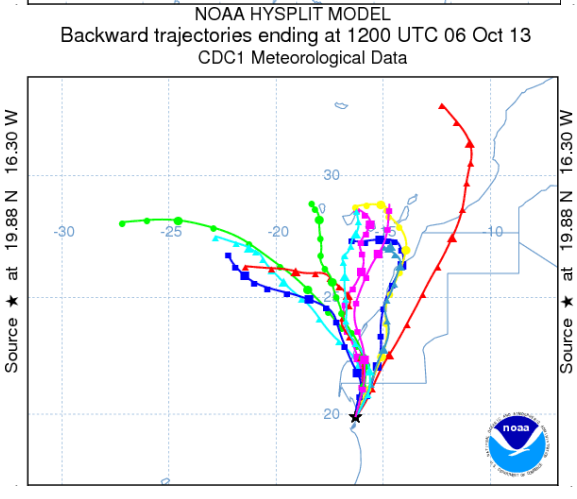

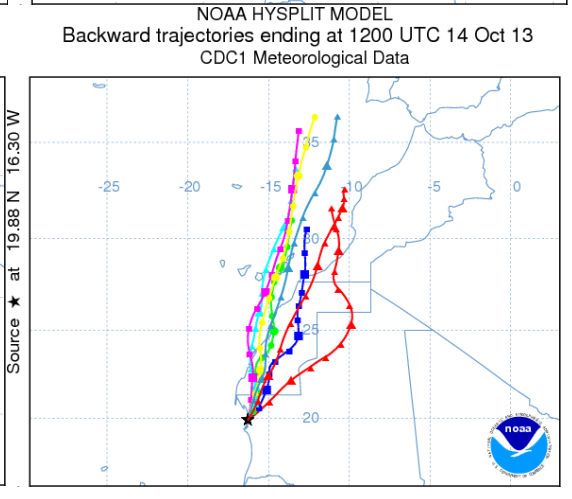

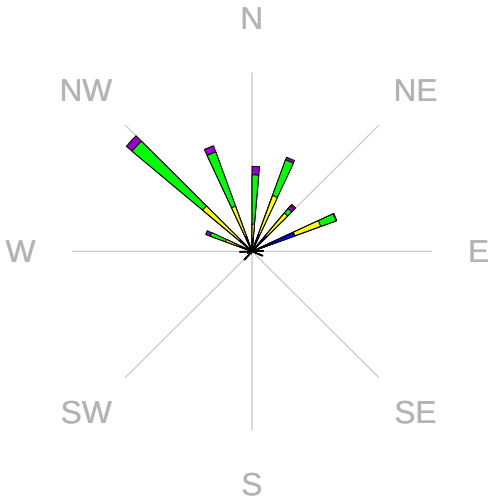

October-November 2013

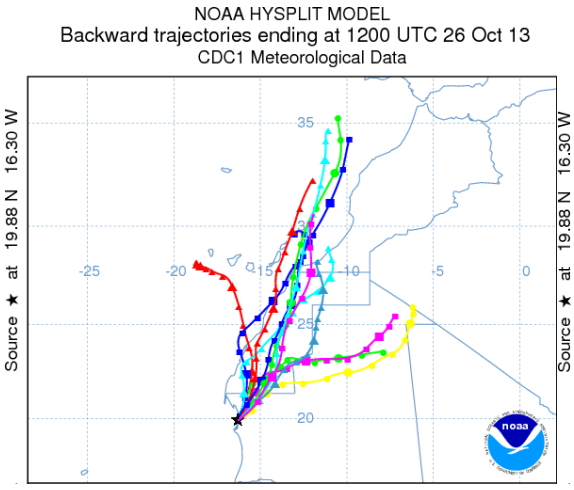

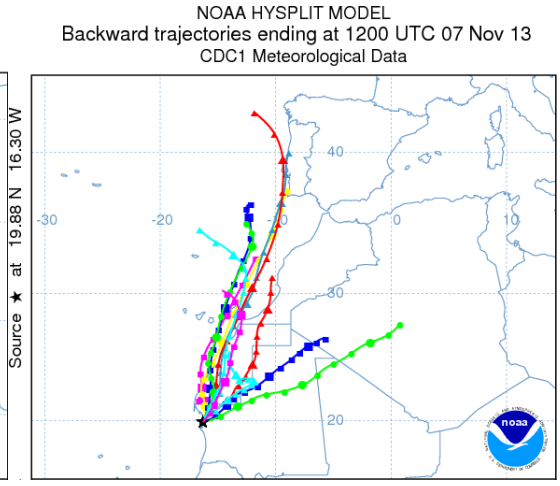

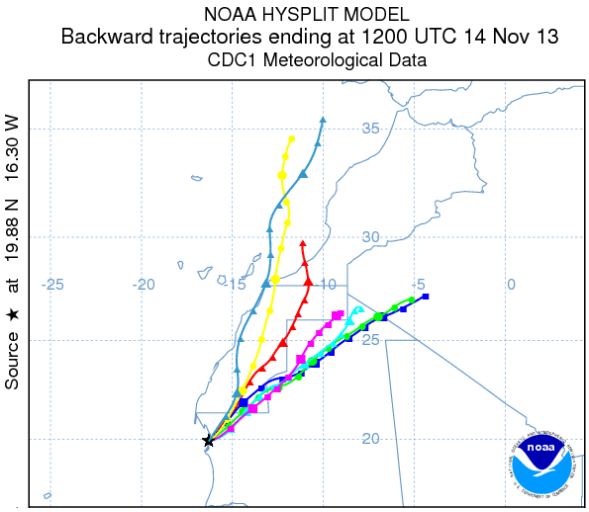

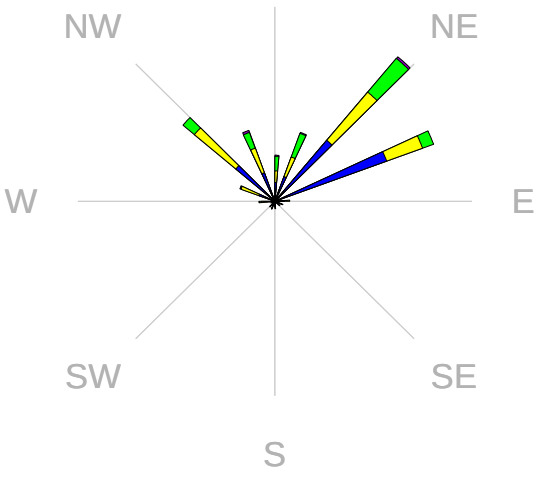

November-December 2013

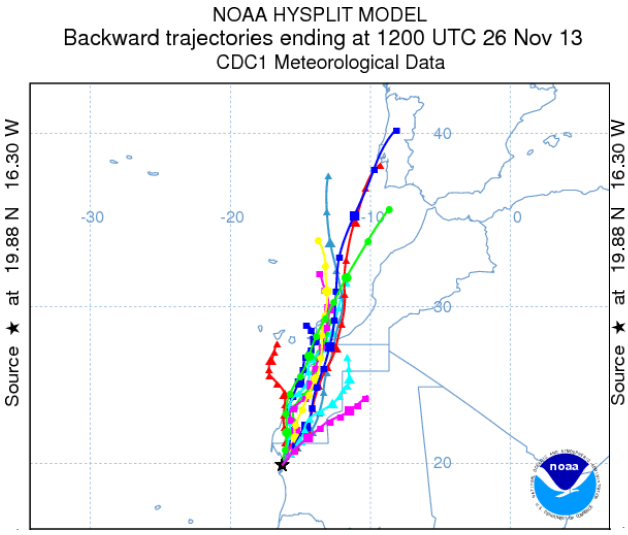

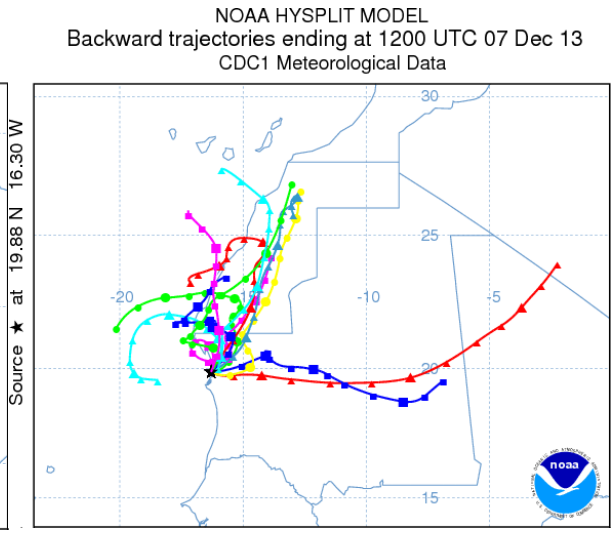

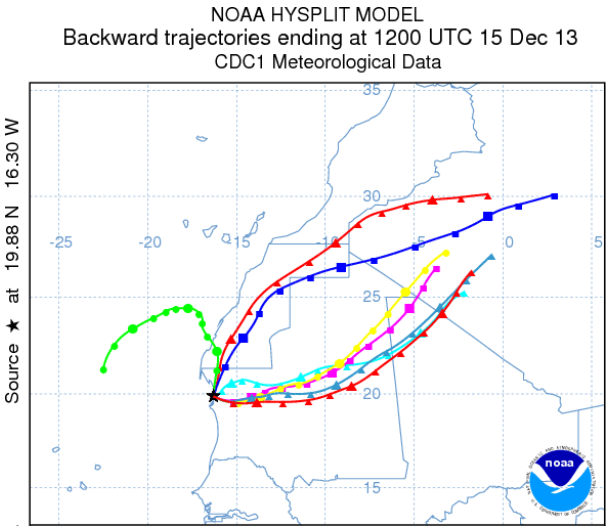

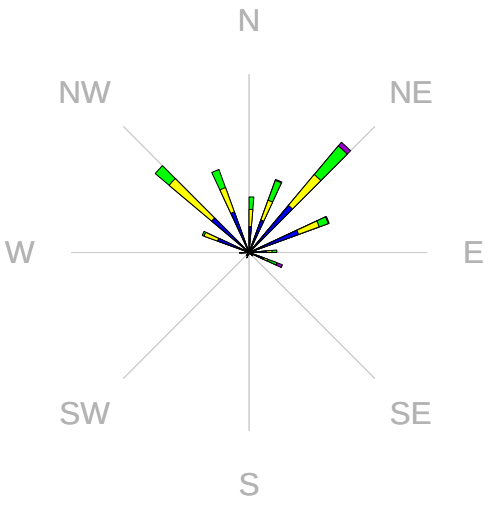

December 2013- January 2014

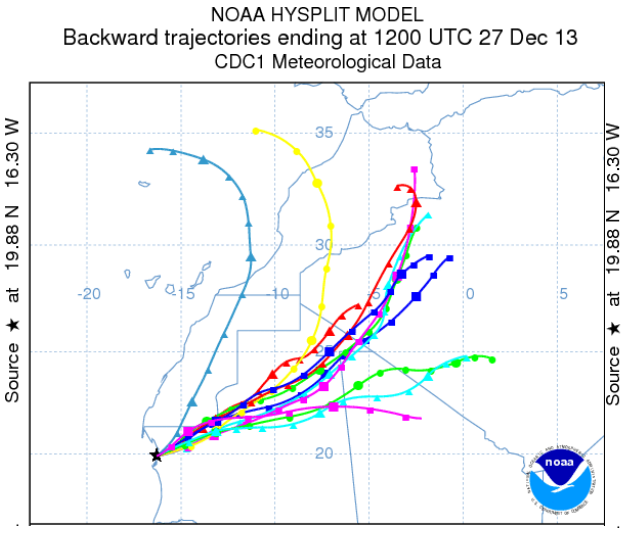

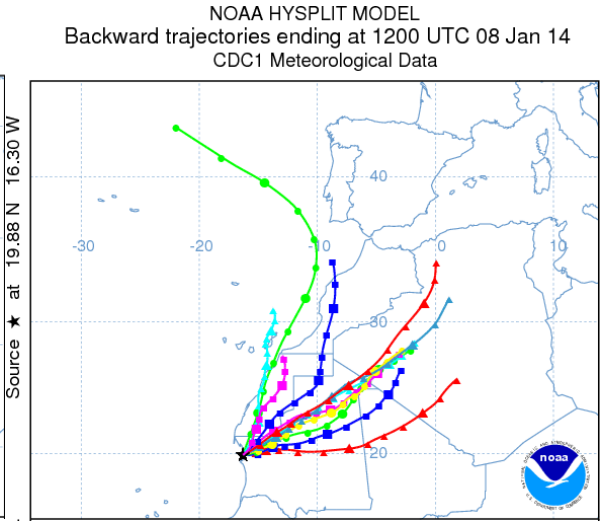

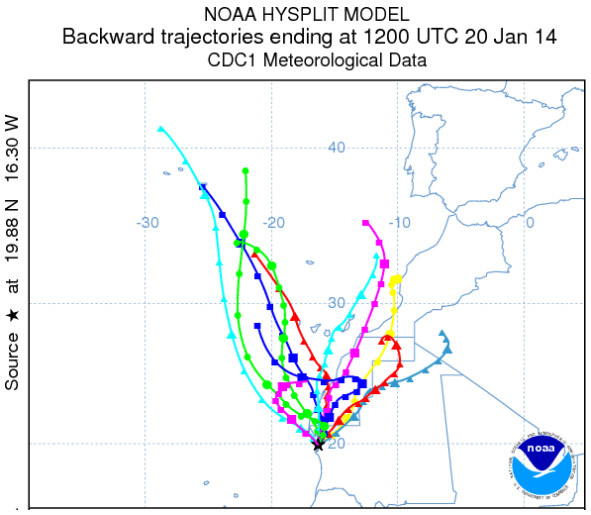

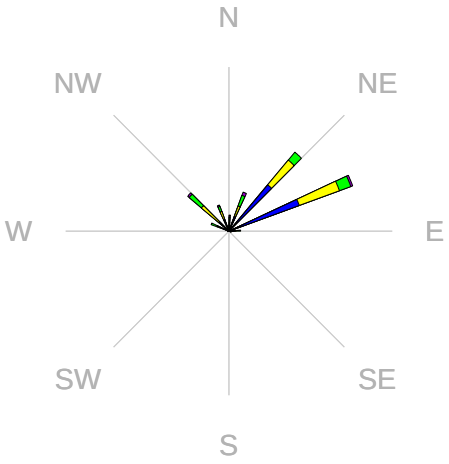

January-February 2014

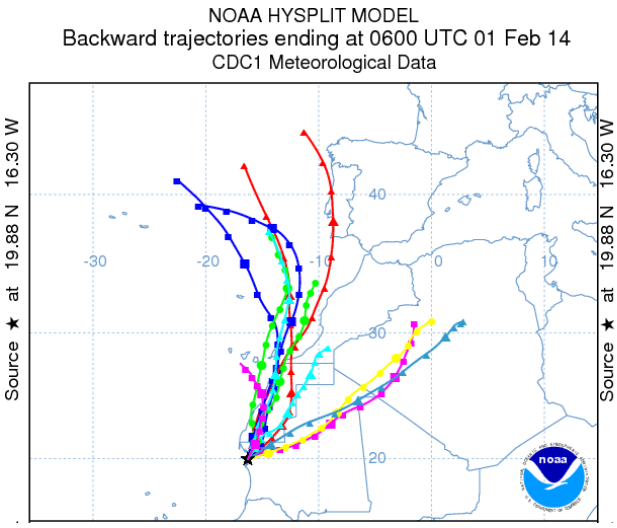

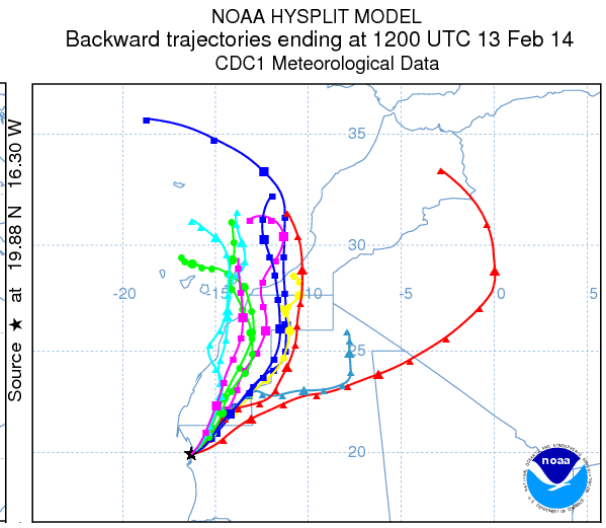

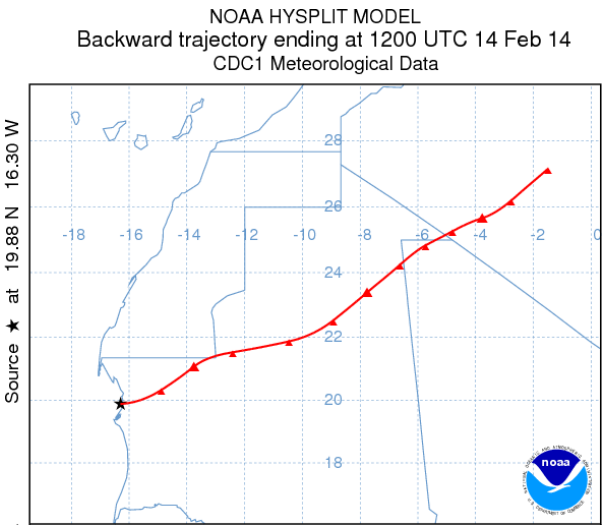

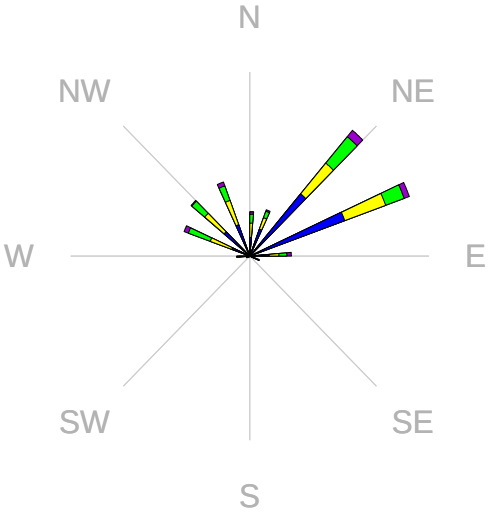

February-March 2014

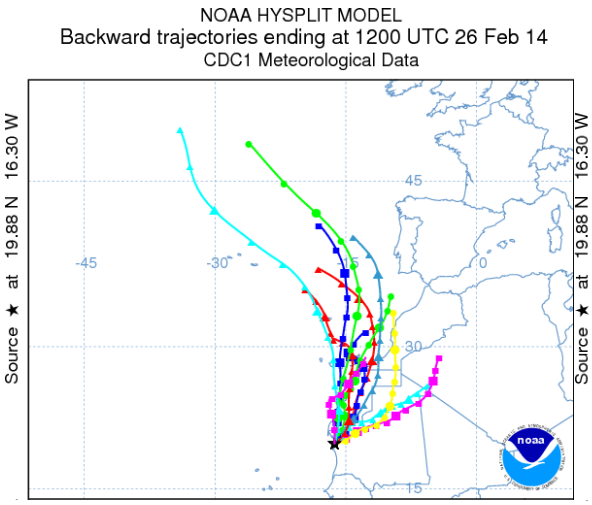

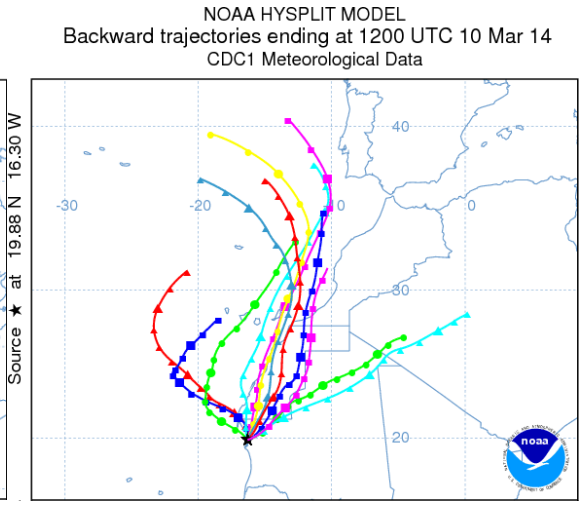

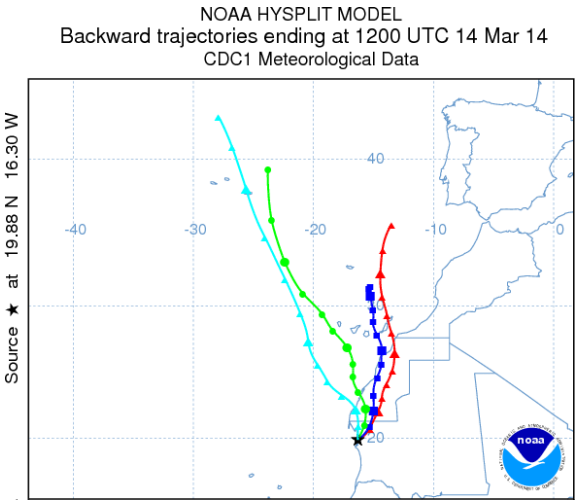

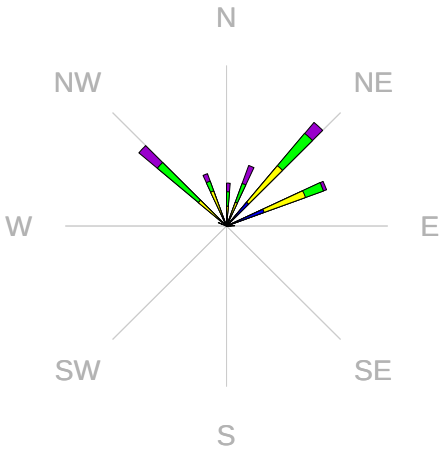

March-April 2014

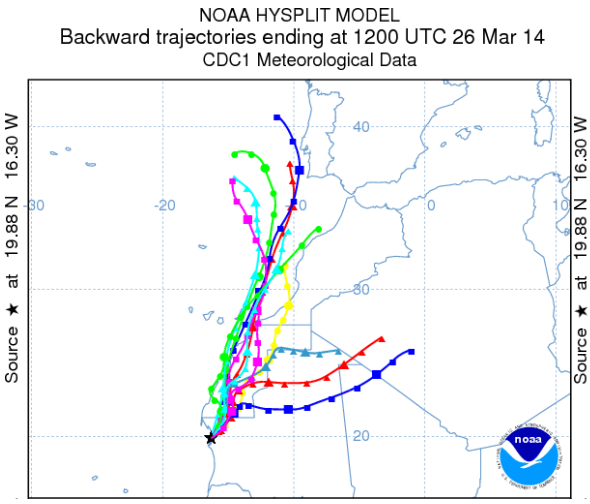

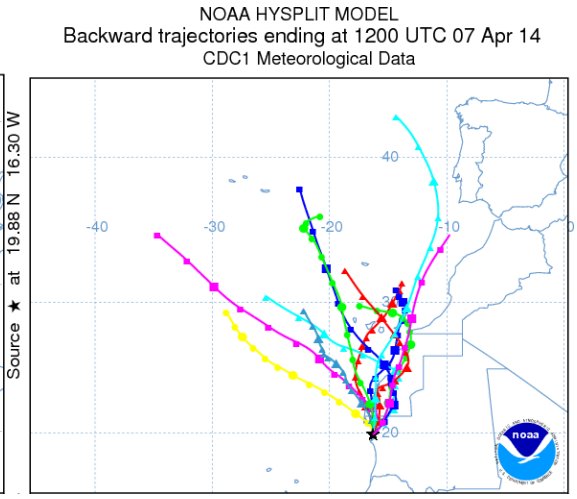

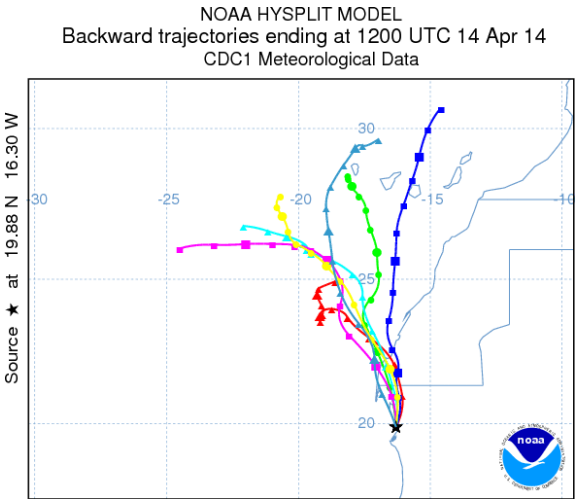

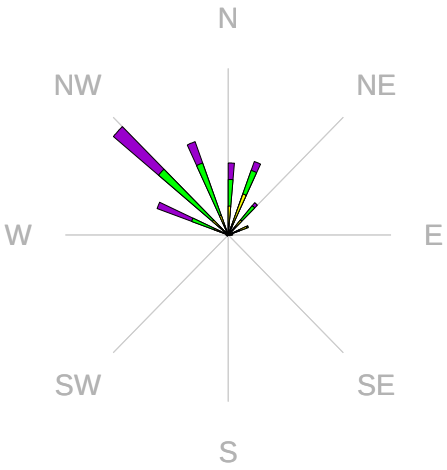

April-May 2014

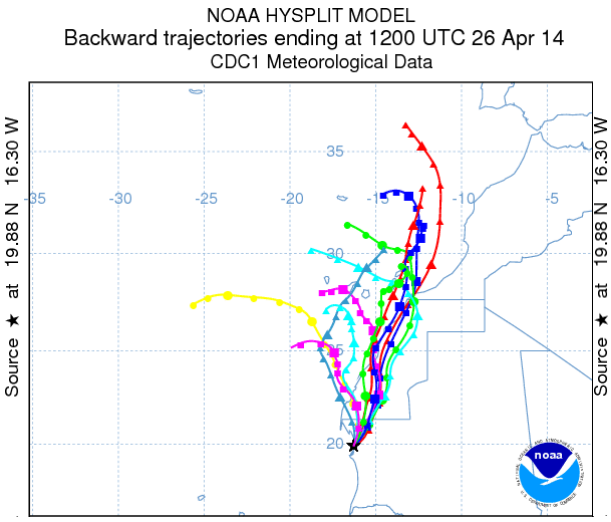

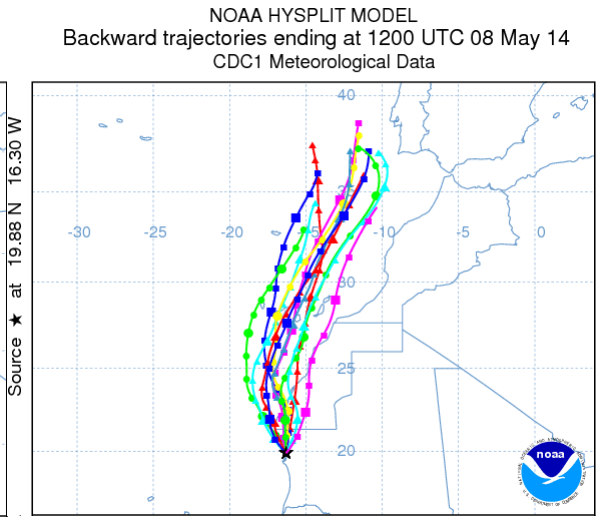

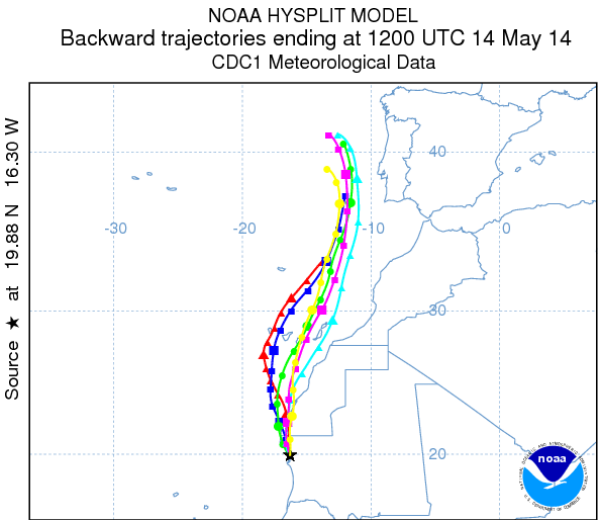

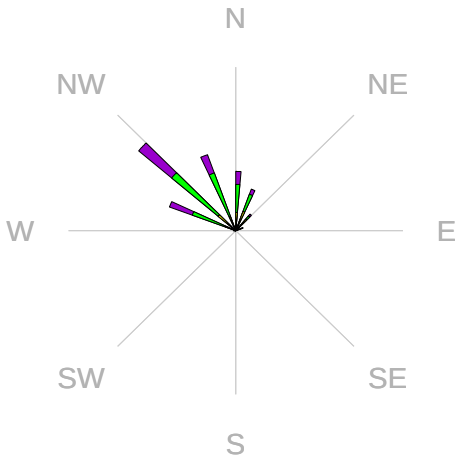

May-June 2014

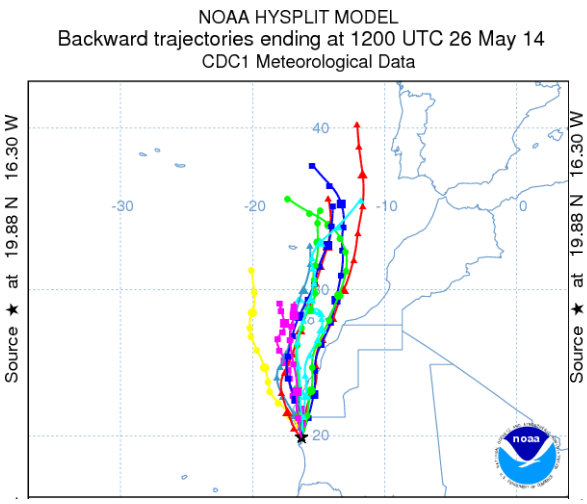

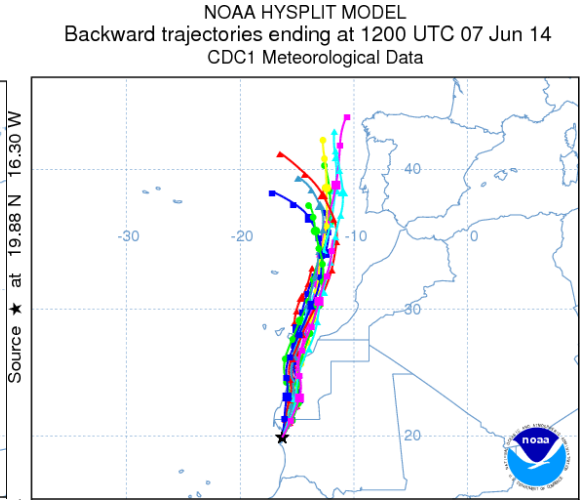

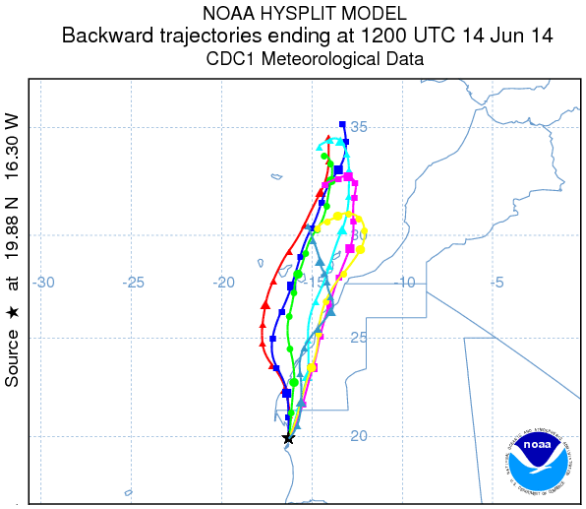

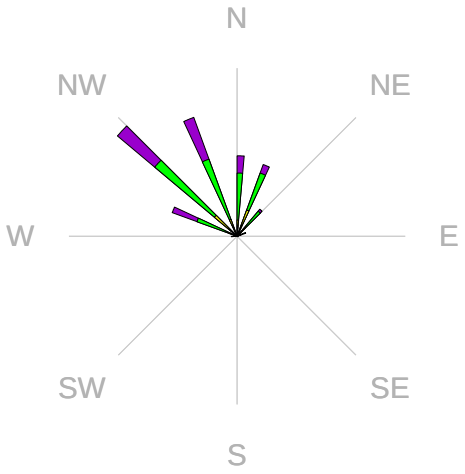

June-July 2014

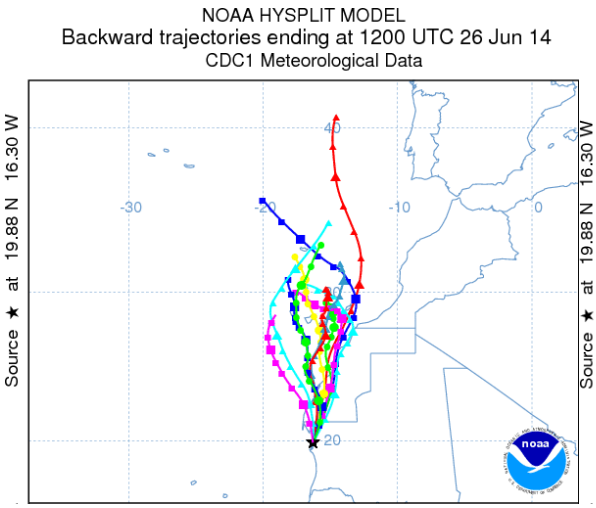

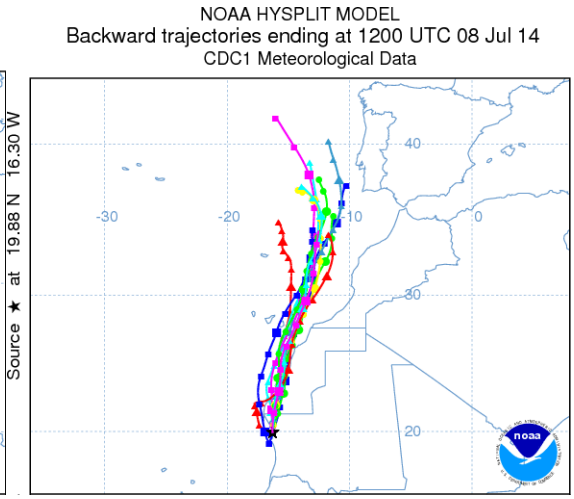

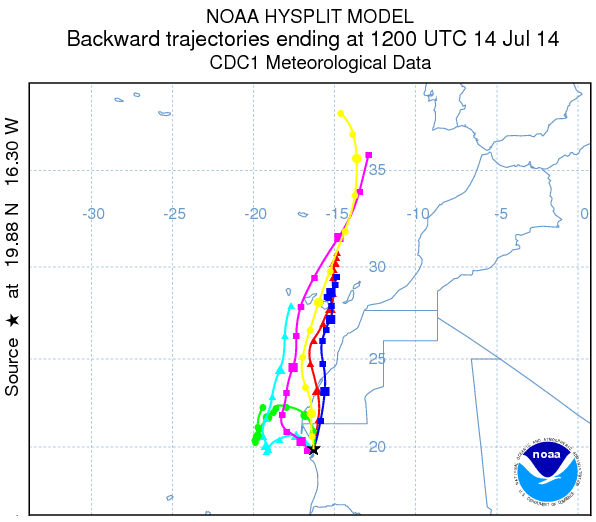

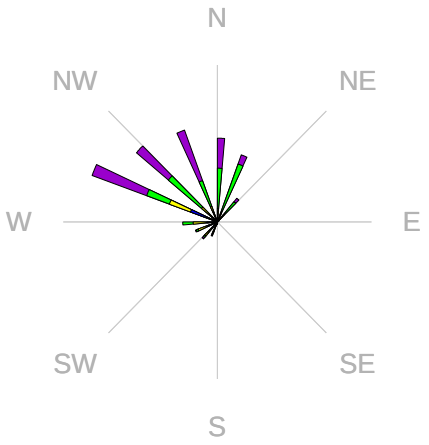

July-August 2014

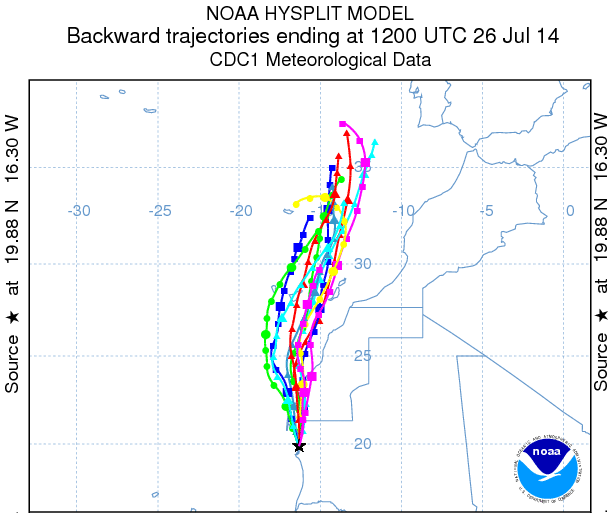

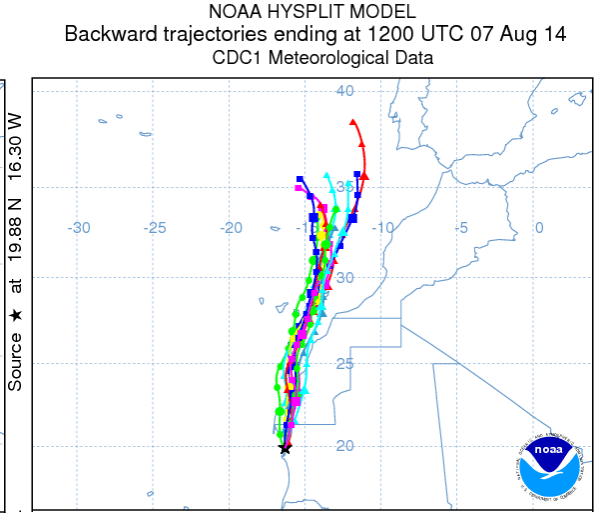

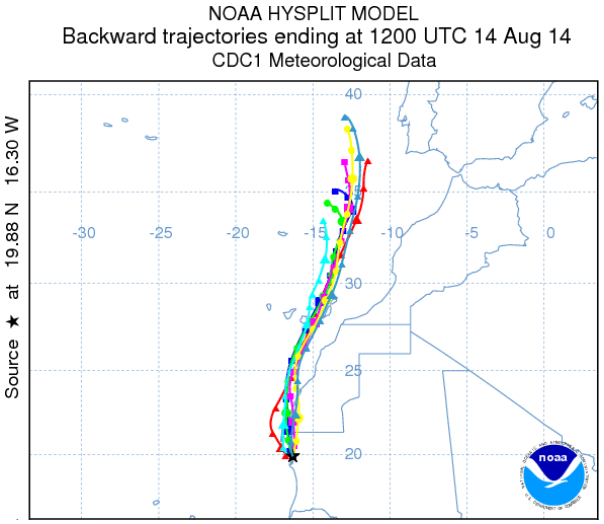

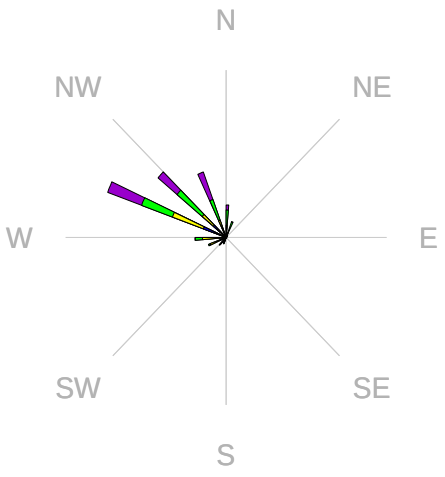

August-September 2014

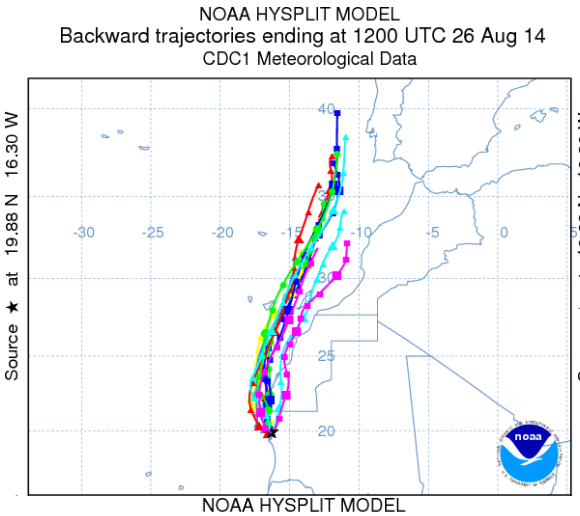

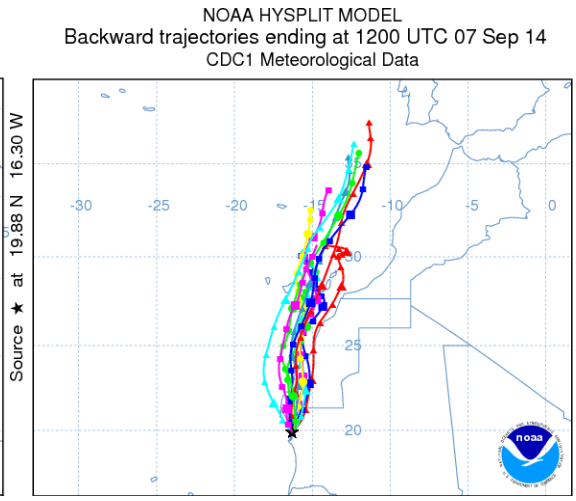

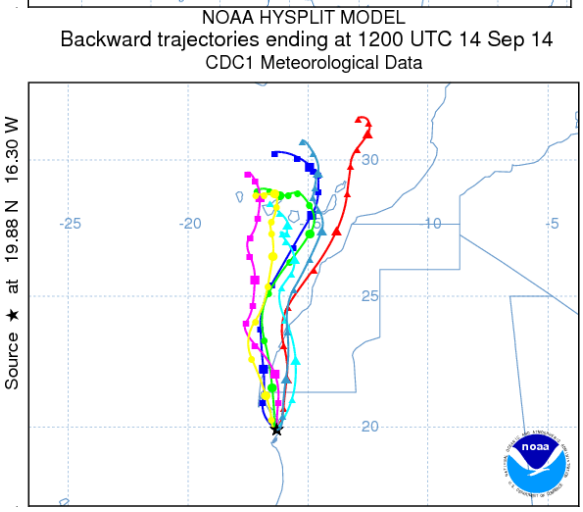

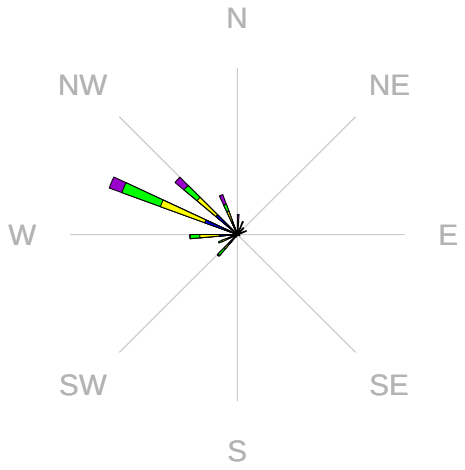

September-October 2014

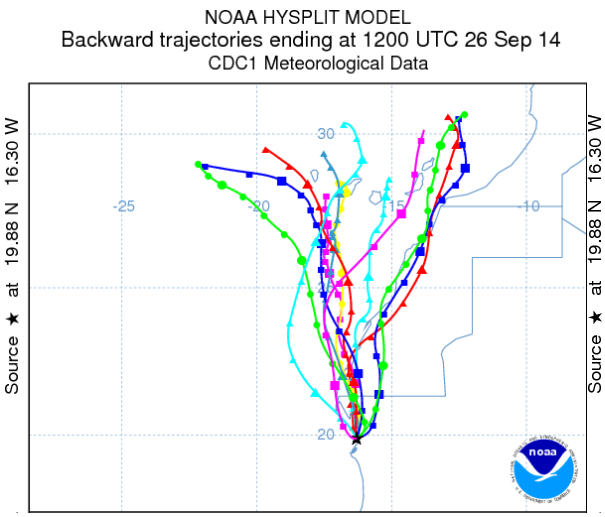

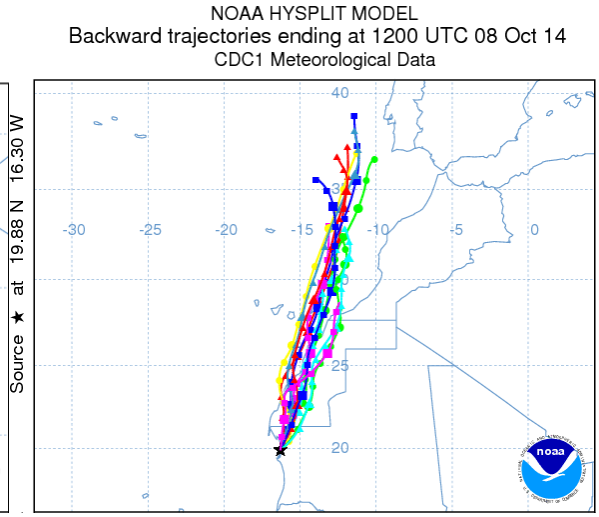

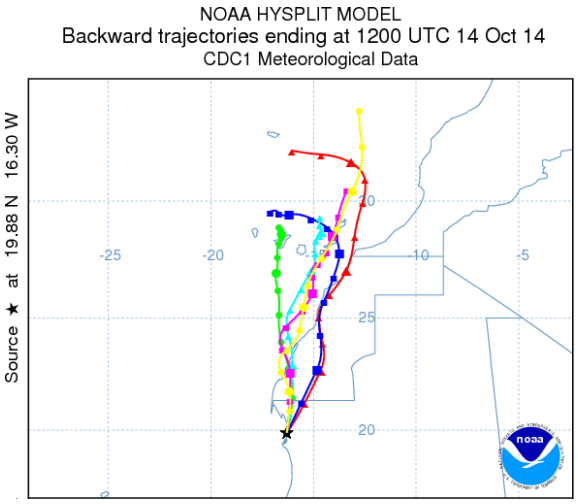

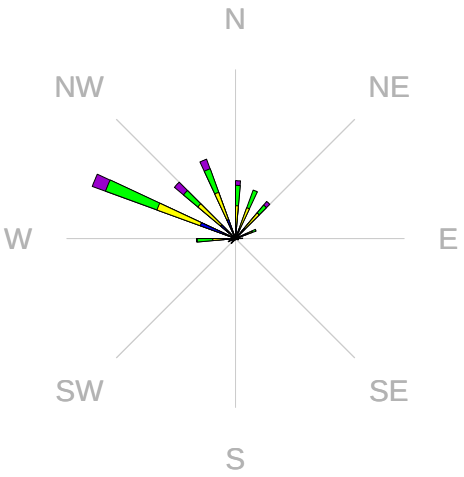

October-November 2014

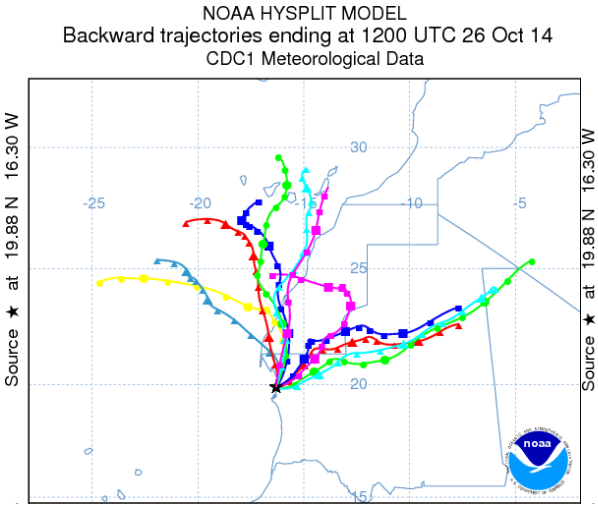

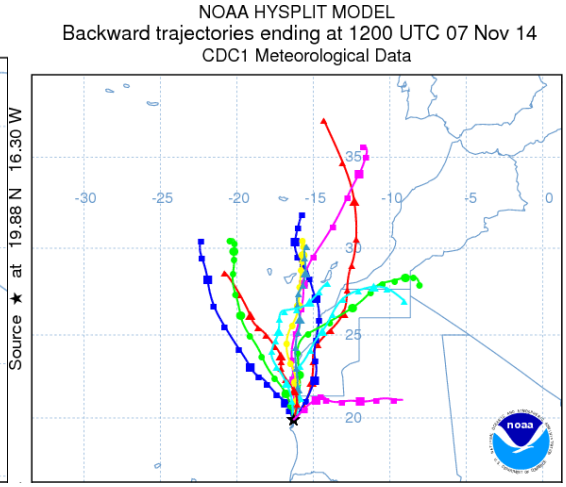

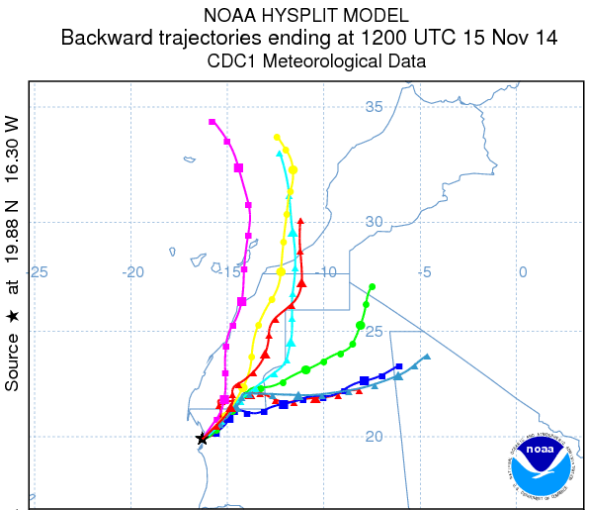

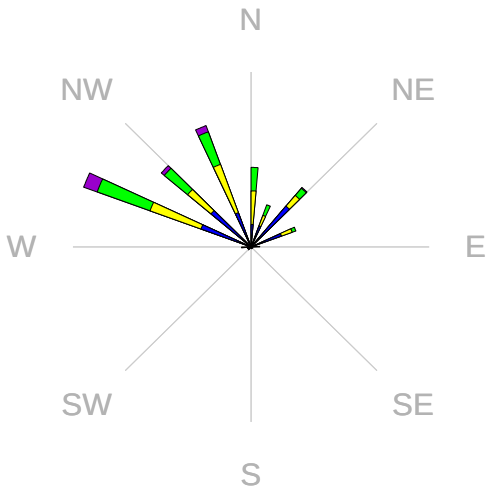

November-December 2014

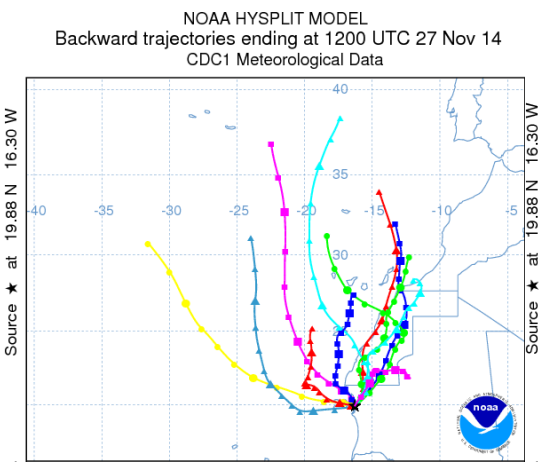

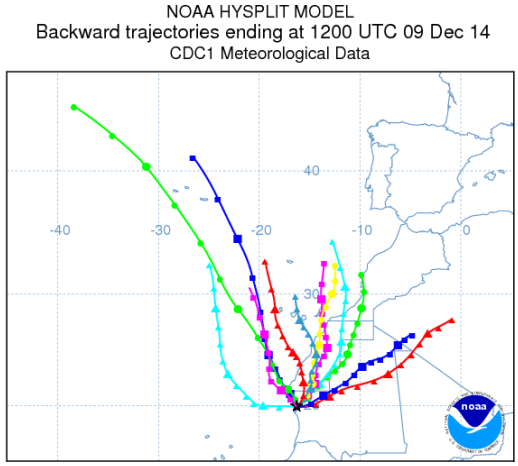

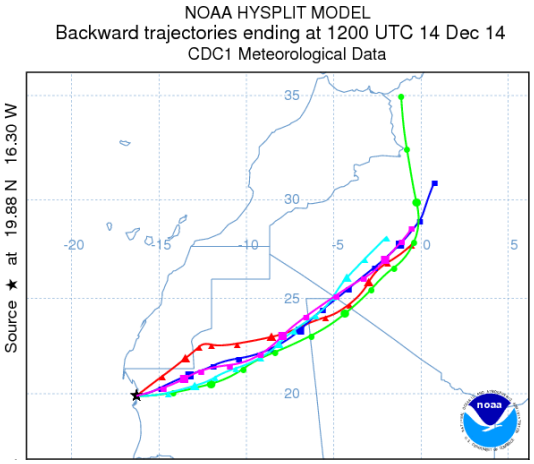

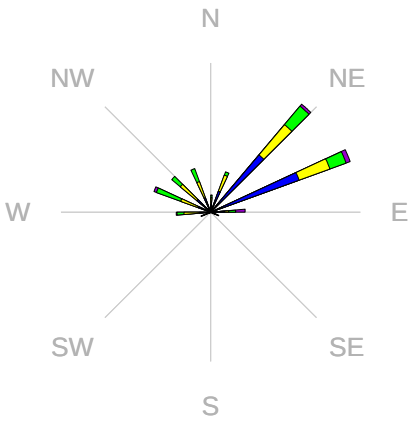

December 2014-January 2015

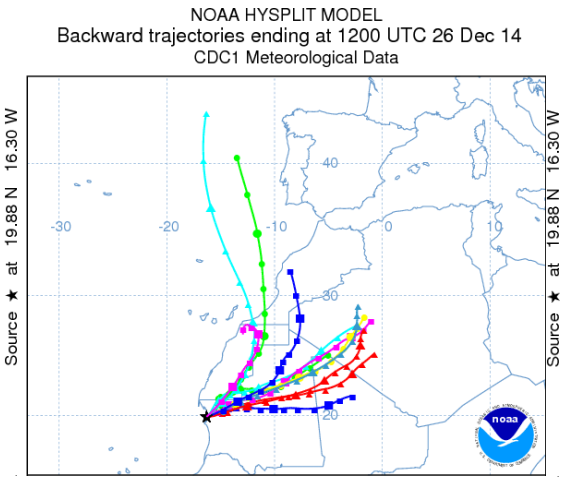

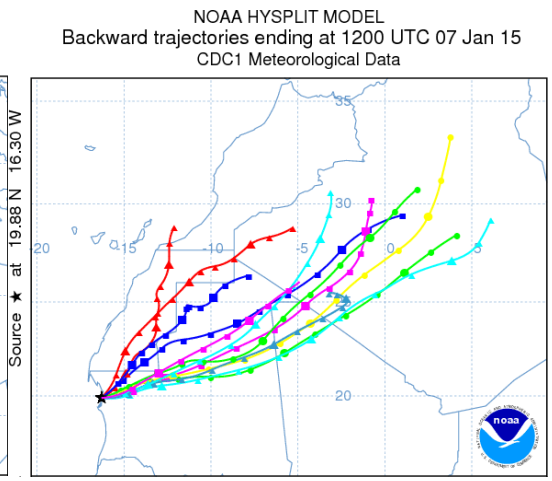

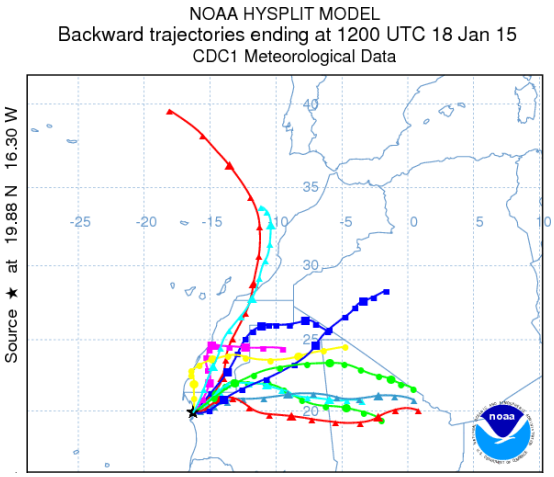
NOAA HYSPLIT MODEL
Backward trajectories ending at 1200 UTC 18 Jan 15
CDC1 Meteorological Data
Source ★ at 19.88 N 16.30 W
40
35
30
25
20
-25
-20
-15
-10
-5
0
5
10
noaa

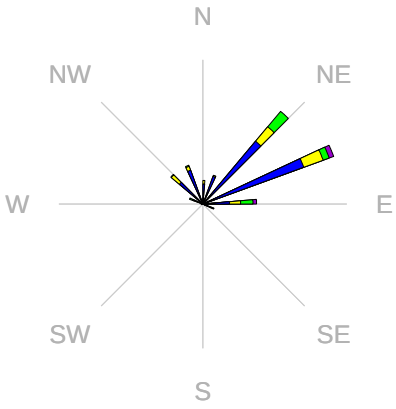
N
NW
NE
W
E
SW
SE
S